TECHNICAL REPORT STANDARD TITLE PAGE

1. Report No.	2. Government Accession No.	3. Recipient's Catalog No.

4. Title and Subtitle
EVALUATION OF THE COMPOSITE WING GIRDER BRIDGE AT BEAR CREEK

5. Report Date
November 1984

6. Performing Organization Code

7. Author(s)
Christopher D. White and John E. Breen

8. Performing Organization Report No.
Research Report IAC(84-85)-0799-1F

9. Performing Organization Name and Address
Center for Transportation Research
The University of Texas at Austin
Austin, Texas 78712-1075

10. Work Unit No.

11. Contract or Grant No.
Study No. IAC(84-85)-0799

12. Sponsoring Agency Name and Address
Texas State Department of Highways and Public Transportation; Transportation Planning Division
P. O. Box 5051
Austin, Texas 78763

13. Type of Report and Period Covered
Final

14. Sponsoring Agency Code

15. Supplementary Notes
Research Study Title: "Measuring and Predicting Stresses of Bear Creek Bridge on FM 1626"

16. Abstract

This report documents the construction monitoring and subsequent field testing to evaluate the performance of an innovative "loose-fit" composite post-tensioned concrete wing girder bridge constructed over Bear Creek, south of Austin, Texas. The structure was built as a trial evaluation of an early proposed design for an elevated interstate highway expansion.

Monitoring of the bridge was carried out both during critical construction steps and by truck testing after completion. Results of both construction measurements and service load level loading tests were compared to analytical predictions. Recommendations for improvement of the present design with regards to both constructability and structural performance are made. The suggested revisions should result in both easier and quicker construction with improved appearance and durability at a reduced cost.

17. Key Words	18. Distribution Statement
	No restrictions. This document is available to the public through the National Technical Information Service, Springfield, Virginia 22161.

19. Security Classif. (of this report)	20. Security Classif. (of this page)	21. No. of Pages	22. Price
Unclassified	Unclassified	174	

Form DOT F 1700.7 (8-69)

EVALUATION OF THE COMPOSITE WING GIRDER BRIDGE AT BEAR CREEK

by

Christopher D. White and John E. Breen

Research Report IAC(84-85)-0799-1F

Research Project IAC(84-85)-0799

Measuring and Predicting Stresses of Bear Creek Bridge on FM 1626

Conducted for

Texas
State Department of Highways and Public Transportation

In Cooperation with the
U.S. Department of Transportation
Federal Highway Administration

by

CENTER FOR TRANSPORTATION RESEARCH
BUREAU OF ENGINEERING RESEARCH
THE UNIVERSITY OF TEXAS AT AUSTIN

November 1984

The contents of this report reflect the views of the authors who are responsible for the facts and accuracy of the data presented herein. The contents do not necessarily reflect the views of policies of the Federal Highway Administration. This report does not constitute a standard, specification or regulation.

There was no invention or discovery conceived or first actually reduced to practice in the course of or under this contract, including any art, method, process, machine, manufacture, design or composition of matter, or any new and useful improvement thereof, or any variety of plant which is or may be patentable under the patent laws of the United States of America or any foreign country.

P R E F A C E

The study described herein was administered through the Center for Transportation Research at The University of Texas at Austin under the sponsorship of the Texas State Department of Highways and Public Transportation--Research Study IAC (84-85)-0799. Although the actual testing program was executed in the field, most of the program planning and fabrication of instrumentation took place at the Phil M. Ferguson Structural Engineering Laboratory at The University of Texas Balcones Research Center.

Much of the success of the project depended on the cooperation of all parties involved, from the designer, T. Y. Lin International, and contractor, Bill Shannon, Inc., to the Texas State Department of Highways and Public Transportation. In this respect, all the individuals who participated in the project should be commended on their openness and willingness to share information. The authors would like to thank the following individuals for their contribution to this study: Mr. William Garbade, SDHPT; Mr. Randy Cox, Mr. Bobby Hunt, Mr. Carl Amelung, and Mr. David Balli, engineering staff members from the SDHPT; Mr. Bill Shannon, Mr. Kevin Monk, and Mr. Wallace Jackson of Bill Shannon, Inc.; Mr. Bob Lochausen, the precasting contractor; and Mr. Charles Redfield and Professor T. Y. Lin of T. Y. Lin International. Although many other individuals played a role in the day-to-day efforts of the project, they are too numerous to mention here. However, their assistance was greatly appreciated.

Individuals who participated in other phases of the project were Dr. C. P. Johnson and Mr. Pyong Soo Lee from The University of Texas at Austin, who developed the finite element model for the Bear Creek structure. Mr. Gordon Clark from the Ferguson Structural Engineering Laboratory also assisted in the preparation and testing of the structure. All of these individuals deserve the author's gratitude for their cooperation.

Finally, the authors would like to thank their friends and colleagues at the Ferguson Structural Engineering Laboratory who were "drafted" into service for the week of final testing in July. Their perseverance through the heat and rain and the countless barbecue lunches is a credit to the profession.

The success of this study demonstrates how much can be accomplished when all individuals involved in a project are committed to working together in a positive spirit. The field of structural engineering would benefit greatly from continued cooperation between designers, contractors, owners and other parties involved.

S U M M A R Y

This report documents the construction monitoring and subsequent field testing to evaluate the performance of an innovative "loose-fit" composite post-tensioned concrete wing girder bridge constructed over Bear Creek, south of Austin, Texas. The structure was built as a trial evaluation of an early proposed design for an elevated interstate highway expansion.

Monitoring of the bridge was carried out both during critical construction steps and by truck testing after completion. Results of both construction measurements and service load level loading tests were compared to analytical predictions. Recommendations for improvement of the present design with regards to both constructability and structural performance are made. The suggested revisions should result in both easier and quicker construction with improved appearance and durability at a reduced cost.

I M P L E M E N T A T I O N

This project was undertaken on a "real time" scale to provide factual information and observations to both District 15 project staff and to Bridge Division personnel concerning the proposed "loose-fit" bridge system proposed for the San Antonio expressway project. The wisdom of trying this innovative design and construction concept on a modest scale at the Bear Creek crossing has been amply justified by the subsequent changes made as the design proceeded on the main freeway project. The observations of both construction problems and structural performance were shared with representatives of owner, designer, and constructor much earlier than the completion of this report. It is felt that this free interchange of documented observations aided in developing new solutions for problems observed and clearly showed the attractiveness and robustness of the proposed design.

C O N T E N T S

Chapter Page

T A B L E S

F I G U R E S

C H A P T E R 1

INTRODUCTION

1.1 General

An improvement program is currently under design to expand the traffic flow and ease congestion at the "Y" intersection of IH-35 and IH-10 in downtown San Antonio, Texas. Because of limitations on space and new right-of-way acquisitions, the additional lanes will be provided by elevated structures.

One of the structural systems proposed to meet the stringent demands was a composite wing girder design featuring a partial cast-in-place spine beam and precast wings as shown in Fig. 1.1. The structure is a combination of precast slab units made composite by cast-in-place closure joints and post-tensioning. The design is a novel concept developed by T. Y. Lin International. Although the overall concept is not entirely new (a variant was used successfully by Lin at the San Francisco International Airport), the design techniques and construction processes are quite unique. The proposed design has been subsequently substantially revised, partially due to observations made in this program.

In order to evaluate design techniques and assess construction benefits and potential problems, an experimental two-span full-scale prototype bridge based on this design concept was constructed on FM 1626 over Bear Creek south of Austin. The proposed construction sequence and processes, as well as many aspects of the limited access constraints,

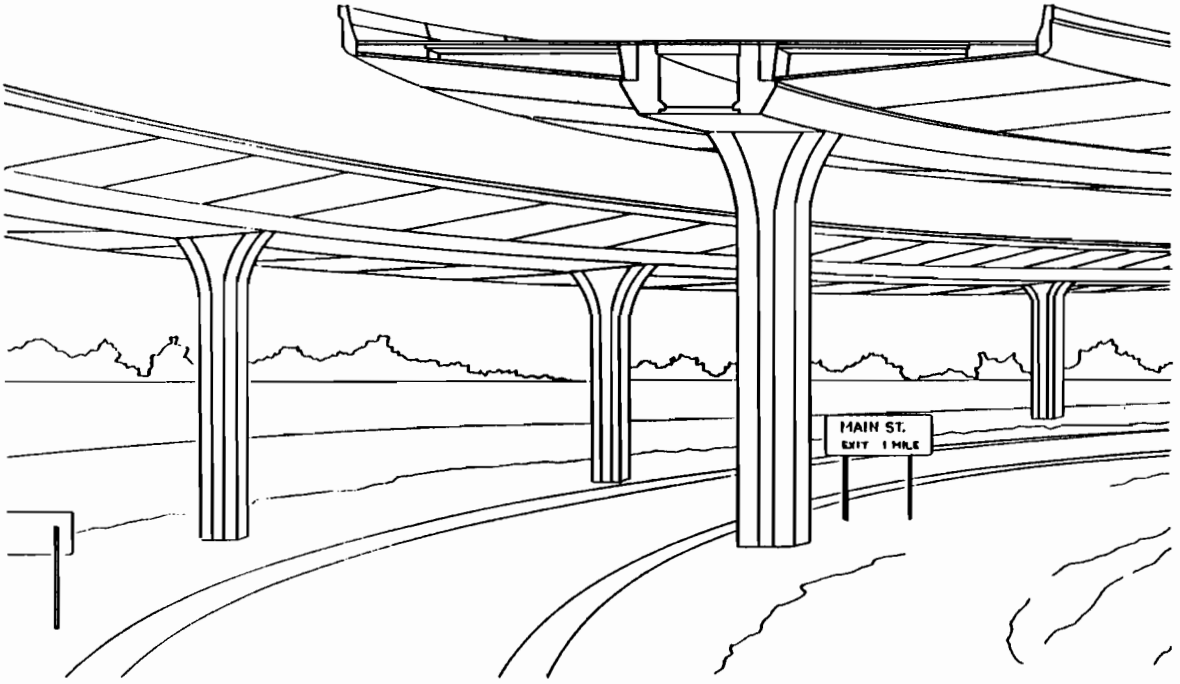

Fig. 1.1 Proposed composite wing girder design featuring a partial cast-in-place spine beam and precast wings

were incorporated at the site in order to closely replicate the conditions expected in San Antonio. A team from the Ferguson Structural Engineering Laboratory, acting through The University of Texas Center for Transportation Research, was utilized to document bridge behavior during construction and under typical service loads upon subsequent completion of the structure. Through a series of displacement, distortion, and slip measurements, the behavior of the component units and the degree of composite load carrying action of the entire structure were evaluated.

1.2 Related Research

The instrumentation and testing of the prototype bridge at Bear Creek was only one phase of the current comprehensive study of the proposed composite wing girder structure. Related research undertaken includes:

1) Analytical Model of the Bear Creek Bridge. A finite element analysis program was developed to aid in interpretation of test results and to facilitate the extension of design techniques to the more complex structures involved in the San Antonio project. Results from the analytical model are compared herein with the experimental results to establish the predictive capability of such a program in determining the distribution of stresses, deformations, and the degree of composite load transfer in the structure.

2) Model Testing. Because it would be undesirable to subject the Bear Creek structure to excessive overloads, and since it would be very beneficial to study the full load range characteristics of the proposed system, a half-scale model of a portion of the structure was also tested to destruction at the Ferguson Structural Engineering Laboratory [1]. The model, which consisted of four sets of precast panels and wings, was loaded to induce shear and torsional stresses and distortions and to study the load transfer between adjacent wing units and from wing unit to spine beam. Loading was taken to complete failure to verify the actual safety of the system and indicate needed improvements in details.

1.3 Objectives and Scope of Study

The unique design techniques and construction processes utilized in the proposed composite wing girder system necessitated a better understanding of the performance and load transfer behavior of the bridge during construction and under service loads. Thus, appropriate instrumentation devices were implanted at various stages of construction of the Bear Creek bridge to obtain information on displacements, distortions, and slip. These devices were monitored, and deformations were recorded at critical phases of the construction operation and under static service level loadings upon completion. These observations, along with careful observations of construction problems and concrete cracking, were then used to evaluate the nature of composite action in the bridge and to suggest details needing improvement.

1.4 Report Contents

Design details and specifications are presented in Chapter 2 along with a description of construction operations and observations. Detailed plans for selected portions of the Bear Creek bridge are given in Ref. 2. Chapter 3 describes the installation and location of instrumentation and details the test setup and loading sequence used. Chapter 4 presents the test results and their interpretation and compares these results with data from analytical models. Finally, Chapter 5 provides recommended changes to facilitate design and construction of similar structures in the future, and Chapter 6 provides a brief summary of the study and the resultant conclusions.

C H A P T E R 2

DESIGN AND CONSTRUCTION OF THE BEAR CREEK BRIDGE

2.1 Specifications and Guidelines

2.1.1 General. The Lin design for the Bear Creek project consists of two 100 ft spans supported on bearing pads at either abutment and continuous through the integral cast-in-place pier cap at the center as shown in Fig. 2.1. The composite design concept separates the construction sequence into two distinct phases: (1) the fabrication, casting, and initial stressing of the spine beam and (2) the placement of the wings and deck slab.

The spine beam shown in Fig. 2.2 is made up of precast compression struts and panels joined by cast-in-place construction. The precast units shown in Fig. 2.4 act as flanges in conjunction with the cast-in-place webs. The spine beam cross section is the same throughout with the exception of a 10-ft section at either abutment and a 20-ft section at the center pier. At these locations the top and bottom flanges taper out from a uniform section to the typical midspan thicknesses. Post-tensioning in the longitudinal direction ties the spine beam together prior to setting the wing units. At this stage only half the tendons are stressed to allow the spine beam to carry its own dead weight as well as the dead weight of the wings and deck.

The wing units, which cantilever out from either side, join the spine beam at a cast-in-place closure joint and are held in place by transverse post-tensioning. The wing-spine connection, shown in Fig.

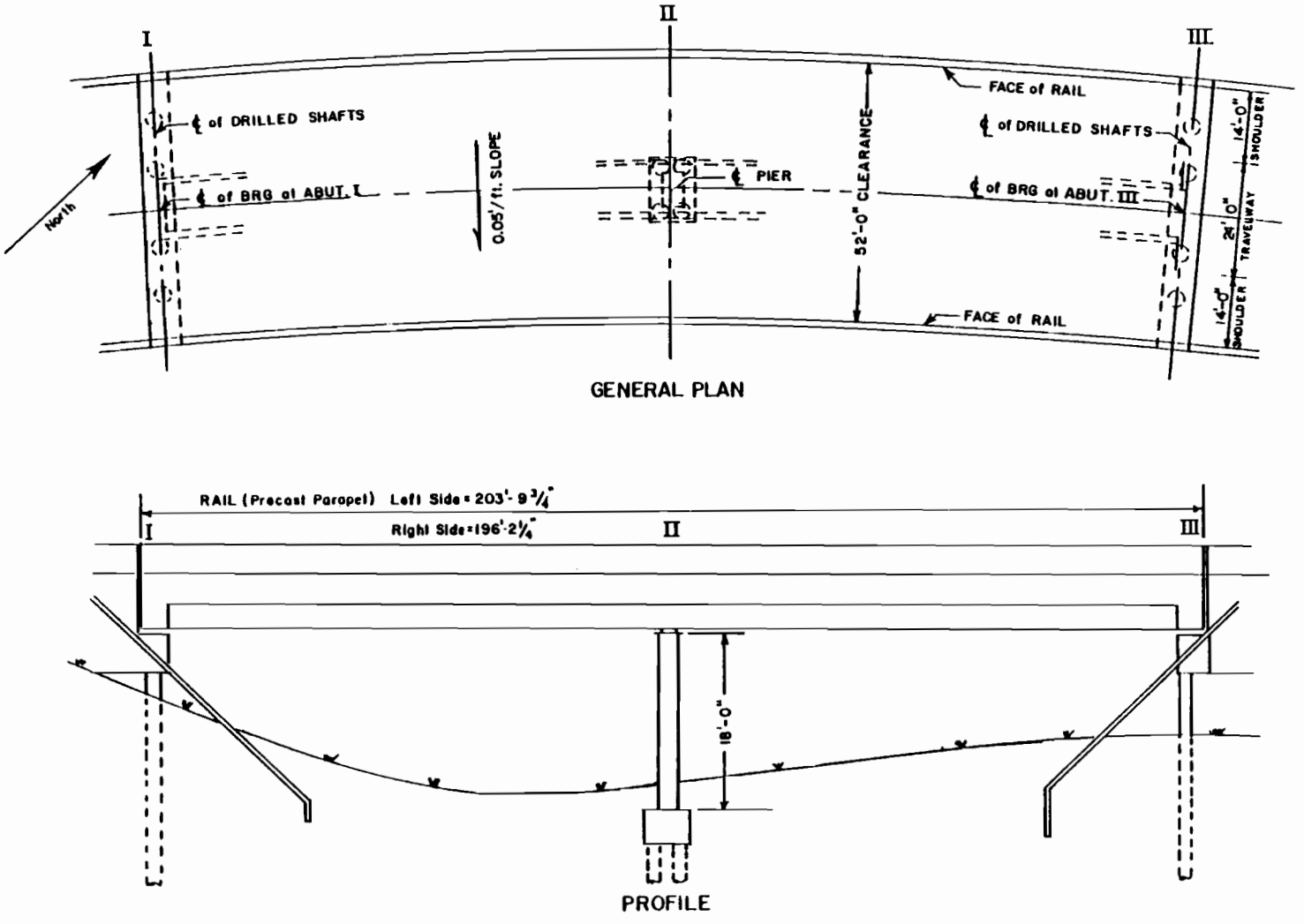

Fig. 2.1 Plan and elevation views of the bridge at Bear Creek - Travis Co., Texas

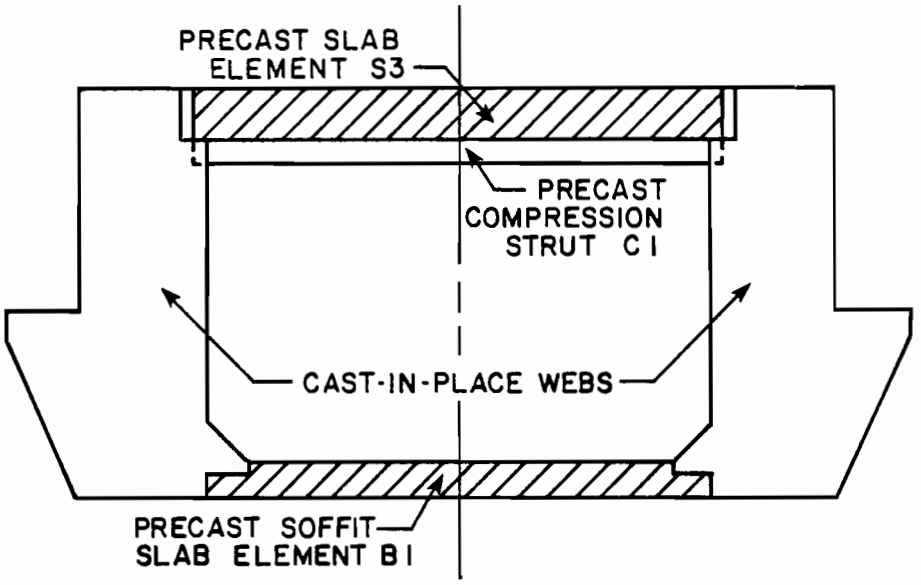

Fig. 2.2 Typical spine beam cross section prior to wing or deck placement

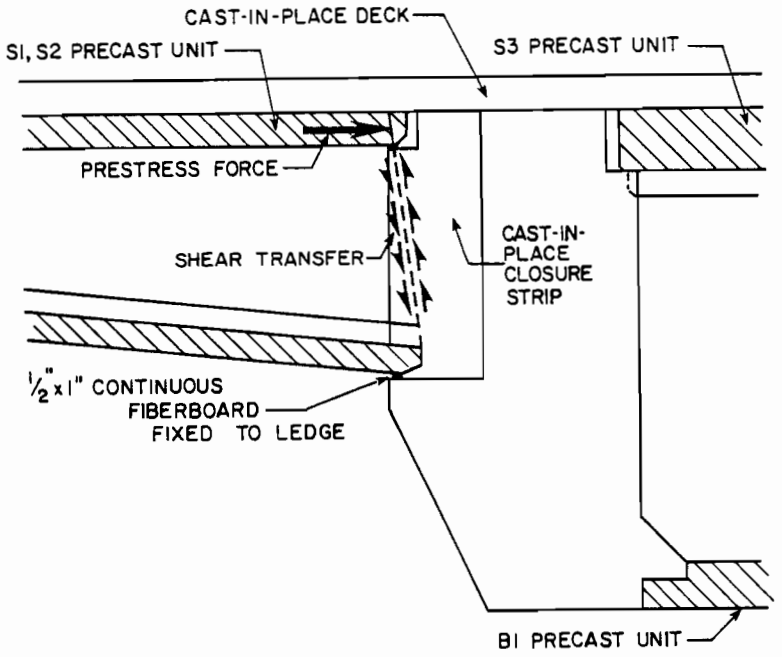

Fig. 2.3 Wing-spine connection showing clamping force due to prestress and shear transfer mechanism

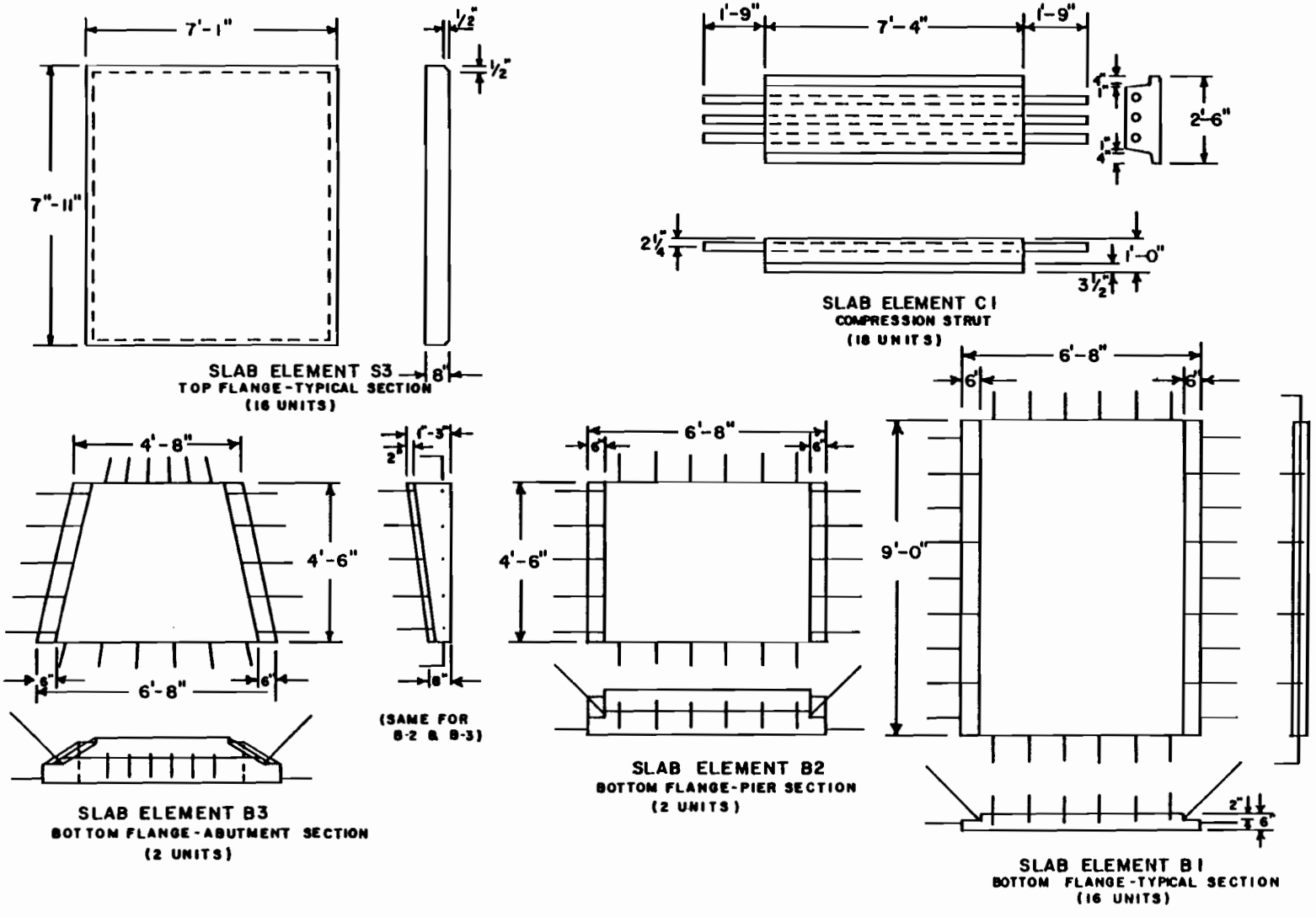

Fig. 2.4 Precast slab units with nominal dimensions

2.3, was designed to prevent the wing from bearing directly on the spine beam haunches. Thus, shear friction due to the transverse post-tensioning provides the load transfer mechanism from wing to spine beam. Precast slab panels are supported between adjacent wings by the center ribs of the wings. These panels act as permanent forms for casting the deck and allow a void to be maintained between adjacent wing ribs. Figure 2.5 shows the precast wing units and panels with their nominal dimensions.

As shown in Fig. 2.6, the bridge is made composite by a 4-in. deck and final post-tensioning in the longitudinal and transverse directions. To complete the bridge, 10-ft long precast parapet units are set in place, and a 5-ft wide solid closure strip is cast at the wing-parapet connection. A detailed set of design plans are presented in Appendix A of Ref. 2.

2.1.2 Design Specifications. The criteria used for design were the 1977 AASHTO Standard Specifications for Highway Bridges. Four lanes of AASHTO HS20-44 truck and lane loadings were applied for maximum effects with a 25% reduction in live load stresses as permitted in AASHTO Section 1.2.9. Additional loads considered included those resulting from temperature changes ranging from $-40^{\circ}F$ to $+35^{\circ}F$ and a differential support settlement of 0.1 ft.

The 4° curve at Bear Creek and the 52-ft width reflect prototype geometry needs. Support conditions at abutment I simulate the bearing conditions at a typical expansion joint for the San Antonio project. Consequently, the bridge behaves as somewhat simply-supported in

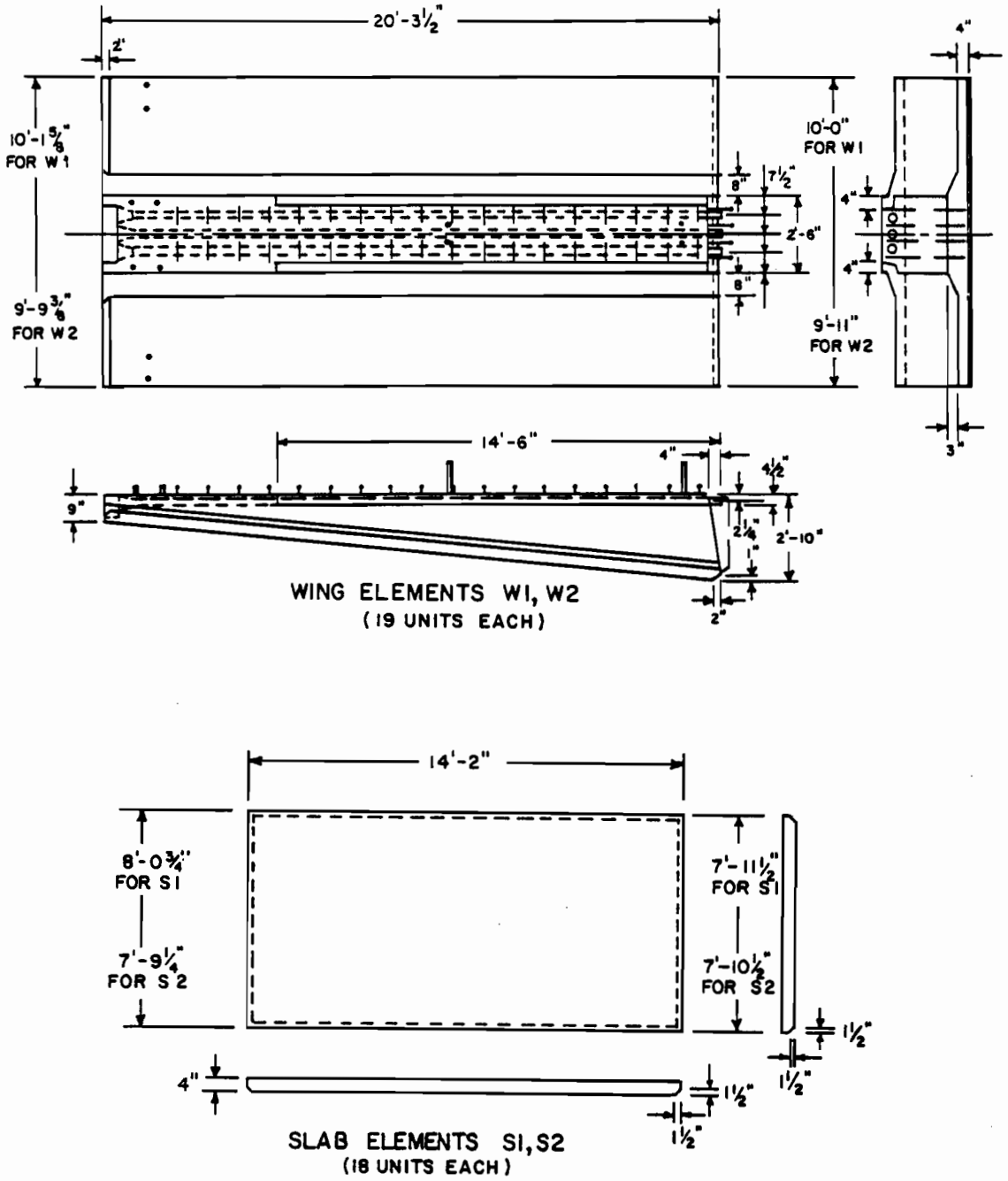

Fig. 2.5 Precast wing units and wing deck panels with nominal dimensions

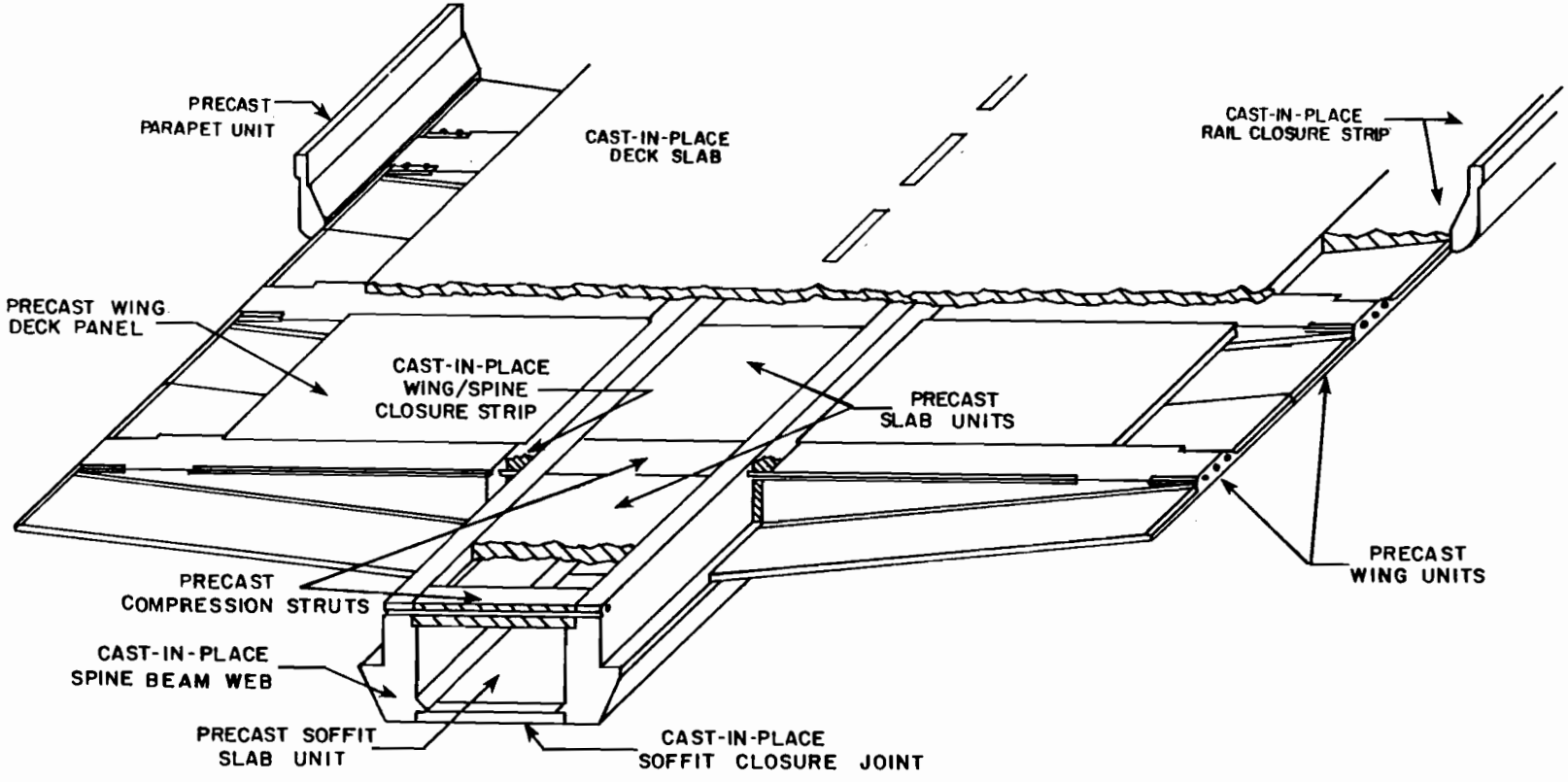

Fig. 2.6 Conceptual view showing assemblage of cast-in-place and precast construction

resisting rotation at the abutment I end. At abutment III,the support conditions more closely resemble a typical end abutment. The result is a more flexible support in the longitudinal direction with increased stiffness in regards to transverse rotation.

2.1.3 Specific Construction Requirements. To model the conditions envisioned in the San Antonio environment, construction at Bear Creek was required to advance longitudinally forward from the abutment I end of the bridge. All materials were delivered from that end, and casting and transport had to proceed forward accordingly. Although the San Antonio project calls for contractors to support the spine beam during forming operations entirely from overhead, the prototype bridge was constructed using ground shoring to minimize costs.

2.2 Materials

2.2.1 Concrete. Design calculations were based on concrete strengths of f'_c = 3500 psi at 48 hours for post-tensioning operations and f'_c = 5000 psi at 28 days for the superstructure. Actual strengths were greater than 5000 psi and most exceeded 6000 psi based on 6- x 12-in. cylinder tests. B1, C1 and S slab units had an average 7-day strength of 6200 psi while the wing and parapet units had bimodal 10-day strengths of 5900 psi and 6800 psi. Cast-in-place web concrete strengths were about 6400 psi at 28 days and 7575 psi at 231 days [2].

2.2.2 Mild Steel Reinforcement. Grade 60 steel was used for all portions of the superstructure. No verification tests were performed.

2.2.3 Post-Tensioning Steel. All post-tensioning tendons were composed of 1/2-in. diameter Grade 270 stress-relieved 7-wire strands. Wing tendons contained 7 strands per duct while the longitudinal tendons in the spine beam and abutments ranged from 31 to 36 strands per duct in number.

Transverse wing tendons were to be tensioned to 75% of ultimate and the remaining tendons to 80% of ultimate at jacking. This assumed a resultant stress of 70% would remain after seating. Long term losses were assumed to be 15% of the seating stress.

2.3 Construction Operations and Observations

2.3.1 Sequence of Construction. The sequence of construction, as shown in Fig. 2.7(a)-(i), proceeded as planned for the most part [3]. Certain stages were modified slightly, and consecutive activities overlapped where practical.

2.3.2 Precasting Operations. All the precasting was carried out at a small yard in Seguin, Texas. The B and S slab elements were cast along with the C1 compression struts in the early stages of precast operations using wood forms with a turnover rate of approximately a unit per day.

Turnover time for the wing units shown in Fig. 2.8 was slightly longer than for the slab elements due to the more involved steel arrangement and forming procedure. The P1 and P2 parapet units were cast using standard steel forms. Channel sections protruded out from the member for attachment to the wing units through bolted connections. For the S1, S2 deck panels the contractor had the option of using permanent

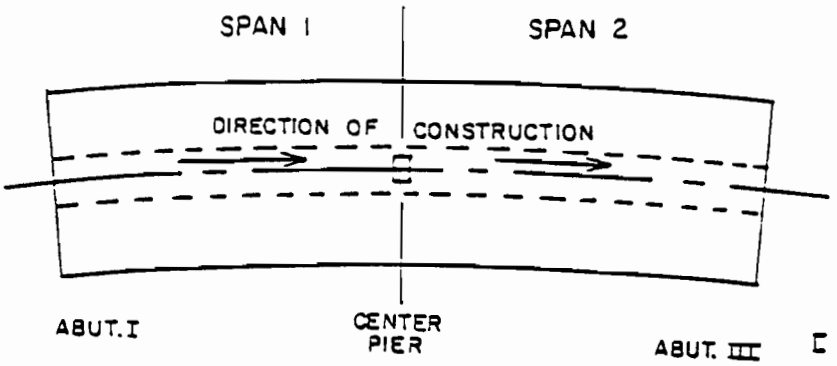

REFERENCE PLAN

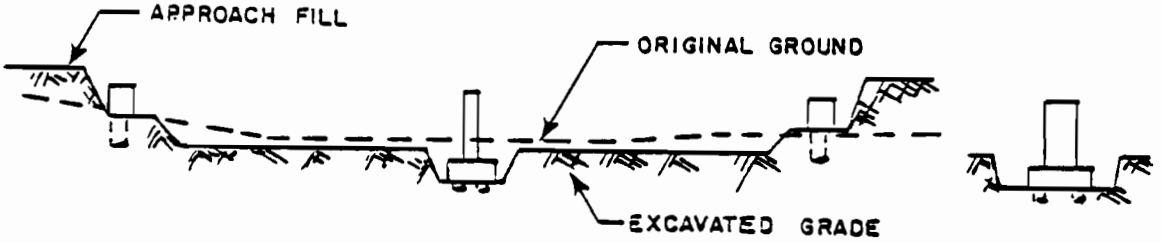

a) PHASE 1
1) Excavate to design grade
2) Construct foundation for abutment and pier
3) Construct abutment seat and central pier

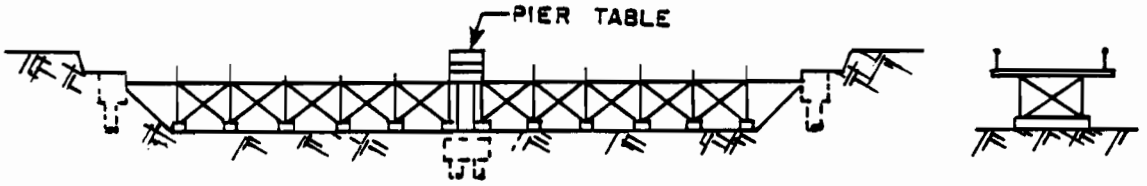

b) PHASE 2
1) Erect falsework for both spans
2) Cast pier table over center pier

Fig. 2.7 Sequence of Construction

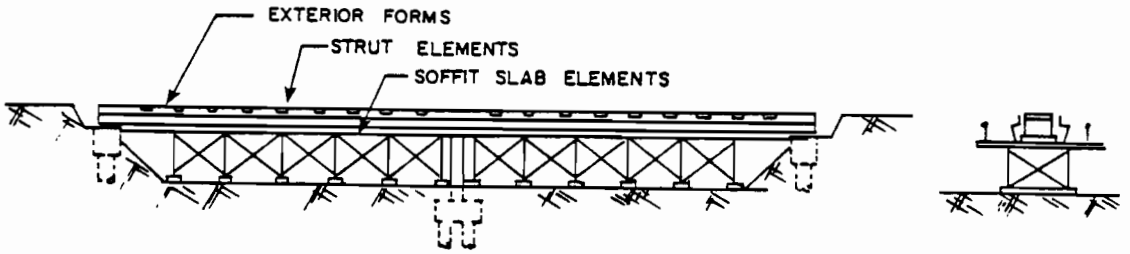

c) PHASE 3
1) Set soffit slab elements in spans 1 and 2
2) Set interior formwork and strut elements in span 1
3) Place spine beam reinforcement and ducts in span 1
4) Set exterior forms for spine beam in span 1
5) Cast soffit closures and spine beam webs in span 1

PHASE 4
1) Repeat Phase 3 above for span 2
2) Remove interior forms from spine beam in spans 1 and 2 after one day cure

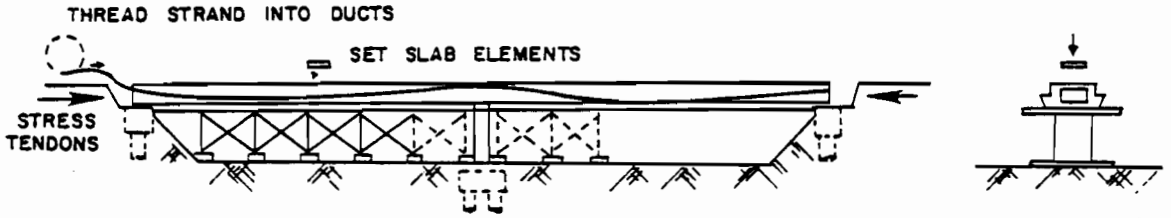

d) PHASE 5
1) Set slab elements in spans 1 and 2; grout joints
2) Thread longitudinal strand through ducts in spine and transverse strands through ducts in abutment III diaphragm beam
3) Stress tendons in diaphragm beam and longitudinal tendons after two days cure and when f'_c=3500 psi
4) Remove falsework from under spine

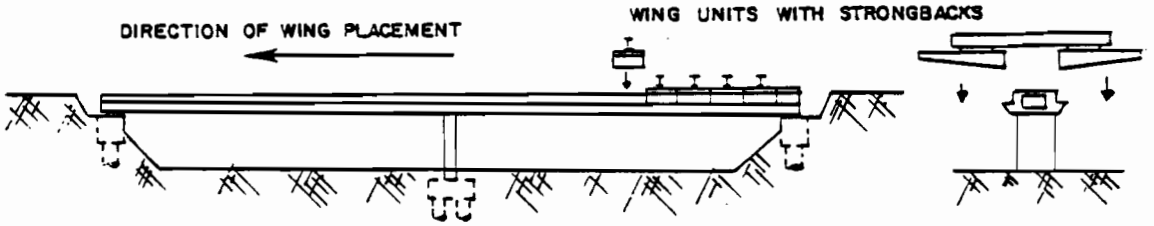

e) PHASE 6
1) Place and align wing elements with strongbacks starting at abutment III
2) Splice transverse ducts at wing-spine connection
3) Place reinforcement in wing-spine connection
4) Cast wing-spine connection after each set of five wings have been set in place

Fig. 2. 7 (cont.)

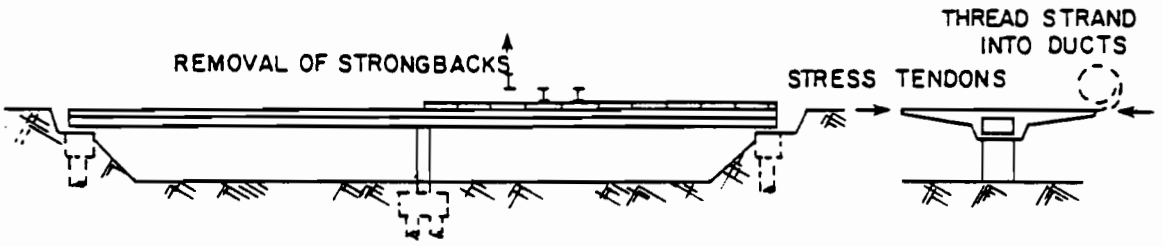

f) PHASE 7
1) Thread transverse strand through ducts
2) Stress first-stage transverse tendons for each set of five wings after two days cure and when f'_c=3500 psi
3) Remove strongbacks from post-tensioned wing units

PHASE 8 Repeat Phases 6 and 7 for the remaining sets of five wings

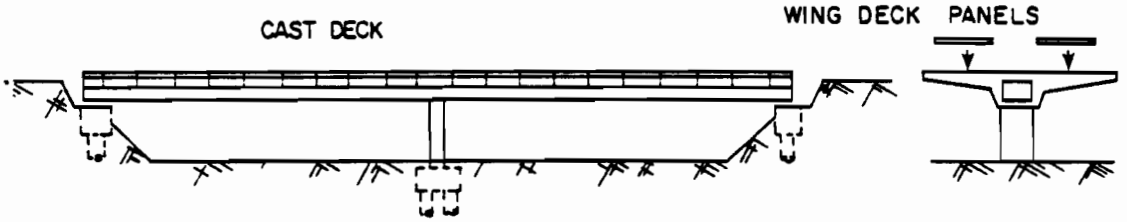

g) PHASE 9
1) Set wing deck panels in span 2; block ends
2) Set wing deck panels in span 1; block ends
3) Place deck reinforcement mat for both spans
4) Cast deck except for parapet closure strips on sides

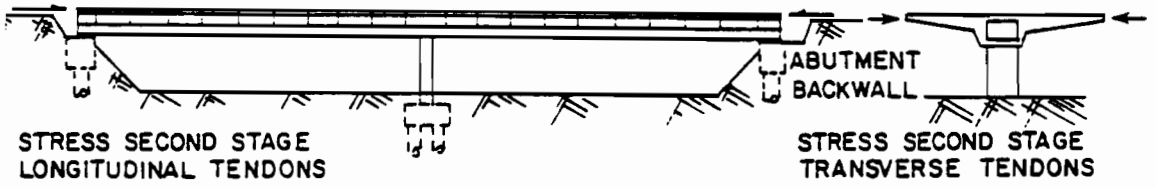

h) PHASE 10
1) Stress second-stage transverse tendons in both spans after two days cure and when f'_c=3500 psi
2) Stress transverse tendons along abutment I
3) Stress second-stage longitudinal tendons
4) Complete abutments

Fig. 2. 7 (cont.)

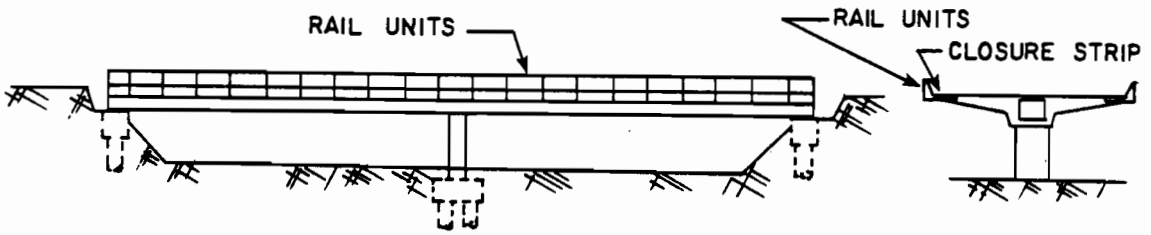

i) PHASE 11 1) Place parapet units in both spans
2) Cast parapet closure strips in both spans

Fig. 2.7 (cont.)

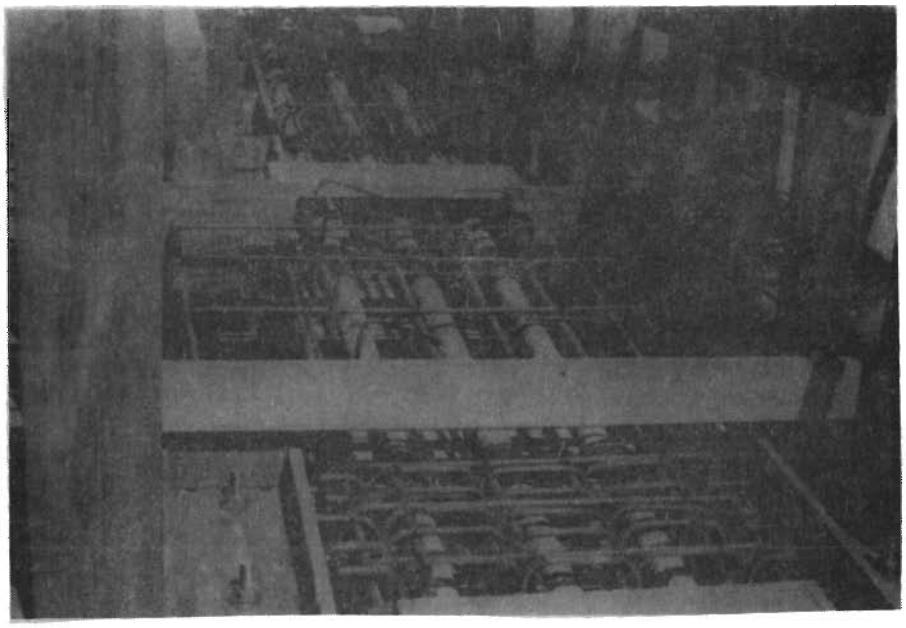

(a) Wing forms with reinforcing steel and transverse tendon ducts in place prior to casting. Post-tensioning anchorage zone is visible in background

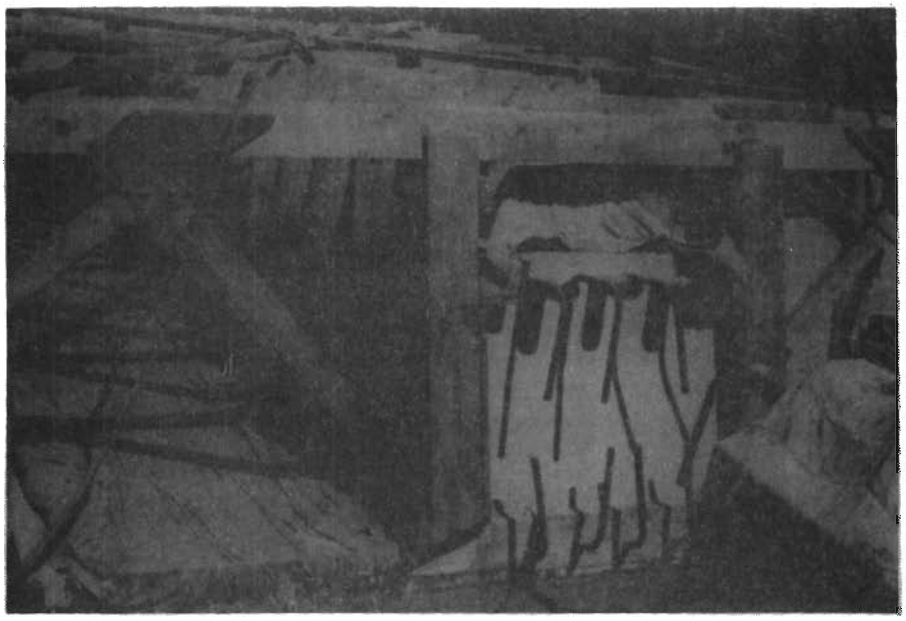

(b) Completed wing unit being cured in formwork

Fig. 2.8 Wing casting operations

metal deck forms with an additional layer of deck reinforcement or the 4-in. thick precast units as detailed earlier in Fig. 2.5. The latter option was chosen for this project.

2.3.3 Construction Stages

2.3.3.1 Erection of Center Pier and Abutments. Abutments and wing walls were supported on drilled shafts. The center pier was also supported on drilled shafts. The pier itself was 4 ft x 8 ft in cross section and 18 ft in height. Longitudinal steel extended up from the pier into the spine beam (Fig. 2.9). Once the ground shoring was in place, a solid pier cap was cast integrally with the pier reinforcement (Fig. 2.10).

2.3.3.2 Construction of Spine Beam. Once the ground-supported shoring was erected, the B1, B2 and B3 soffit slab units were set in place, as shown in Fig. 2.11. The B units had bent reinforcement bars extending out from the slab in both the longitudinal and transverse directions. These were tied together between adjacent units longitudinally and extended at a 45° angle into the cast-in-place webs in the transverse direction.

The partially completed web reinforcement cage was then set alongside the slab units, prestress ducts inserted (see Fig. 2.12), the interior spine beam forms erected, and C1 compression struts were set atop the interior forms.

The erection of the exterior forms completed forming operations in span 1 except for the transverse duct connections and reinforcement in the abutment region. The anchor blocks were positioned in the end

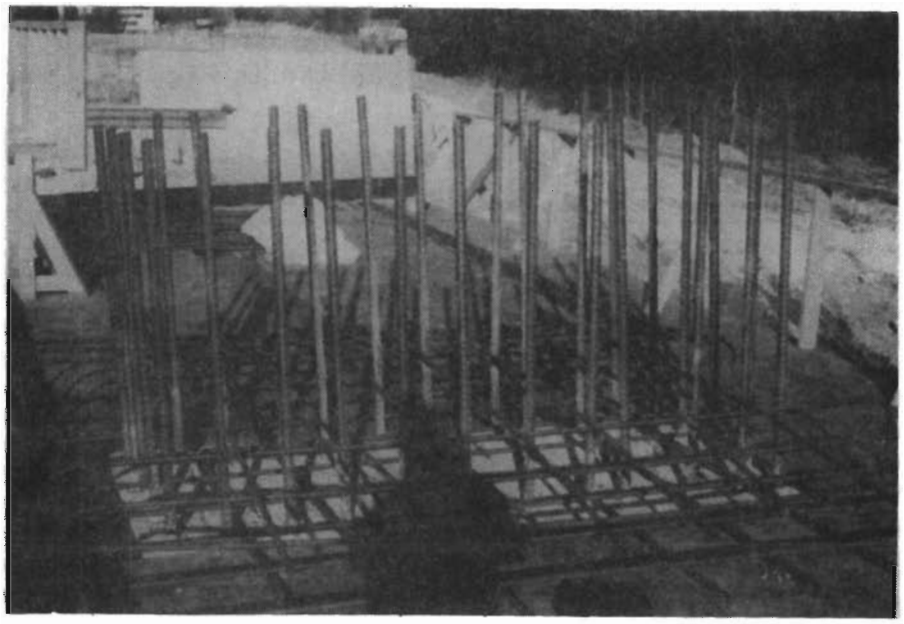

Fig. 2.9 Steel extending up from the center pier to provide continuity between the pier and the cast-in-place pier cap

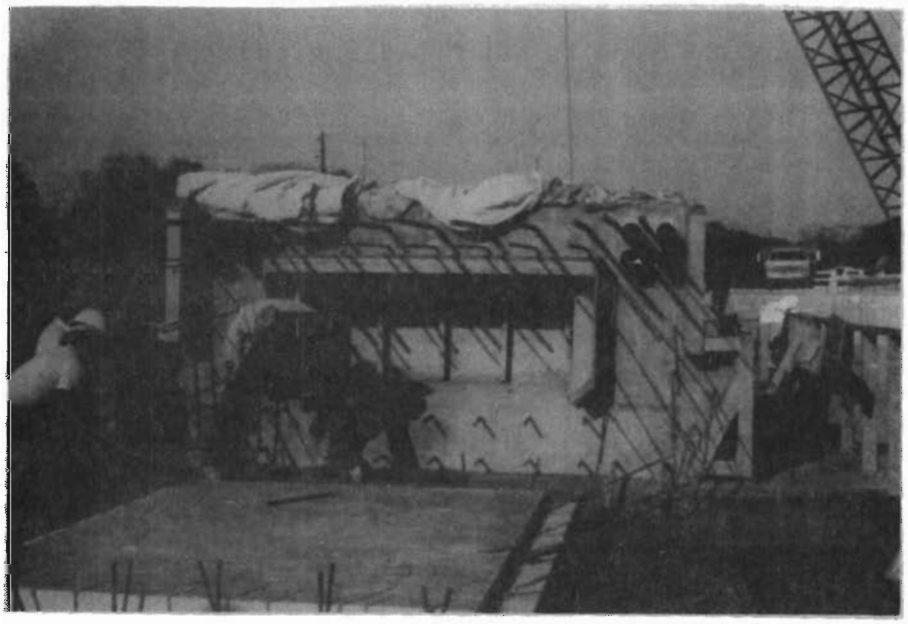

Fig. 2.10 Pier cap with portion of formwork removed

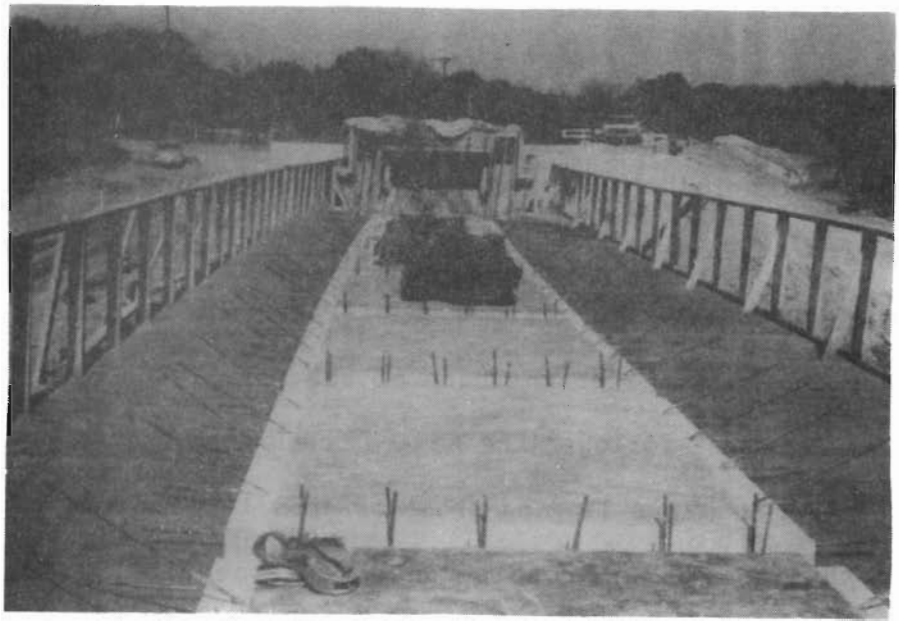

Fig. 2.11 B1 soffit slab units in place

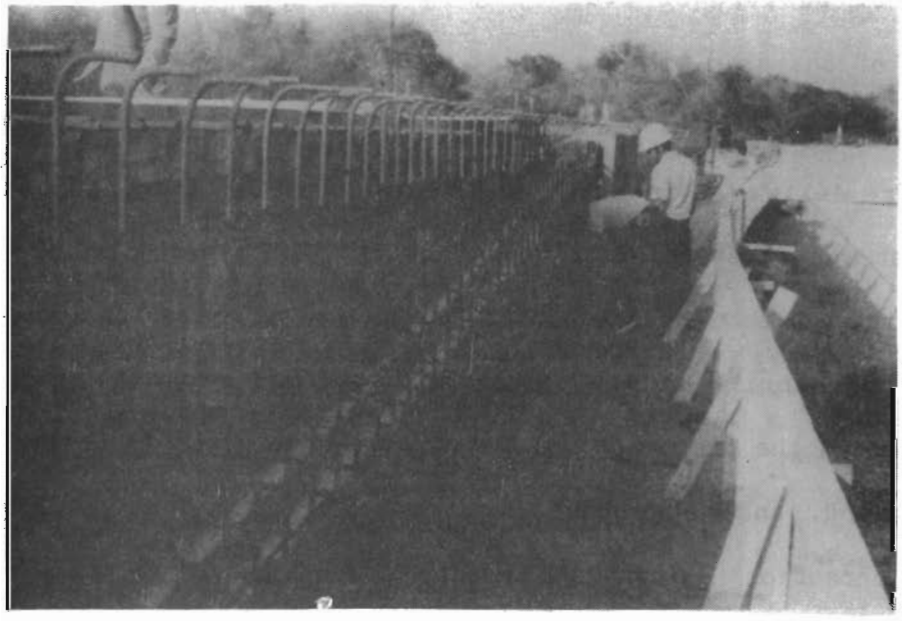

Fig. 2.12 Spine beam web reinforcement and post-tensioning ducts

region of abutment I by means of a large wooden template, and the anchorage zones and diaphragm region were heavily reinforced

Concrete was pumped from a truck located on the abutment I approachway. The interior of the spine beam was enclosed to prevent concrete from spilling over as it was pumped into the top of the forms. The closure joint between soffit elements was cast by pulling concrete in through the openings at the base of the forms. The casting of the spine beam in span 2 followed the same procedure as the first span with corresponding operations lagging those of span 1 by several days. After removing the formwork, the spine beam was essentially completed by dropping the S3 slab units in place and grouting them. First stage post-tensioning of half the longitudinal tendons and both transverse tendons in the diaphragm beam allowed the bridge to carry its own weight as well as that of additional dead weight to be added in the future upon wrecking of the shoring.

2.3.3.3 Placement and Positioning of Wing Units. The wing units were delivered from the abutment I end of the bridge and placed one set at a time starting at abutment III. The wings were supported by a strongback which was transported the length of the bridge by means of a motorized carrier developed by one of the subcontractors. Once the wings were in the proper position, they were released from the carrier, repositioned, and attached to the adjacent wing unit with a bolted channel connection. After each set of five wings was in place (see Fig. 2.13), a 1-ft wide closure strip was cast between the wing and spine beam web. The center tendon in each of the five wings was then post-

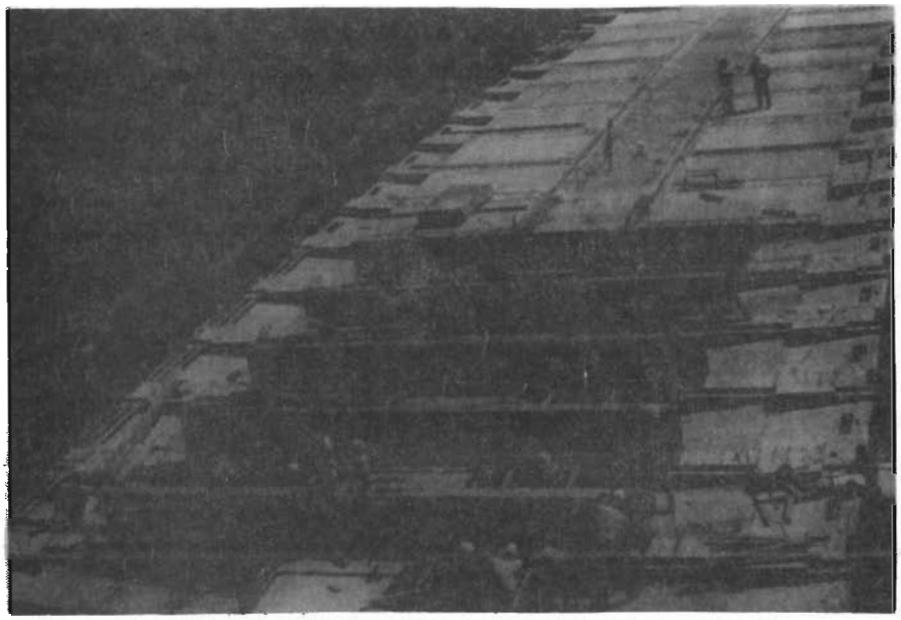

Fig. 2.13 Overview of wing placement operation

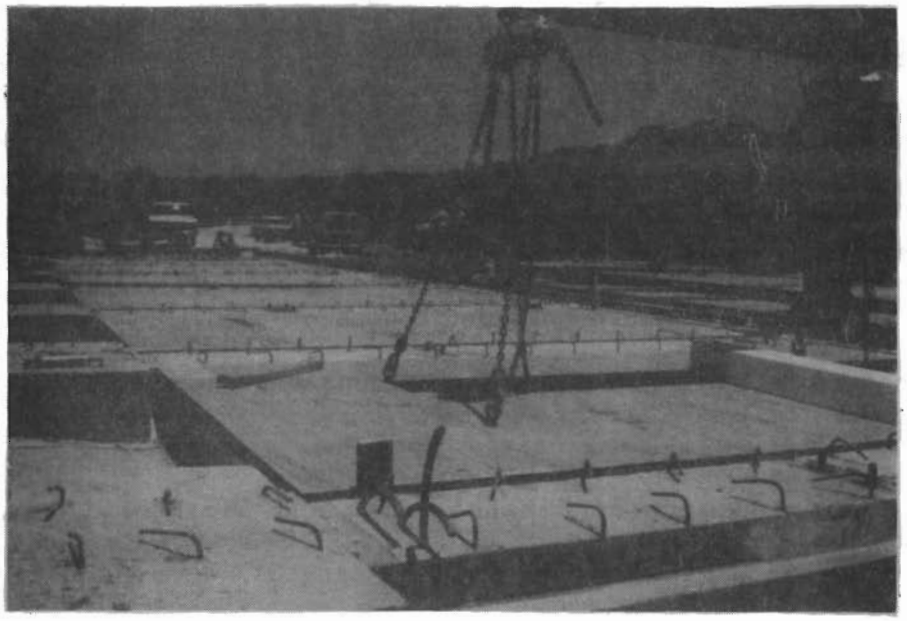

Fig. 2.14 S1,S2 deck panel being set in place

tensioned after two days' cure when a minimum closure strength of 3500 psi was achieved. The strongbacks were removed, and the process was repeated until all twenty wings were set and post-tensioned.

With the partially post-tensioned wings carrying their own weight, the S1 and S2 panels were dropped into place between adjacent wing units (Fig. 2.14). The panels were supported on foam strips by the wing ribs on two sides and the spine beam on a third. The edge nearest the wing tip had previously been blocked off with styrofoam to create a void underneath the panels. These panels were not grouted prior to casting the deck.

2.3.3.4 Deck Placement. The deck slab was placed by pumping the concrete from the abutment I approachway. The entire deck was cast at one time with the exception of 5-ft wide strips on either side along the wing tips which were cast after the parapet units had been bolted in place.

After the deck concrete strength reached 3500 psi, second stage post-tensioning was performed. This included the four remaining longitudinal tendons, the two outside tendons on each wing, and the five transverse tendons at abutment I. The tendons were then grouted and the remainder of the backwall was cast at each end.

2.3.3.5 Placement of Parapet Units and Closure Strips. The parapet units, which were precast in 10-ft lengths, were attached to the center rib of each wing by bolting two channel sections anchored in the parapet to an inset on the wing tip. Closure strips were cast to complete the superstructure.

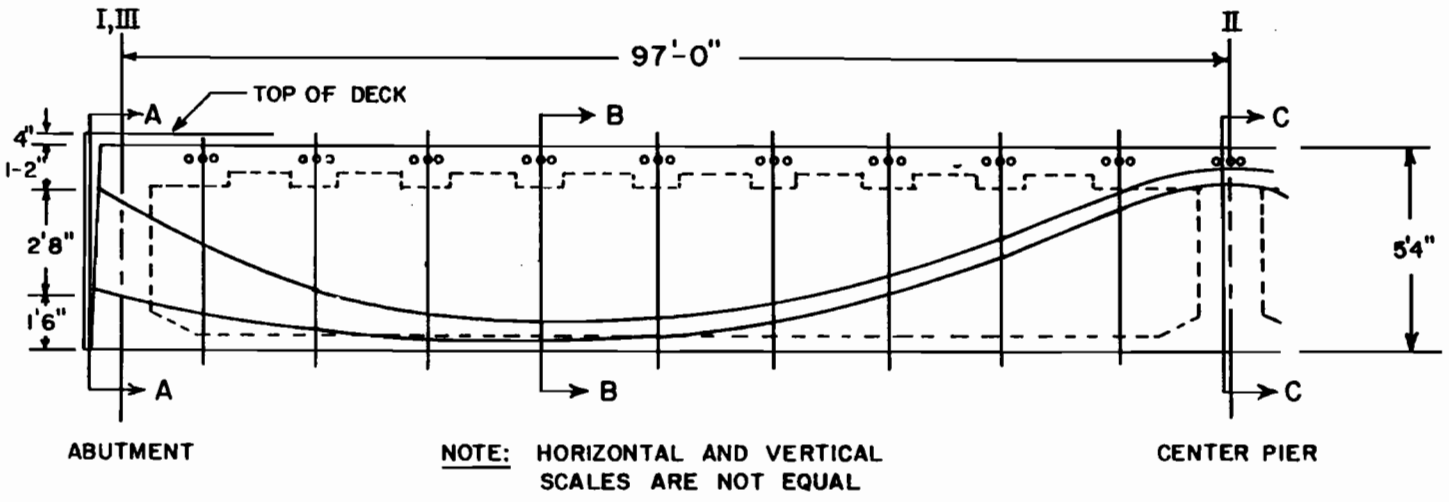

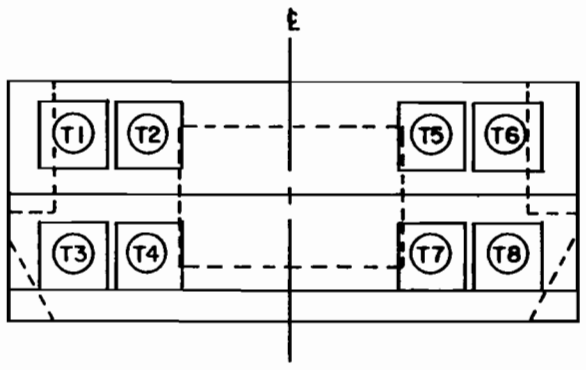

SECTION A-A
END ABUTMENT DETAIL

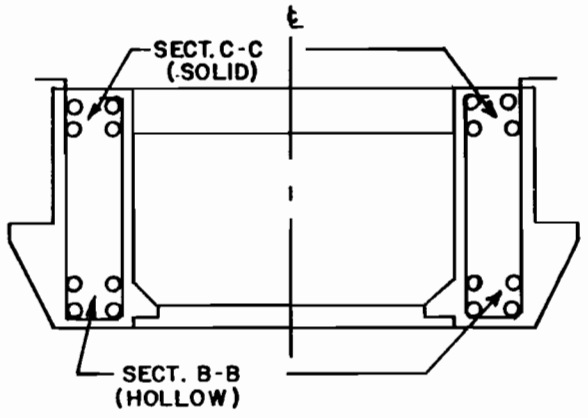

SECTIONS B-B, C-C

Fig. 2.15 Arrangement of longitudinal prestressing tendons

2.3.3.6 Post-Tensioning Operations. Longitudinal and transverse post-tensioning operations were each carried out in two separate stages. The longitudinal tendon arrangement consisted of eight sets of tendons in two separate parabolic drapes as shown in Fig. 2.15. The final configuration consisted of 34 strands in each of tendons T1, T6, T3, and T8; 35 strands in each of tendons T4 and T7; and 36 strands in each of T2 and T5.

The transverse prestressing in the wing units consisted of three tendons with seven 1/2-in. strands each. The exception was the cast-in-place wing unit at abutment I which contained five sets of seven strands. The three-tendon wings were stressed in two stages while the latter was stressed entirely after placement of the deck.

The longitudinal tendons in the spine beam were originally to be stressed to approximately 80% of their ultimate strength at jacking. The actual forces measured after seating were as follows: tendons T1 and T6--1770 kips total; tendons T3 and T8--1820 kips total; tendons T2, T4, T5 and T7--3620 kips total. The transverse wing tendons were stressed to 75% of ultimate at jacking. Long-term losses were assumed to be 15% of the stresses immediately after seating.

The sequence and order of stressing was as follows:

1. First stage longitudinal
   - Transverse beam at abutment III; order at contractor's option
   - Half of longitudinal tendons in the following order: T1, T8, T6, T3

2. First stage transverse

   - Stress middle tendon in each wing from abutment III end to abutment I end

3. Second stage transverse

   - Stress remaining outer two tendons in wings; order at contractor's option

   - Stress all transverse tendons along axis I

4. Second stage longitudinal

   - Stress remaining longitudinal tendons, T2, T4, T5 and T7; order at contractor's option

All conduits were to be grouted not later than one month after completion of the tensioning operation for that respective tendon.

2.3.3.7 Problems During Construction. As is generally the case with any type of structure incorporating novel design concepts and construction techniques, certain difficulties and shortcomings arose during the construction of the Bear Creek bridge. These problem areas will be documented in this section with the ultimate aim of facilitating and improving the construction of similar projects in the future. A list of recommendations will be presented in Chapter 5 to help minimize further occurrence of these events in general and to specifically improve the constructability of this type of wing-girder structure.

The problems encountered during the Bear Creek project can be attributed to both errors in construction and deficiencies in detailing. Errors in construction generally involved post-tensioning operations, while inadequate detailing led to problems in the constructability of the bridge as designed.

Most of the problems in detailing were the result of congestion in the spine beam web. The web itself was 1'-8" wide with #6 stirrups and 1-1/2 in. clear cover. Through the center of each web ran four 4-in. diameter post-tensioning ducts. These ducts were arranged in two rows and were draped from a position near the top of the web at the center pier and at each abutment to a position at the bottom of the web near midspan. This can be seen in the profile and cross-sectional views in Fig. 2.15. Near the center pier additional longitudinal reinforcement caused considerable difficulty in coupling the post-tensioning ducts. Some of the bars had to be shifted to accommodate the ducts, since the design drawings had both occupying the same space in the cross section. Also, near the abutment ends of the bridge, additional shear and bursting reinforcement made it impossible to properly position the ducts and anchorage hardware without moving or cutting several reinforcement bars. Besides requiring field changes in effective steel areas and placement, the congestion made proper concrete placement nearly impossible because the minimal clearance available between the post-tensioning ducts and the reinforcing steel at the center pier.

The web cross section in Fig. 2.16 shows the position of the tendon ducts at the pier section (top of web) and near midspan (bottom of web). In going from one configuration to the other along the length of the spine beam, it is inevitable that at some point the ducts must pass through the horizontal legs of the stirrups near middepth of the web. The design drawings did not indicate this clearly although careful

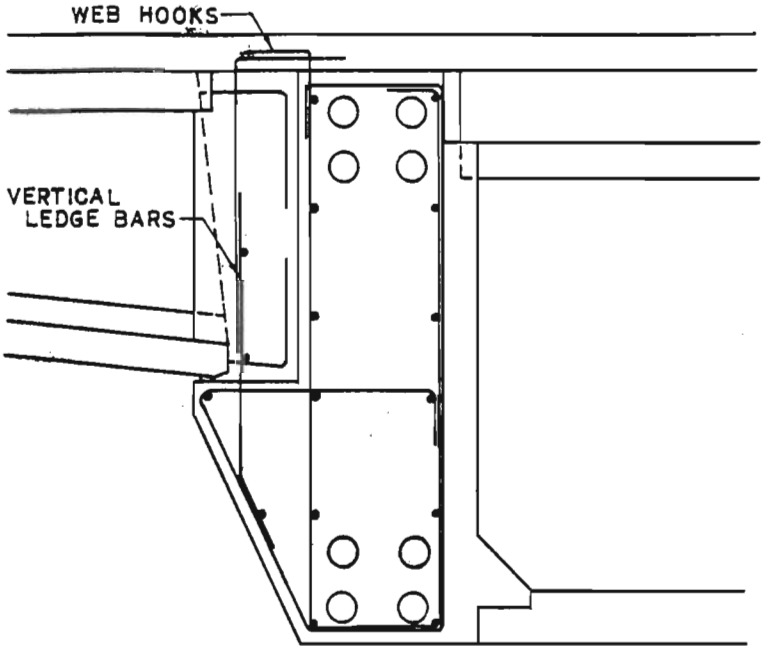

Fig. 2.16 Prestress duct arrangement in spine webs as presented in working drawings

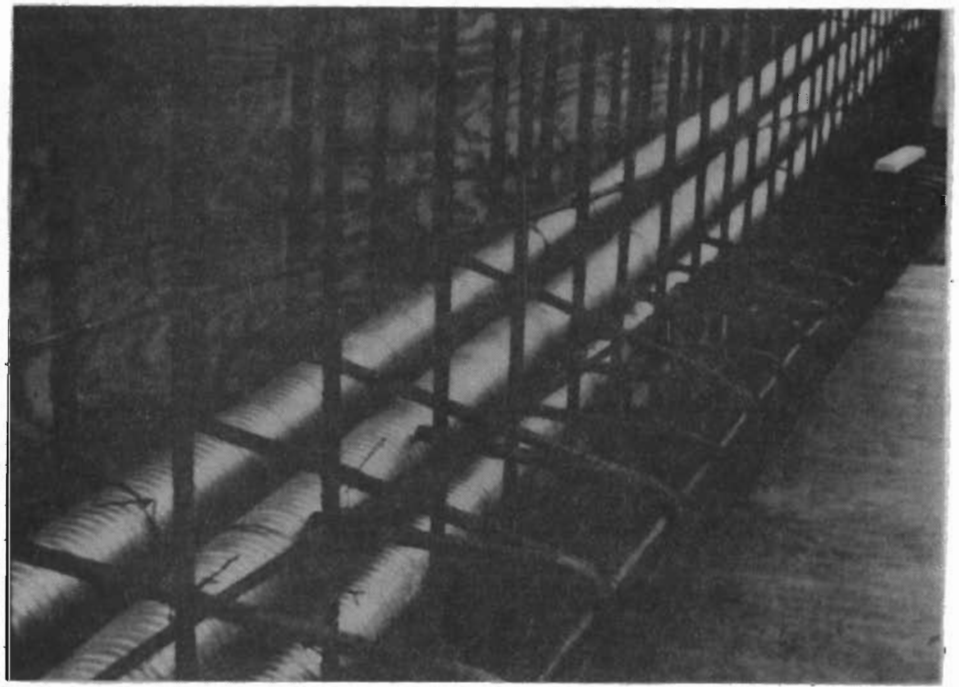

Fig. 2.17 Location where stirrup bars had to be cut and then wired back in place to accommodate drape of web tendon ducts

study would show this to be the case. This was not realized in the working drawing stages, because conventional reinforcement and post tensioning details were not handled in common. All web reinforcement was fabricated as shown on the design drawings and bar schedules and was placed prior to inserting the ducts. Consequently, it was necessary for the contractor to burn off sections of large numbers of the horizontal bars at this intersection. New bars were then lap spliced on to the existing bars to accommodate the tendons as shown in Fig. 2.17. This is not good engineering practice. The designers should make sure the design is constructable as drawn or at least make provision for acceptable means of handling any inconsistencies. Shop drawings which show both nonprestressed and prestressed reinforcement on the same sheets should be specifically required.

This inattentiveness to detail is shown again in Fig. 2.18 where the wing reinforcement was incompatible with the transverse tendon ducts and couplers. Field changes were required to enable placement. Another detail which is not particularly desirable from a serviceability point of view is the deck reinforcement cutoff locations shown in Fig. 2.19. The #10 bars over the first 25 ft of span from each abutment were cut off right at the S1,S2 panel edges. Since any sharp change in geometry results in areas of stress concentration and is a prime candidate for formation of future cracks, it would be advisable to extend the bars into the closure area a short distance. The cutoff locations should be staggered so that such an abrupt change does not take place.

Fig. 2.18 Difficult arrangement of reinforcement and transverse ducts in coupling region of wing-spine closure strip

Fig. 2.19 Deck reinforcement cutoff detail over precast panels

The wing placement operation went fairly smoothly once the contractor's crew had gained some learning experience from the first few units placed. There was, however, one set of details which caused considerable hindrance throughout the duration of wing placement operations. The 6-in. hooks extending into the deck from the top surface of the web and the vertical bars extending from the spine beam wing ledge into the closure strip (shown in Fig. 2.16) made transport and positioning of the wings rather difficult. The contractor was concerned over the stability of the units during the period in which they were being moved out along the span and wished to carry them in a position which straddled the spine beam. The designer had envisioned that they would be transported horizontally at a much higher elevation and then lowered into position. Details of reinforcement were selected with this option in mind but were not changed when the contractor's lower travel position was chosen. Figure 2.20 shows the first wing unit placed at abutment III. The web hooks can be seen clearly along the top of the spine beam. The ledge vertical bars have been bent to allow clearance for the wings. The ledge bars made it difficult to carry the wings in a straddle position along the ledge while the top bars prevented the contractor from carrying the wings at a higher level unless they were carried completely above the spine. Misalignment between the first two wing units resulted from clearance problems between the wing and spine beam. In addition to causing wing placement problems, both sets of bars were a nuisance during wrecking of the spine beam forms.

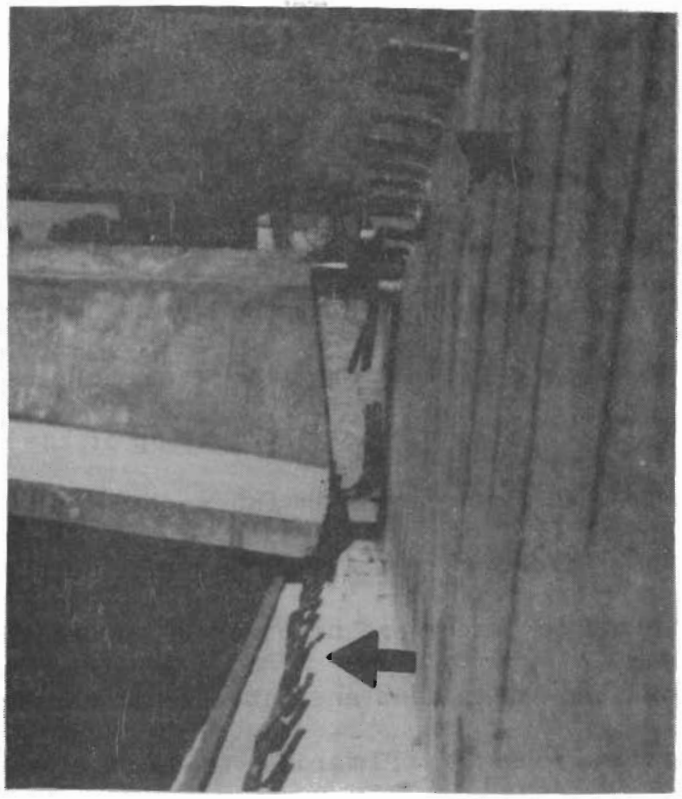

Fig. 2.20 Wing unit in place at abutment III; web hooks at the deck level and vertical closure bars protruding from the wing ledge are clearly visible (arrows)

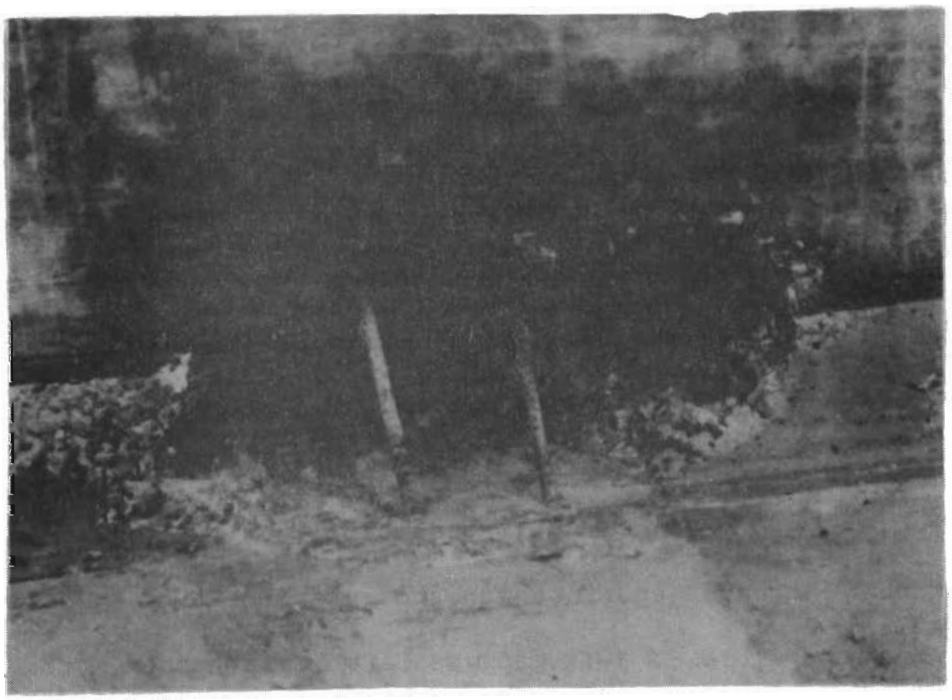

Fig. 2.21 Void at soffit panel closure joint formed during casting of the spine beam webs

The awkward arrangement of the external spine beam reinforcement cited above did not present a major deterrent to completion of the bridge. However, the inconveniences caused were totally unnecessary in light of the purpose the protruding bars were meant to serve. The quantity of steel and number of hooks at the top of the spine beam are probably not enough to effectuate shear interaction between the spine beam and deck. The hooks as detailed are much too short to provide effective development for anchorage or bar splice purposes. It appears that the web hooks and ledge bars are intended to confine the closure strip. They probably serve primarily to hold the minimum area longitudinal closure steel in place. A more efficient means of handling the closure steel should be devised. A system of threaded connector bars could possibly be used to splice the bars after the wings are positioned.

The construction operation itself went as planned for the most part. The completion time was considerably longer than originally anticipated, but some delay would generally be expected when new and unfamiliar methods of construction are involved. The substantial amount of in-place reinforcement placement and the limited work space and access caused substantial delays. One of the few problems that did arise during onsite casting involved the B1 soffit closure joints near the web in span 1. With the B1 units positioned on the formwork, the web reinforcement cages and interior and exterior forms were set in place along either side. A 1-ft gap was left between the bottom slab units. This was to be cast integrally with the spine beam webs. The

spine beam was cast in three lifts, and the closure joint was filled by concrete flowing down through the bottom of the spine beam forms. While placing the second lift in span 1, the contractor's crew revibrated the 1-ft closure joint between bottom slab units which had recently been cast with the first lift. This caused more concrete to flow under the forms at the closure joints and resulted in large voids on the superelevated side of the bridge as shown in Fig. 2.21. These voids were grouted up in span 1, and the contractor was successful in preventing a similar occurrence in span 2 by exercising caution when vibrating near the closure joints.

The only other significant problems during construction involved post-tensioning operations. These were the result of using either improper equipment or using the proper equipment incorrectly. When stressing the transverse diaphragm beam at abutment III, the post-tensioning jack was not centered correctly on the bearing surface. Several of the strands sheared off before reaching the design prestress level. The tendons had to be destressed, and the damaged strands were removed and replaced.

For transverse wing stressing operations, an oversized jack was used throughout construction. The jack pressed against the 2-in. thick ledge at the base of the stressing pocket and cracked the ledge in a majority of the wing units. Some of the ledges were broken off completely. Although the cracked ledges did not affect the bridge structurally, they nevertheless had to be repaired. Thus, a reasonable effort should be made to prevent their occurrence.

Overall, construction proceeded without serious incident. A major concern of the authors is the speed at which successive spans can be erected in a large-scale project if so many field placement operations are required. In particular, the construction of the spine beam webs in situ appears to be very time consuming.

This section dealt mainly with problems in the present scheme of construction and proposed only minor recommendations for improvement. Other matters of concern regarding the performance of the structure, such as observed cracking, etc., will be discussed in Chapter 4. Chapter 5 makes recommendations for improving the present design and expediting construction as well as recommendations of a more general nature.

CHAPTER 3

INSTRUMENTATION AND TESTING

3.1 General

The evaluation program was broken up into two separate phases. The first phase involved the observation of behavior of the bridge during construction. Measurement of elevations at critical stages of construction was carried out by the Texas State Department of Highways and Public Transportation resident engineering staff. Internal and external surface strains and temperature gradients during this phase were measured by staff from the Ferguson Structural Engineering Laboratory. The second phase was aimed at evaluating the performance of the completed bridge structure under service level loads. In addition to the above-mentioned measurements, relative slip characteristics between elements, changes in longitudinal and transverse slopes, and transverse spine beam diagonal distortions were also monitored.

3.2 Installation and Locations of Instrumentation

3.2.1 Deflections. Elevations were measured during both phases using an automatic level and rod. During construction, readings were made to 1/100 of a foot at 10 ft or 20 ft intervals along the bridge at the wing tips and over the center of each spine beam web. During the service load tests, a vernier was used to increase the accuracy of these readings. Figure 3.1 shows the rod locations for vertical deflection measurements.

3.2.2 Longitudinal Strains. Longitudinal surface strains were measured using a mechanical strain gage with an 8-in. gage length at six cross-sectional locations along the length of the bridge, as shown in Fig. 3.1. Two sections corresponded to the expected regions of maximum positive and negative moment, respectively.

Gage points were positioned as shown in Fig. 3.2 to allow determination of the strain distribution on both sides of the spine beam.

An initial set of readings was taken upon completion of casting of the spine beam and prior to first-stage post-tensioning, and all subsequent readings were referenced back to it. Readings were taken at each major construction phase.

The only problems encountered in using the Demec gage were with the internal surface gage points in span 1 which fell off due to a combination of poor epoxy and high humidity. The points were replaced and performed satisfactorily as noted in the results section. The external gage points were utilized only during initial stages of construction. The removal of the shoring and addition of the wings precluded their use at later times.

3.2.3 Temperature Distributions. Internal temperature measurements were made using an electronic thermocouple device in conjunction with a multiple switching unit. The thermocouple probes were iron-constantine wires which were exposed and placed in contact with each other at the location where temperature was to be measured.

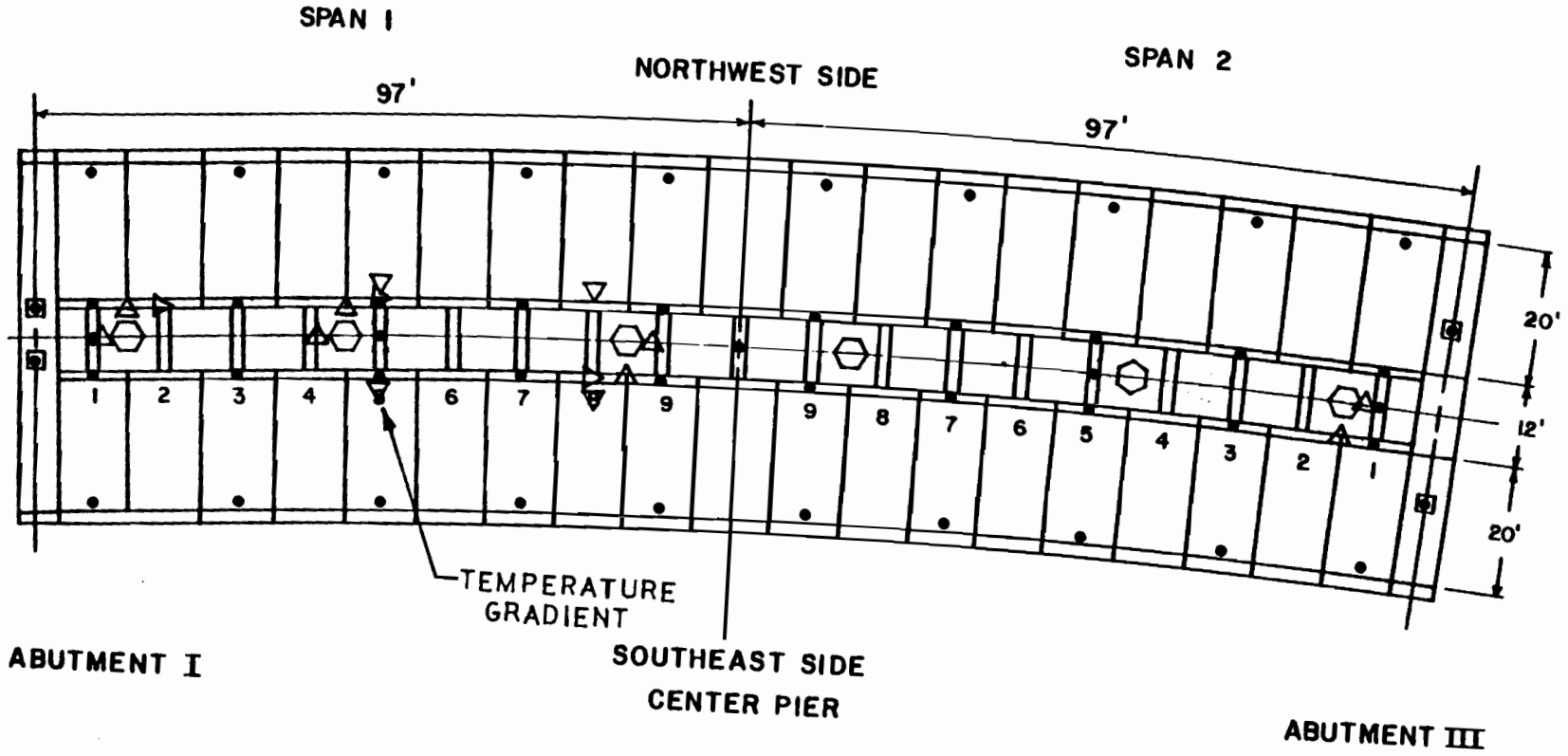

Fig. 3.1 Location of vertical deflection, temperature gradient, slip, and longitudinal strain measurements

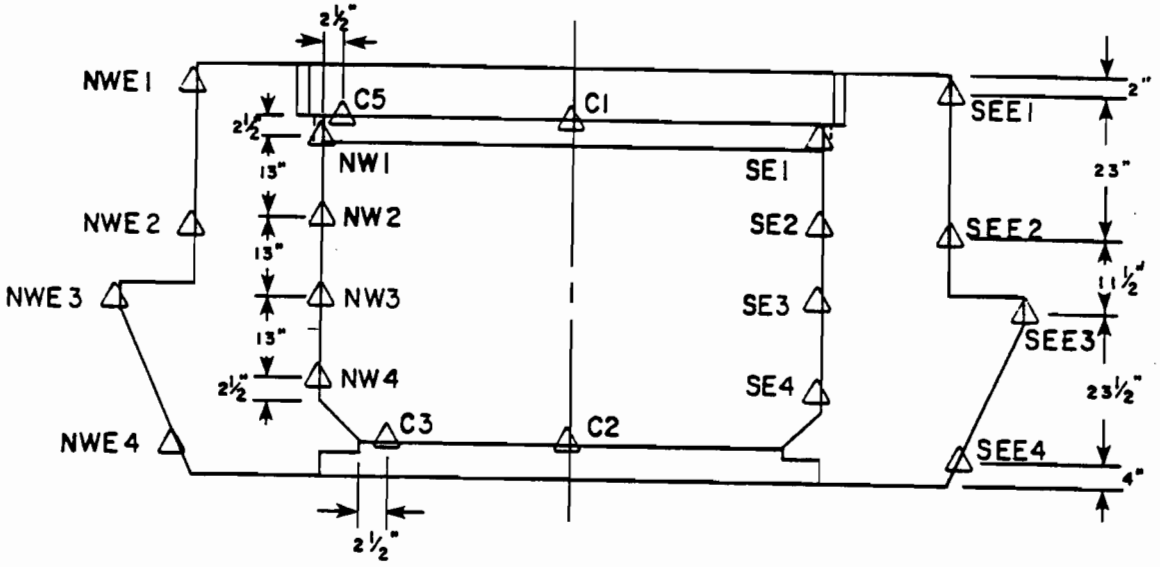

Fig. 3.2 Arrangement of strain points over cross section

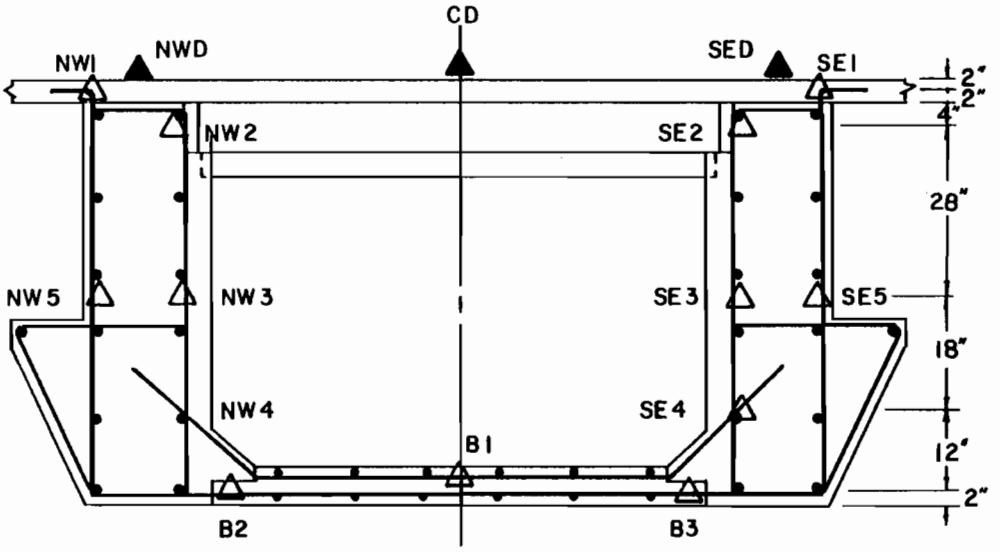

△ ELECTRONIC THERMOCOUPLE

▲ SURFACE THERMOMETER

Fig. 3.3 Distribution of thermocouple probes over the spine beam cross section

The differential resistance change could then be transformed into temperature and displayed directly on an LED readout.

Temperature instrumentation was installed at the station shown in Fig. 3.1 around the cross section, as shown in Fig. 3.3. The probes were tied into the reinforcement cage and insulated from the reinforcement with rubber to represent the heat flow characteristics of the concrete. Readings were taken during construction and during service load tests. Ambient temperatures and surface temperatures (Fig. 3.3) were also measured during the service load tests.

3.2.4 Measurement of Slip. The composite wing girder design and the loose-fit concept use drop-in panels held in place by prestressing and transmitting loads across construction joints by shear friction with no reinforcing steel to prevent the opening of cracks along the joints or to resist sliding along these surfaces. To measure any slip which might occur, the sections shown in Fig. 3.1 were equipped with slip gages. These sections corresponded to regions of high torsional stresses with the exception of section 5 in span 1 used for comparison. At each section slip was measured on three surfaces, as shown in Fig. 3.4. In addition, sections 5 and 8 in span 1 were instrumented for slip at the wing-wing closure strip joint.

The instrumentation scheme used is shown in Fig. 3.5 and was a modification of methods used to measure the slip of anchor bolts embedded in concrete. Steel plates were cast into the B1, C1, and W units flush with the surface at which slip was to be measured. Each plate had three small holes drilled in it. These holes corresponded to

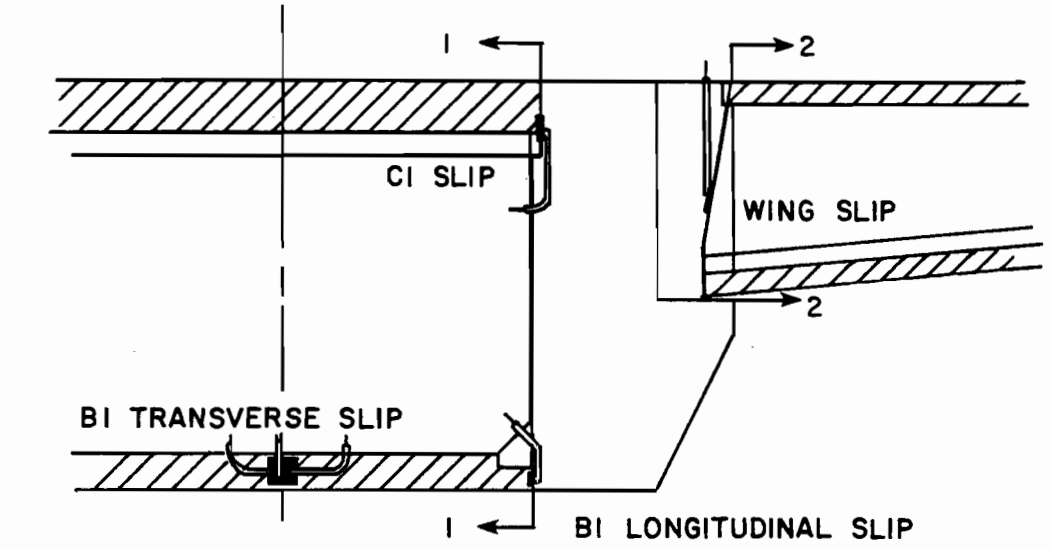

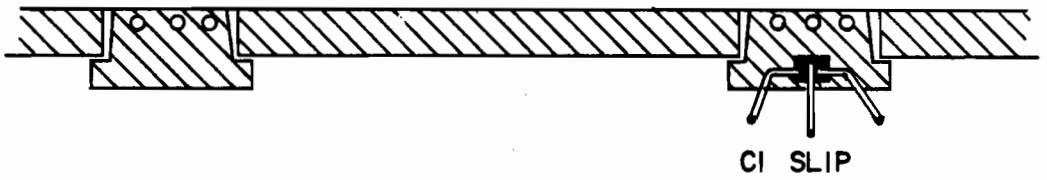

INTERIOR SURFACE OF
SPINE BEAM WEB

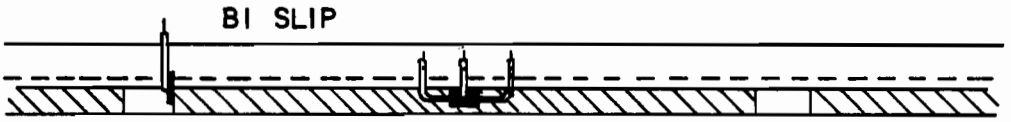

SECTION 1-1

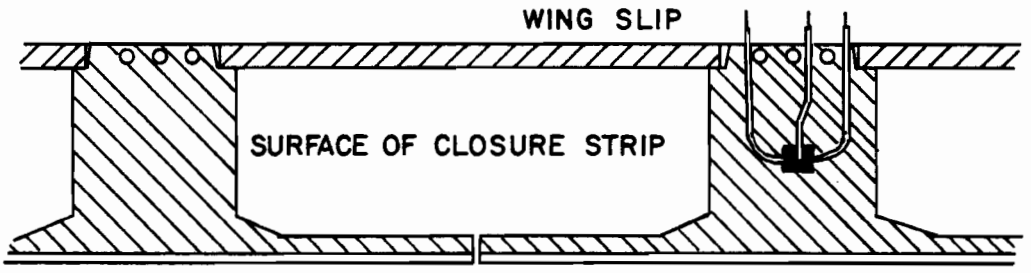

SECTION 2-2

Fig. 3.4 Location of slip measuring devices on instrumented sections

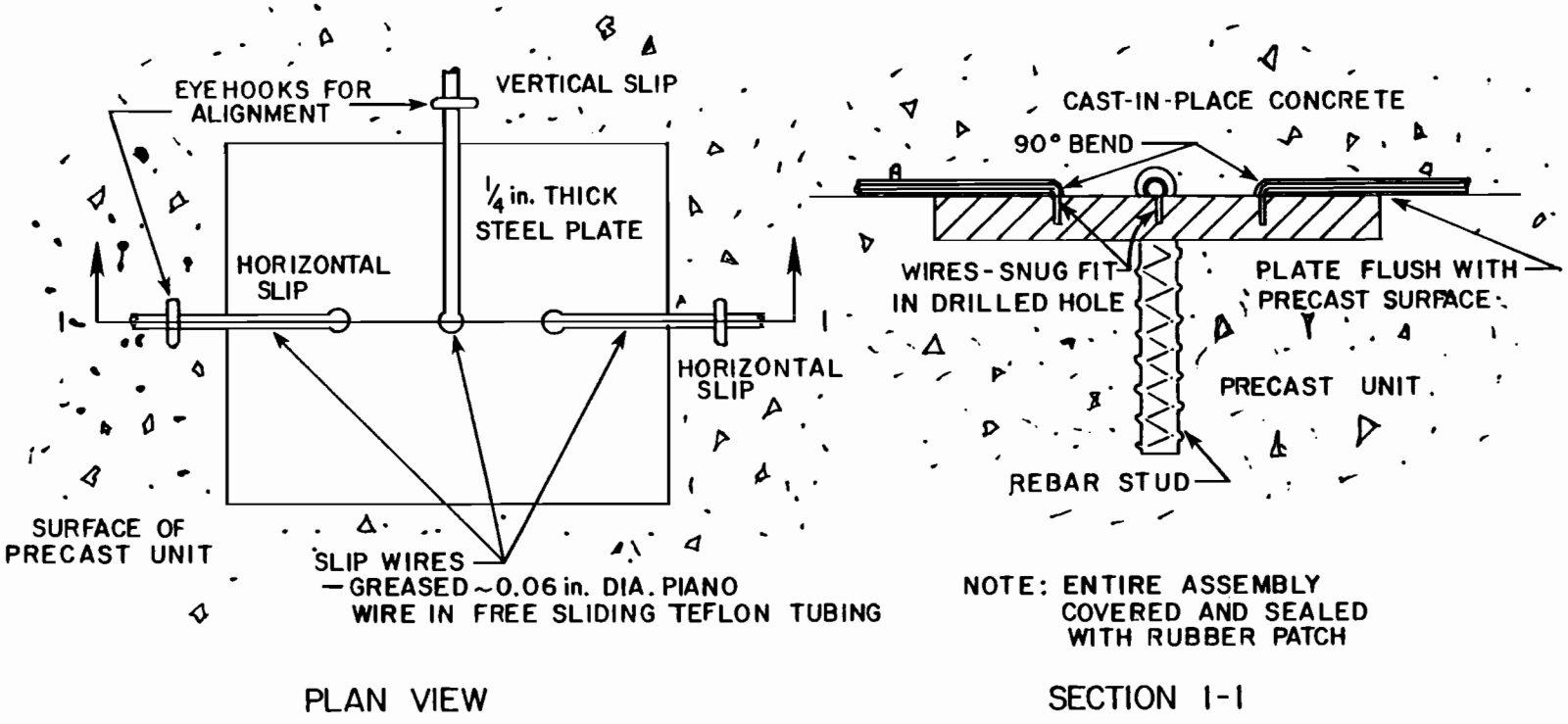

Fig. 3.5 Plate-wire assembly for measuring slip

movement in the vertical direction and in each direction horizontally. Once the instrumentation units were set in place and prior to casting the spine beam webs and closure joints, a stiff wire was attached to the steel plates and fixed in place. A 90^{o} bend was made at the tip of the wire to allow it to run parallel along the surface of the plate in the direction of expected slip. The wire was greased and encased in a plastic sheath permitting it to slide freely. The plate-wire assembly was then sealed with a rubber patch to prevent concrete from binding up the wire in the casing. With the plate assembly in place, the encased wire was led into the section to be cast and passed through a convenient location in the formwork.

Any relative movement between the two units would cause the corresponding wire to move along the direction of slip. Since it was free to move within the plastic casing, the displacement of the free end of the wire could be measured thus indicating the amount of slip.

For slip wires mounted on the B1 and C1 spine beam units, the free ends protruded out from the interior surface into the spine beam cavity. On the wing units the wires extended up from the top surface of the deck. The wires were trimmed to within an inch of the surface, and a small plate was attached at the tip to provide a bearing surface. A dial gage measured the displacement of the wire from the surface. Figures 3.6a and 3.6b show a slip wire-plate assembly prior to casting and a dial gage mounted over a wire during testing.

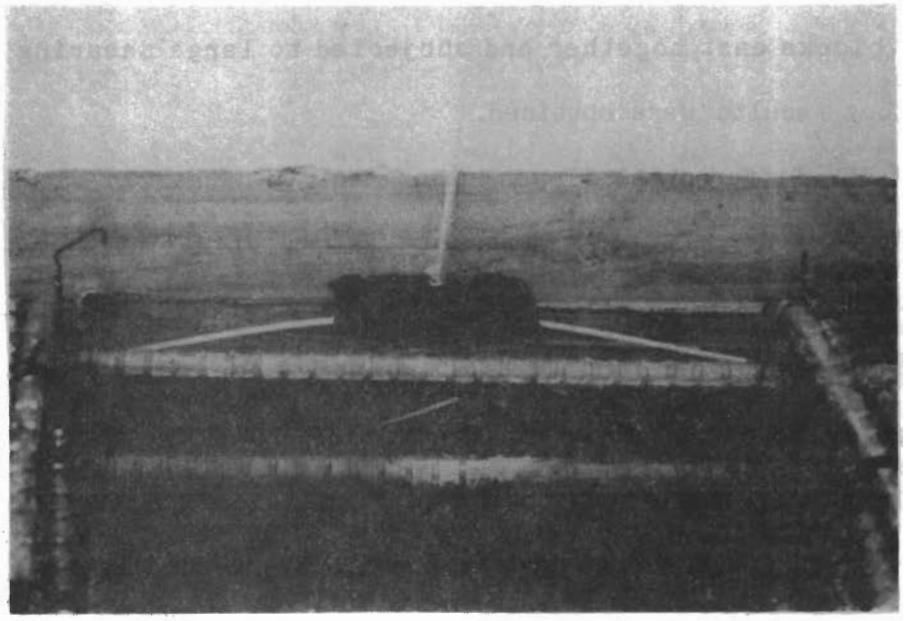

(a) Plate wire assembly installed in B1 unit prior to casting spine beam webs

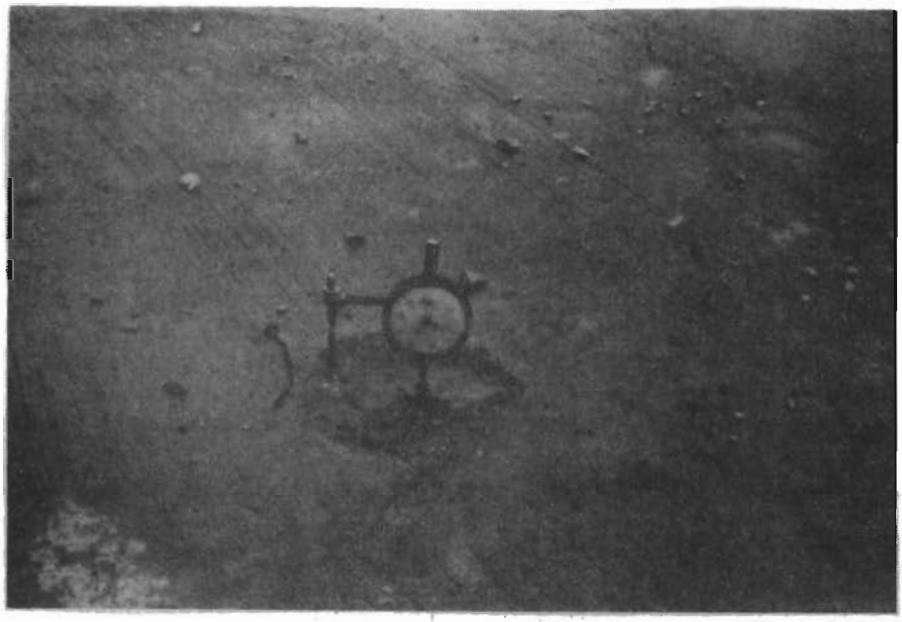

(b) Dial gage used to measure displacement of wire when slip occurs

Fig. 3.6 Slip wire setup

The concept was tested prior to its use on the bridge with two concrete blocks cast together and subjected to large shearing forces. Satisfactory results were obtained.

3.2.5 Differential Slope Measurement. Changes in slope due to service loads were measured by means of a mechanical inclinometer [4], which measured the difference in elevation between pairs of ball bearings cemented to the bridge at a 24-in. gage length. The inclinometer had a slope sensitivity of 4.2×10^{-6} radian. Slope measurements were made in both the longitudinal direction along the centerline of the spine beam and in the transverse direction along the wing ribs (Fig. 3.7).

3.2.6 Cross-Sectional Distortion. Cross-sectional distortion of the spine beam was measured under service loads at eight locations along the bridge (Fig. 3.7).

The instrumentation used to measure diagonal distortions was developed specifically for this project. It consisted of an adjustable aluminum rod anchored at a lower corner of the box with a dial gage mounted at the upper corner immediately opposite, as shown in Fig. 3.8a. As the spine beam displaced along the diagonal in either direction, the amount of movement was measured directly by the dial gage. Each distortion meter was mounted with the dial gage on the southeast side of the bridge. Originally, dial gages with a 0.001-in. sensitivity were used. These were later replaced with 0.0001-in. gages during testing when it was realized that greater precision would be

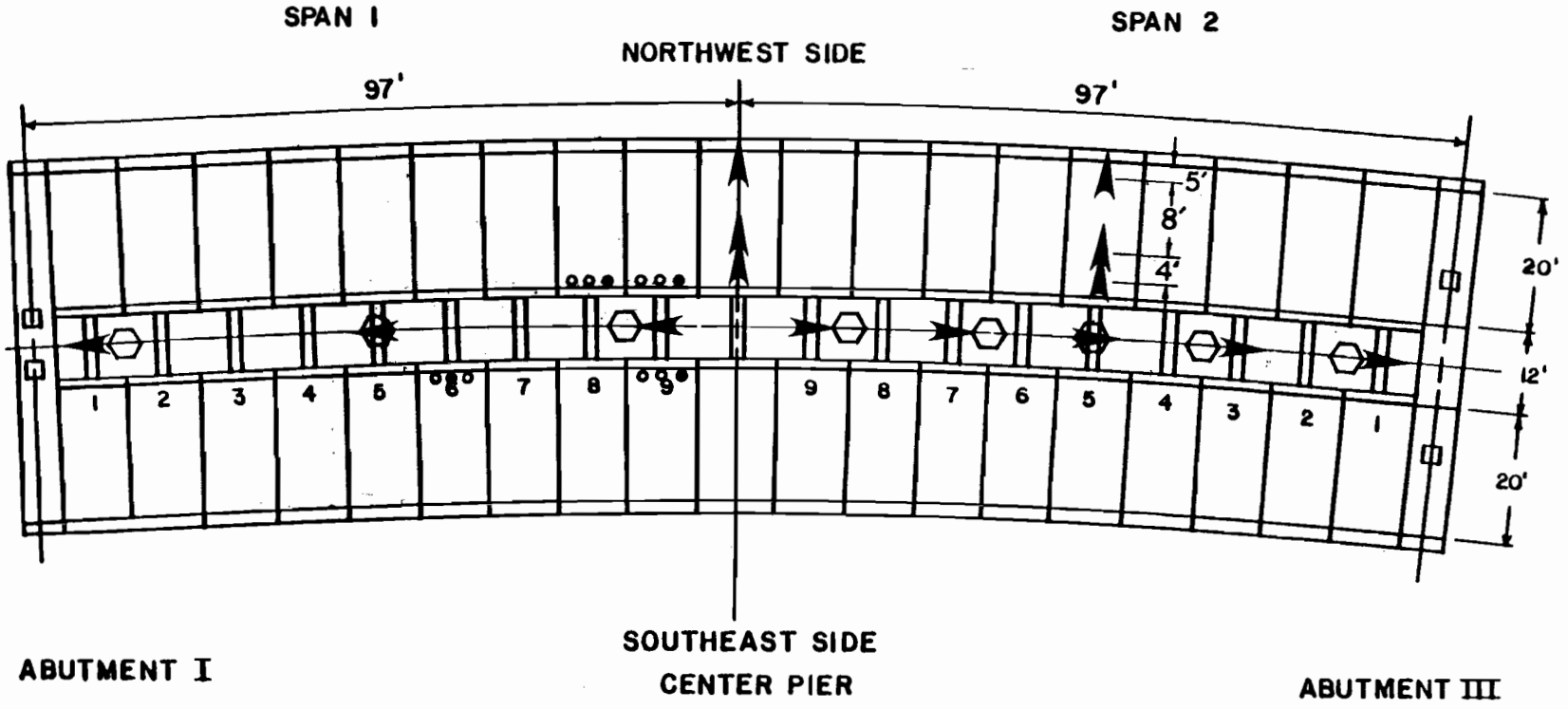

Fig. 3.7 Instrumentation locations for differential slope, cross-sectional displacement, and transverse tendon strain measurements

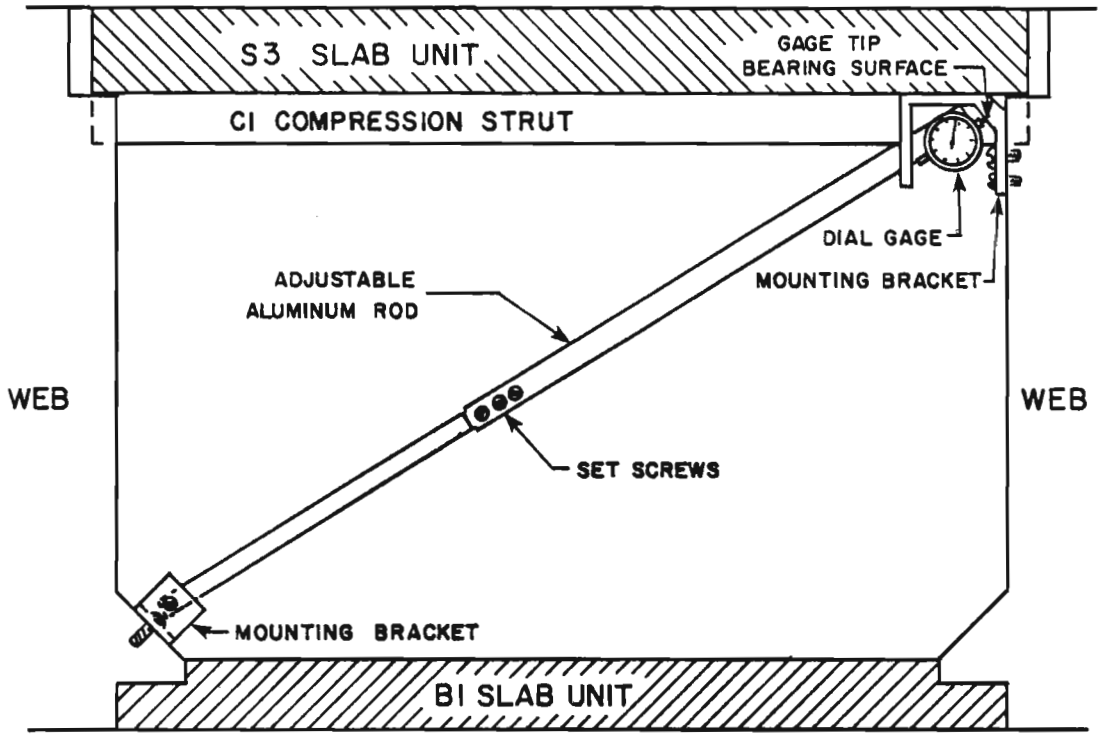

(a) Instrumentation developed to measure cross-sectional displacement

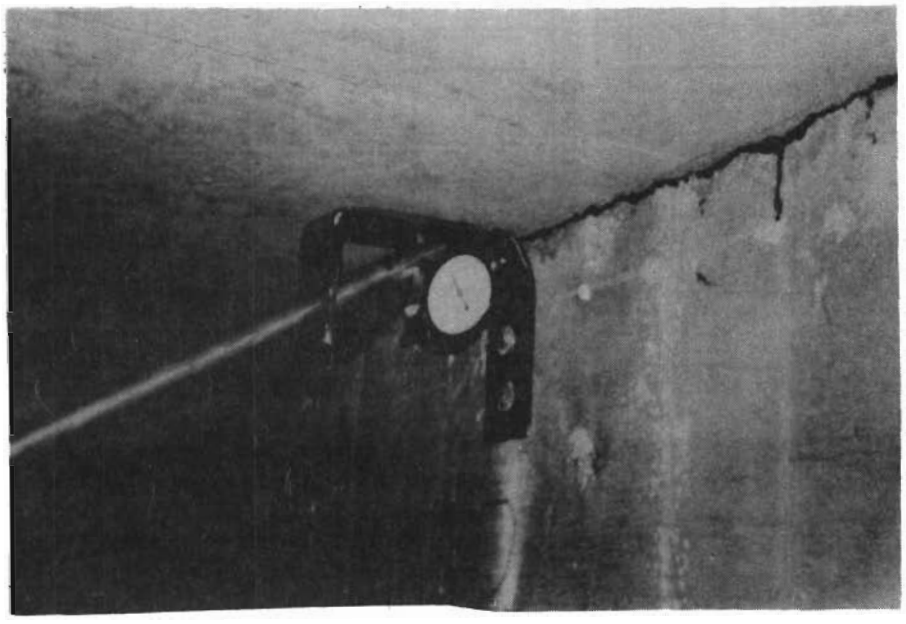

(b) Mounted distortion meter

Fig. 3.8 Diagonal displacements

required. Figure 3.8b shows a distortion meter mounted inside the spine beam.

3.2.7 Transverse Tendon Strains. Electronic strain gages were mounted at the transverse wing tendon locations indicated in Fig. 3.7. The gages were attached to tendons already in place to prevent damage to the gages during threading of the tendons through the ducts [2].

3.3 Testing

3.3.1 General. Testing was in two stages: performance during construction and service load behavior. Construction tests assessed bridge behavior at successive levels of completion as the applied loads and load-carrying mechanisms changed. Longitudinal strains, vertical deflections, and temperature gradients supplied basic information.

Service load testing was somewhat more extensive than construction testing. Cross-sectional distortion, slip, and slope measurements were made in addition to the construction measurement techniques. Truck loads were applied at critical locations along the bridge span, and appropriate readings were taken before and after each loading case.

3.3.2 Sequence and Procedures for Measurements During Construction. The sequence and description of construction steps during which measurements were taken are given in Table 3.1. External strains were measured only during cases 1 through 4. After this time they were impractical, if not impossible, to measure due to shoring removal and placement of the wings.

TABLE 3.1 Sequence and description of construction stages for deflection, surface strain, and temperature measurements

STAGE	DESCRIPTION	SPINE DEFL.	WING TIP DEFL.	EXTERNAL STRAINS	INTERNAL STRAINS	TEMP. GRADIENT
1	After completing spine beam; Prior to first-stage longitudinal post-tensioning	●		●	●	
2	During first-stage post-tensioning (1 axis III tendon, 2 long. tendons stressed)			●	●	
3	Immediately after first-stage longitudinal post-tensioning	●		●	●	
4	After first-stage longitudinal post-tensioning; Prior to wing placement			●	●	●
5	After setting first set of five wings on span 2; Prior to first-stage transverse post-tensioning				●	●
6	After setting second set of five wings on span 2; Prior to first-stage transverse post-tensioning				●	●
7	After setting third set of five wings on span 1; Prior to first-stage transverse post-tensioning				●	●
8	After setting final set of five wings on span 1; Prior to first-stage transverse post-tensioning				●	●
9	After completion of first-stage trans. post-tens; Prior to casting deck	●			●	●
10	After casting deck; Prior to second-stage transverse post-tensioning	●	●		●	●
11	After final transverse post-tensioning; Prior to final longitudinal post-tensioning	●	●			
12	After final longitudinal post-tensioning; Prior to setting parapet units	●	●		●	●
13	After setting parapet units; Prior to casting closure strips				●	●
14	After casting closure strips (Bridge completed)	●			●	●

All temperature readings taken during construction were related directly to a particular set of strain readings. This was done specifically to determine any effects temperature may have had on the measured strains. The results of the construction phase of testing are presented in Chapter 4.

3.3.3 Service Load Tests after Bridge Completion

3.3.3.1 Simulation of Loading. The bridge at Bear Creek was designed for four lanes of HS20-44 loading with a 25% reduction factor. For truck loading the corresponding unfactored design live load plus impact was approximately 88 kips per lane. The design truck load effects were approximated by using SDHPT dump trucks loaded with a dense asphaltic concrete mixture as shown in Fig. 3.9. The test trucks more closely represented overloaded H20 trucks rather than HS20 trucks. They were chosen mainly because they were readily available. However, the smaller stress levels from reduced truck weights are somewhat offset by larger load effects due to closer rear axle spacings so the SDHPT trucks were considered adequate for testing purposes. The trucks were limited to the 62 kip to 65 kip range based on the capacity of the truck loading bed and county road weight restrictions. Actual weights are given in Table 3.2. Figure 3.10 shows the dimensions of the test trucks.

3.3.3.2 Testing Procedures. The live load testing program had five basic load types labeled 1C, 2NS, 3C, 1S, and 2N, and the order of testing was arranged in a logical sequence progressing from lower loads to higher loads (i.e., increasing the number of trucks) and from balanced, flexural loads to eccentric, torsional loads. Thus,

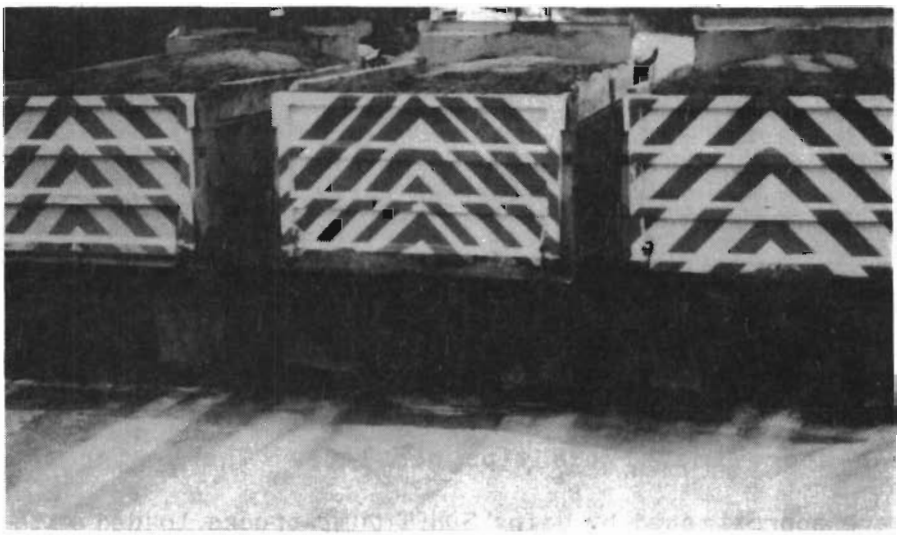

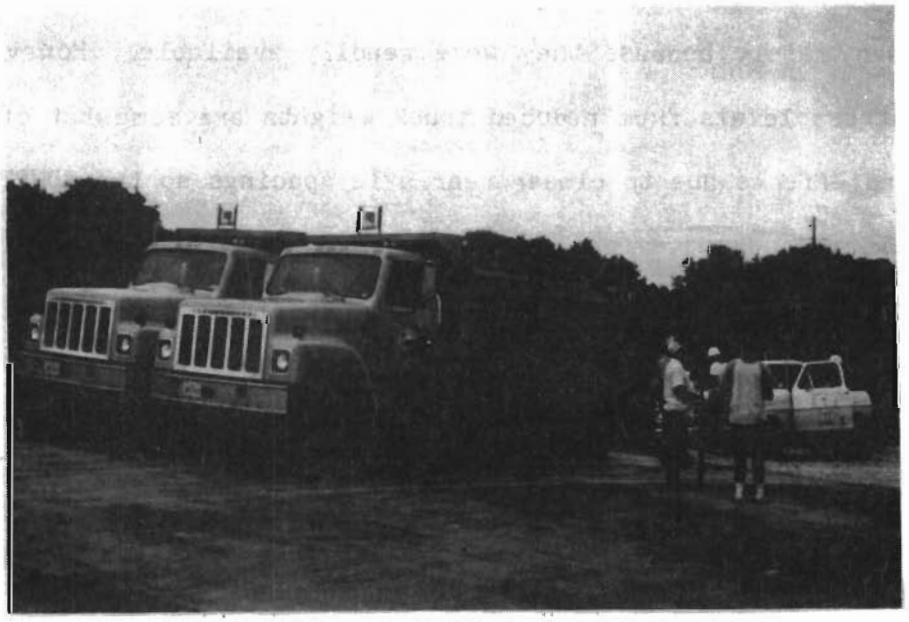

Fig. 3.9 Dump trucks used to simulate design service loads

TABLE 3.2 Axle and total weights of test trucks prior to commencement of service load testing*

TRUCK I.D. NUMBER	WEIGHT (lbs) FRONT AXLE	TOTAL	BACK AXLE
3151	14,020	64,040	50,140
3152	13,780	62,560	48,900
3153	15,040	65,020	50,120

* Truck loads subject to change during course of testing as noted in Sec. 3.3.3.1

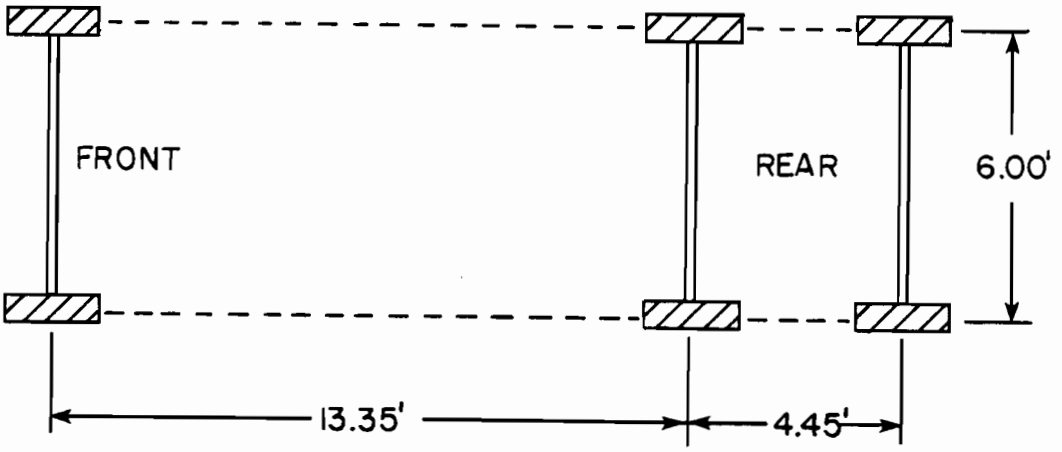

Fig. 3.10 Dimensions of test trucks used in service load testing

consistent with the above pattern, load type 1C involved one truck positioned along the centerline axis of the bridge, type 2NS involved two trucks positioned in parallel with one truck located over each wing tip (north/south side), type 3C consisted of three trucks in parallel symmetrical about the centerline axis of the bridge, and load types 1S and 2N utilized one truck along the south wing and two trucks along the north wing, respectively. Each load type, in turn, was divided into several load cases with truck locations along the length of the span generally corresponding to the quarter, half, and three-quarter points. Figures 3.11 gives the load types and corresponding truck locations for each load case.

An attempt was made to reduce the influence due to temperature and other environmental factors during testing. This was to ensure that results reflected only the effects due to applied truck loads. Frequent "no load" or zero readings were taken both before and after every few sets of readings for ready references.

Table 3.3 lists the loading cases in the proper sequence and gives the types of measurements taken during each case. The results of the service load testing program are summarized in Chapter 4 of this report.

In addition to the quantitative measurements, qualitative observations in the form of crack inspection and crack mapping were performed before and after the service load test programs.

3.3.3.3 Test Conditions. The weather was less than cooperative throughout the duration of testing. The service load tests were

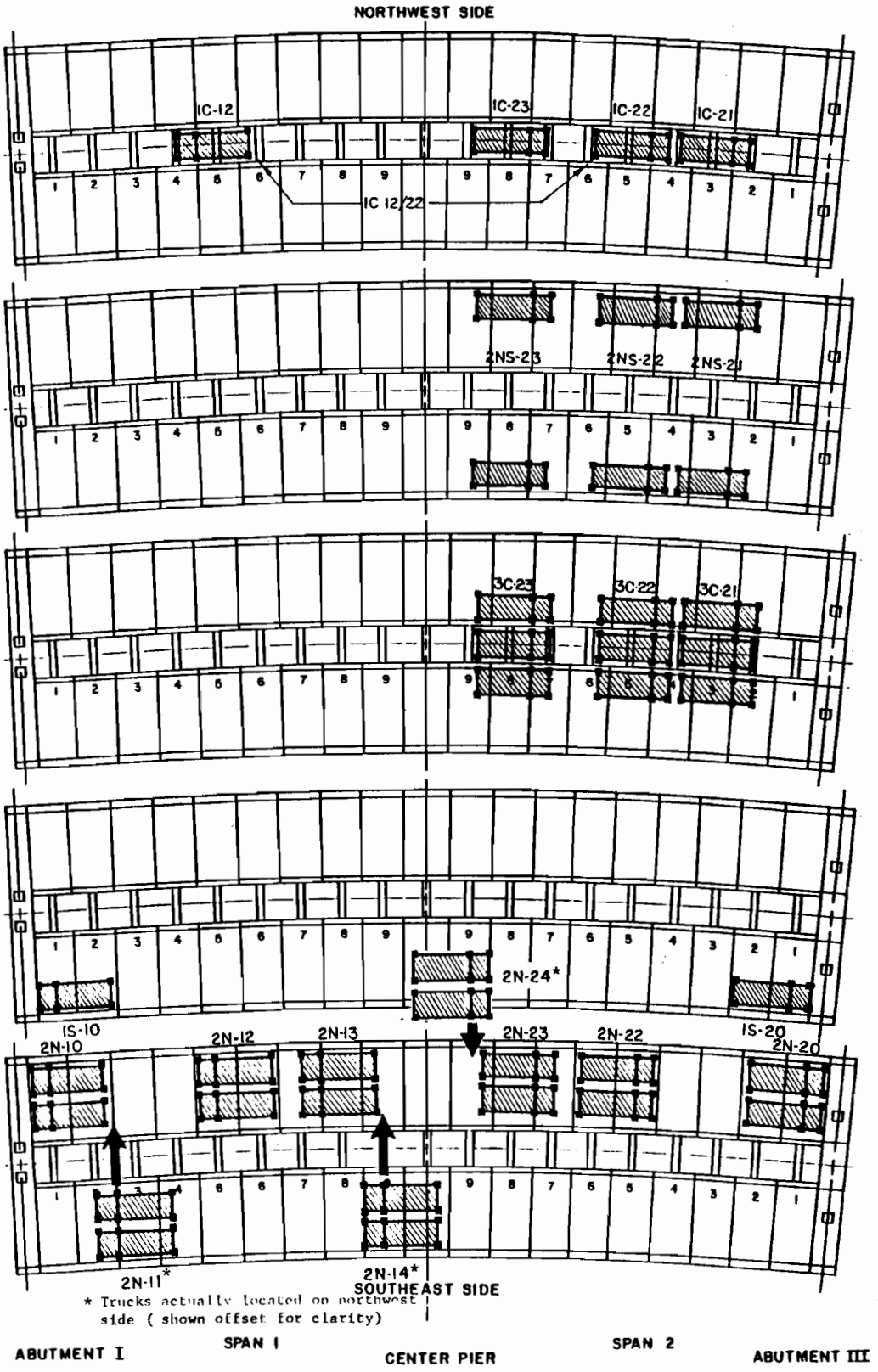

Fig. 3.11 Load positions and designations for service load tests

TABLE 3.3 Sequence of loading and types of response measured for each particular case

DATE	LOAD CASE	DEFL.	SURFACE STRAINS	SLOPE (LONG.)	SLOPE (TRANS.)	X-SECT. DISP.	SLIP	TEMP.
7/11	NO LOAD	•	•	•	•	•	•	•
7/11	1C-21	•	•				•	•
7/11	1C-22	•	•				•	•
7/11	1C-23	•	•				•	•
7/11	NO LOAD	•	•	•	•	•	•	•
7/12	NO LOAD	•	•	•	•	•	•	•
7/12	1C-12	•	•				•	•
7/12	1C-12/22	•	•				•	•
7/12	NO LOAD	•	•	•	•	•	•	•
7/12	2NS-21	•	•	•		•	•	•
7/12	2NS-22	•	•	•	•	•	•	•
7/12	2NS-23	•	•		•	•	•	•
7/12	NO LOAD	•	•	•	•	•	•	•
7/12	1S-10	•	•	•	•	•	•	•
7/13	NO LOAD	•	•				•	•
7/13	3C-21	•	•				•	•
7/13	3C-22	•	•				•	•
7/13	3C-23	•					•	•
7/13	NO LOAD	•		•	•	•	•	•

DATE	LOAD CASE	DEFL.	SURFACE STRAINS	SLOPE (LONG.)	SLOPE (TRANS.)	X-SECT. DISP.	SLIP	TEMP.
7/13	1S-20	•		•		•	•	•
7/13	2N-20	•		•		•	•	•
7/13	2N-22	•		•		•	•	•
7/13	2N-23	•		•		•	•	•
7/13	2N-14	•		•	•	•	•	•
7/13	NO LOAD			•		•		
7/15	NO LOAD	•		•	•	•	•	
7/15	2N-10	•		•	•	•	•	
7/15	2N-11			•	•	•	•	
7/15	2N-12	•		•	•	•	•	
7/15	2N-13	•		•	•	•	•	
7/15	2N-14	•		•		•	•	
7/15	NO LOAD	•		•		•	•	
7/15	2N-20					•		
7/15	2N-21					•		
7/15	2N-22					•		
7/15	2N-23					•		
7/15	2N-24					•		
7/15	NO LOAD					•		

commenced on Monday, July 11, 1983 and were completed Friday, July 15. The temperature was fairly constant in the mid-80 to mid-90^{o}F range throughout the week. The first two days progressed from sunny skies to a heavy overcast with a corresponding increase in humidity. Conditions inside the spine beam became rather intolerable for obtaining measurements.

On Wednesday the weather took a turn for the worse with intermittent rains hampering measurement efforts. Testing was limited to periods between showers, The rains continued into Thursday with increased intensity and frequency. It was decided to postpone testing and complete the program on Friday. By late afternoon, the rains subsided, and testing was completed by early evening.

C H A P T E R 4

TEST RESULTS AND INTERPRETATIONS

4.1 Behavior During Construction

4.1.1 General. The results of test measurements during construction are summarized in the following sections. All results are presented in Ref. 2.

In order to provide some reference frame for evaluation of the results obtained from the field tests, a conventional elastic analysis was carried out for several stages of construction. This analysis, based on a matrix formulation using the direct stiffness method, is in addition to the Lee and Johnson finite element analysis which will be discussed later in this chapter. In order to avoid confusion, the former method will simply be referred to as the conventional analysis, while the Lee and Johnson analysis will be referred to as the finite element analysis.

Figure 4.1 shows the arrangement of elements and nodal points used for the conventional analysis. The cross section was assumed constant along the bridge and the bearing pads incompressible. A rotational spring accounted for the bending stiffness of the pier. Figure 4.2 shows the "assumed" effective cross sections and related properties for various stages of construction. Concrete strength and modulus values were based on strength time relationships from cylinder tests [2]. All results are referenced to locations as indicated in the plan view in Fig. 4.3.

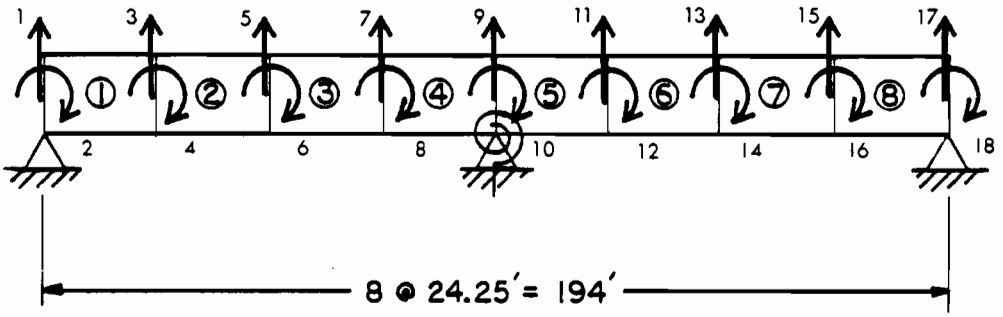

$$K_{\substack{\text{rotation}\\ \text{of pier}}} = \frac{4EI}{L} = \frac{4(4030\text{k/in}^2)(96\text{"}\times 48\text{"}^3/12)}{216\text{"}}$$

$$= 66{,}027{,}520 \text{ in-k/rad}$$

Fig. 4.1 Arrangement of elements and nodal points for conventional analysis

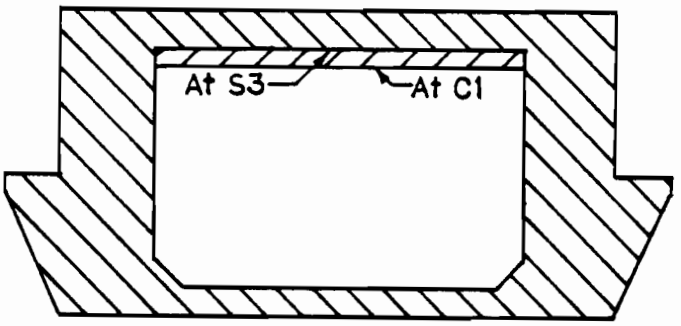

$A_{S3} = 28.60\ ft^2$ $\quad y_t = 2.70\ ft$

$I_{S3} = 90.96\ ft^4$ $\quad y_b = 2.63\ ft$

$I_{C1} = 98.20\ ft^4$

(a) Spine beam

NOTE: S3 CROSS SECTION EXTENDS 7.5 ft AND C1 CROSS SECTION EXTENDS 2.5 ft IN THE LONGITUDINAL DIRECTION; THEREFORE, USE

$$I = \frac{3I_{s3} + I_{c1}}{4}$$

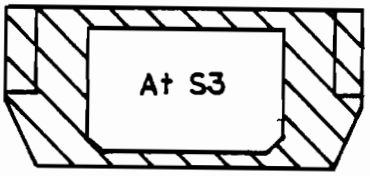

$A_{S3} = 34.35\ ft^2$ $\quad y_t = 2.49\ ft$

$I_{S3} = 102.61\ ft^4$ $\quad y_b = 2.84\ ft$

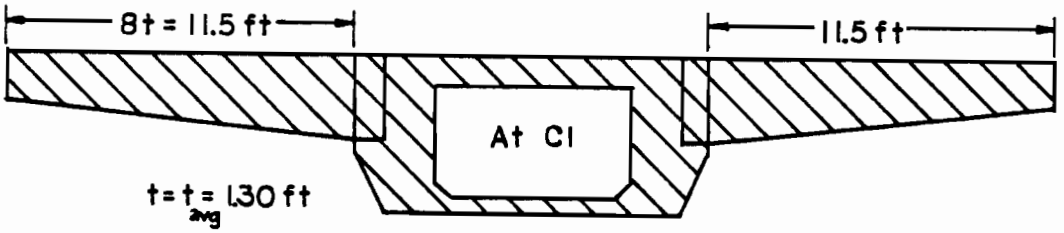

$I_{C1} = 154.29\ ft^4$

(b) Spine beam + wings (no deck)

Fig. 4.2 "Assumed" effective cross sections and related properties for various stages of construction

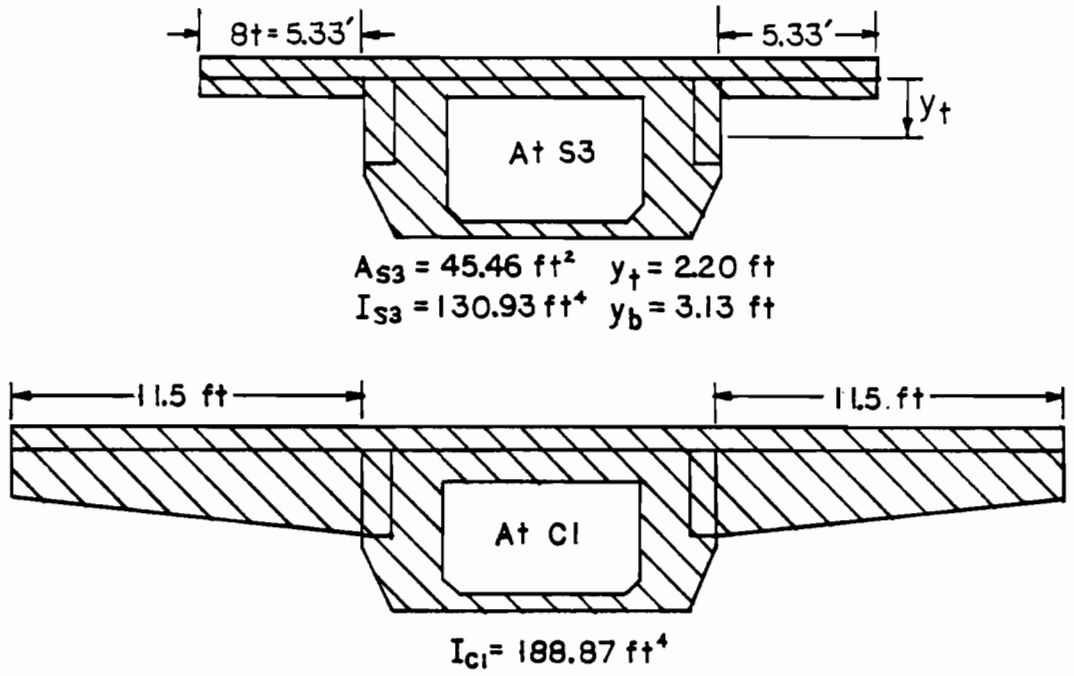

(c) Spine beam + wings + deck

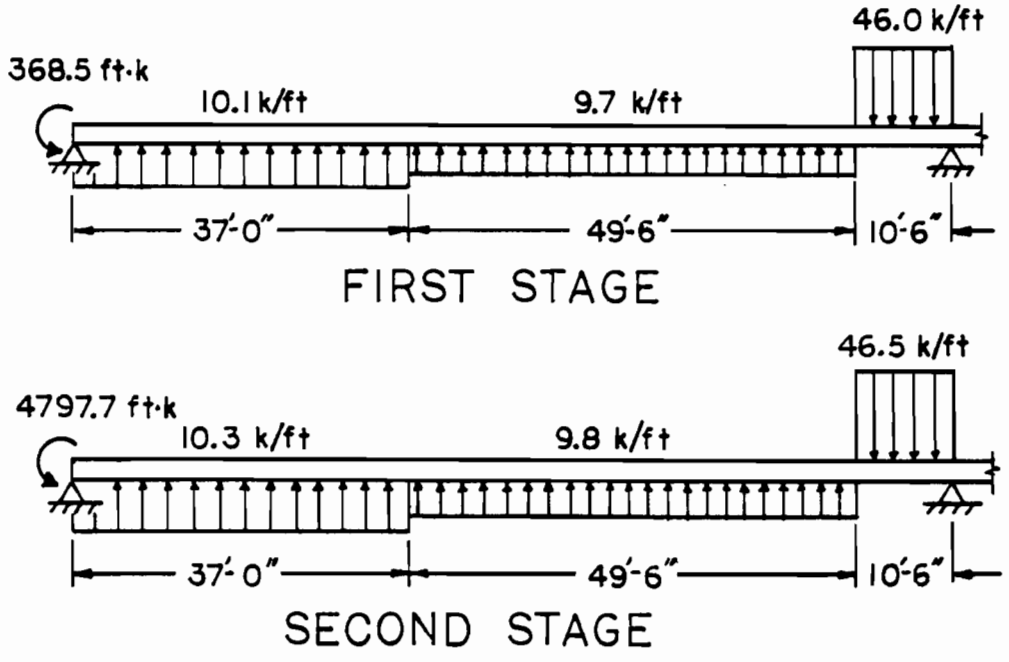

(d) Equivalent transverse loads for longitudinal post-tensioning

Fig. 4.2 (cont.)

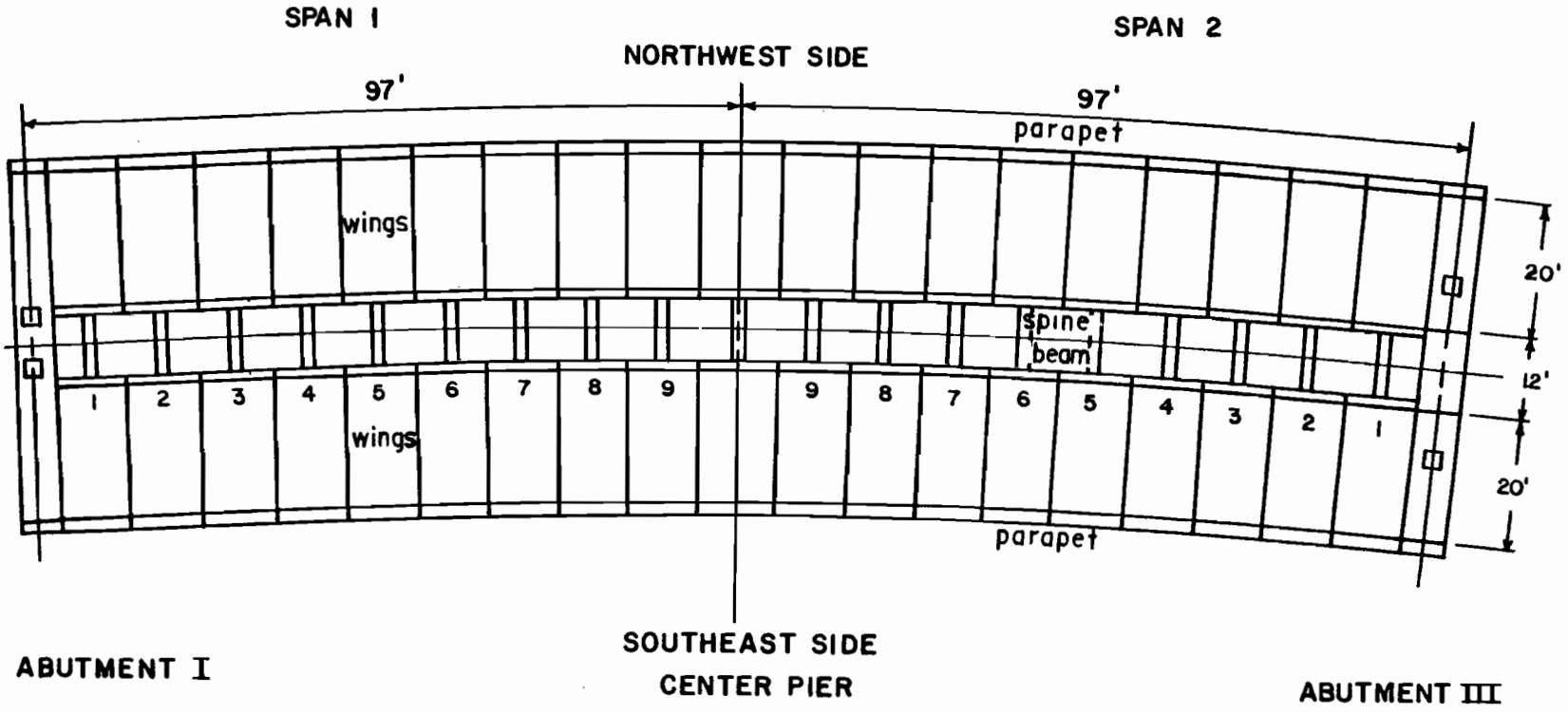

Fig. 4.3 Plan view of bridge showing location identifiers

4.1.2 Deflections. Measurement of elevations along the bridge during construction can be separated into three distinct phases:

1. Elevations of the top surface of the spine beam prior to placement of the deck slab.
2. Elevations of the top surface of the deck slab over the spine beam. These were measured upon completion of the casting of the deck through bridge completion.
3. Elevations of the wing tips. These were measured upon completion of deck casting operations through second stage post-tensioning.

Deflections for the spine beam are plotted in Figs. 4.4 and 4.5 as changes in elevations between successive load cases. Deflection profiles are presented as incremental changes rather than cumulative changes for two reasons. First of all, because elevations were measured at the top surface of the bridge and the top surface changed depending on whether or not the deck had been cast, it was not possible to retain a permanent reference surface. Secondly, the plotting of incremental deflections allows the effects from each particular load case to be examined individually and compared with analytical results. This eliminates carryover effects from previous load cases and reduces time dependent factors.

Figure 4.4 presents average measured changes in elevations for the spine beam webs along with the results from the conventional analysis. The measured profiles resulting from the spine beam dead load and first-stage post-tensioning are similar for spans 1 and 2 with a

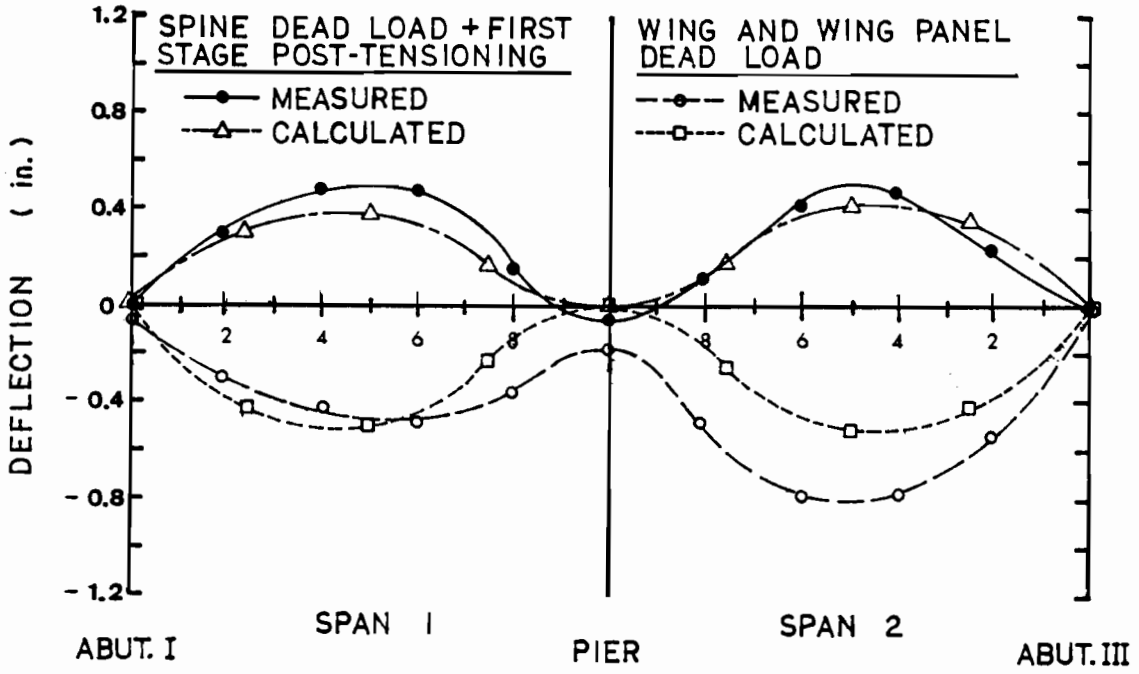

Fig. 4.4 Average differential deflection profiles for the spine beam webs

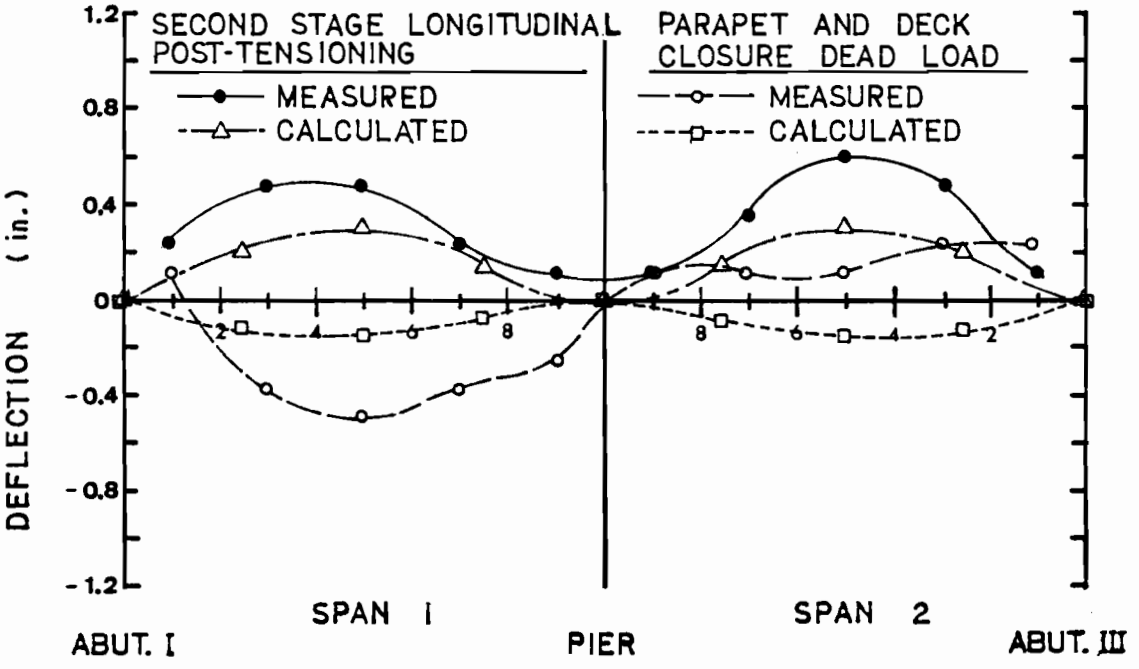

Fig. 4.5 Differential deflection profiles along spine beam centerline

maximum camber of 1/2 in. in either span. The conventional analysis model assumed an effective cross section equal to the entire spine beam cross section as shown in Fig. 4.2a, and concrete strengths of 6220 psi and 5177 psi were used for spans 1 and 2, respectively. The spine beam dead load was 4.36 k/ft, and equivalent transverse loads were used to model the effect of the prestress force. The equivalent loads, shown in Fig. 4.2d, were calculated using the method proposed in Ref. 5 with a total axial force of 0.64 $f_{pu}A_s$ as was measured on the Bear Creek structure. It should be noted that the method for computing equivalent transverse loads in Appendix A.1 of the PTI Manual (Ref. 6), while identical in concept to that of Ref. 5, neglects the induced downward load W_3 over the center support. Because of the sharp curvature of the tendon in the pier region, this component is significant and should not be omitted.

Calculated deflections were in general agreement with measured results. Due to the difference in assumed concrete strengths, span 2 deflections were slightly larger than those in span 1. The calculated maximum deflections underestimated measured values by approximately 20%. Also, the predicted maximums were located at approximately 0.4 L from the abutments while the measured maximum values were shifted towards midspan.

The measured and calculated deflections resulting from the wing and wing panel dead loads are also presented in Fig. 4.4. A vast difference in the magnitude of the measured profiles is apparent between spans 1 and 2. The measured maximum deflection in span 1 is 1/2 in.

while that in span 2 is approximately 3/4 in. No physical reason can be given for such a large difference. Although the difference in concrete strengths and an increasing effective area over a portion of the span as each set of five wings is placed and stressed would have some effect, the difference would be much less significant. This is supported by the results of the conventional analysis. For this analysis the effective cross-sectional area was modified in the portion of the span where wing units and deck panels had already been placed and tensioned. A weighted average of the moments of inertia from the cross sections in Fig. 4.2b was also used to account for the variation in cross section along the span. For the portions of the span where the wing units had not yet been placed and stressed, the spine beam cross section in Fig. 4.2a was considered effective. Concrete strengths were assumed to vary between 6631 psi and 6913 psi for span 1 and between 6925 psi and 6799 psi for span 2 during the four stage wing placement operation. A uniform load of 6.38 k/ft was used for wing and wing panel dead loads. Thus, calculated results from each stage were superimposed to give the deflection profile shown in Fig. 4.4. It can be seen that the calculated deflections differ only slightly between span 1 and span 2 (approximately 5%).

Measured results agree reasonably well with the calculated deflections for span 1 although again, the location of the measured maximum is shifted towards midspan. The span 2 measurements disagree appreciably and may reflect an error as compared with the span 1 and calculated values. Cracking in the span does not appear to be a logical

explanation since later measurements do not indicate similar trends. Furthermore, the 1/4 in. deflection measured at the center pier seems to indicate a measurement error rather than unusual physical behavior of the bridge, since no support problems were noted at that location.

Figure 4.5 shows the deflection profiles resulting from second-stage post-tensioning and from the parapet/deck closure dead loads. Upon stressing, maximum cambers of 0.5 in. were measured in span 1 and 0.6 in. in span 2. This difference may be the result of the difference in concrete strengths or may just indicate variability due to measurement sensitivity.

Due to the dead load of the parapets and deck closure strips, the measured results in span 1 show a maximum deflection of 1/2 in. The profile is relatively smooth, and the maximum occurs near midspan. The span 2 results, on the other hand, are very confusing. The profile is rather uneven and indicates camber along the entire span. This cannot be explained with physical reasoning, since a uniform dead load would cause both spans to displace downwards. Span 1 does not exhibit similar behavior, and the changes in elevation were referenced to readings taken just prior to the application of the load. Therefore, time dependent effects are not significant in explaining the deviation from expected behavior.

Although the measured results due to parapet dead load in span 1 appear reasonable in a qualitative sense, the magnitude of the displacements is questionable. The parapet and closure strip dead load of 2.87 k/ft is less than half the weight of the wing and wing panels

dead load which resulted in the deflections plotted in Fig. 4.4. Undoubtedly, the concrete strengths and the effective moment of inertia of the bridge at the time of parapet placement were also greater than during the earlier loading stage, yet the resulting displacements are nearly the same for both load cases. The sensitivity of the deflection measurement system was marginal for these cases.

The conventional analyses carried out for second stage post-tensioning and parapet/deck closure dead loads [2] predict much smaller vertical displacements than were actually measured. The calculated deflections are approximately 50% to 65% of those actually measured indicating the actual structure is much more flexible than that predicted by the model.

The deflections predicted by the conventional analysis model for the parapet and deck closure dead loads are only a third of those actually measured in span 1. As stated earlier, the weight of the precast rails and the cast-in-place closure joints was 2.87 k/ft. The effective cross section assumed was identical to that used in computing deflections due to second stage post-tensioning, and concrete strengths of 7080 psi and 7036 psi were used. Again, the model seems to predict a much stiffer structure than actually exists for the span 1 displacements. A quantitative comparison of predicted and measured displacements for span 2 does not appear relevant for this particular load case due to the great disparity between the two profiles.

Figure 4.6 presents measured deflections at the wing tips along the northwest and southeast sides of the bridge. The displacements are

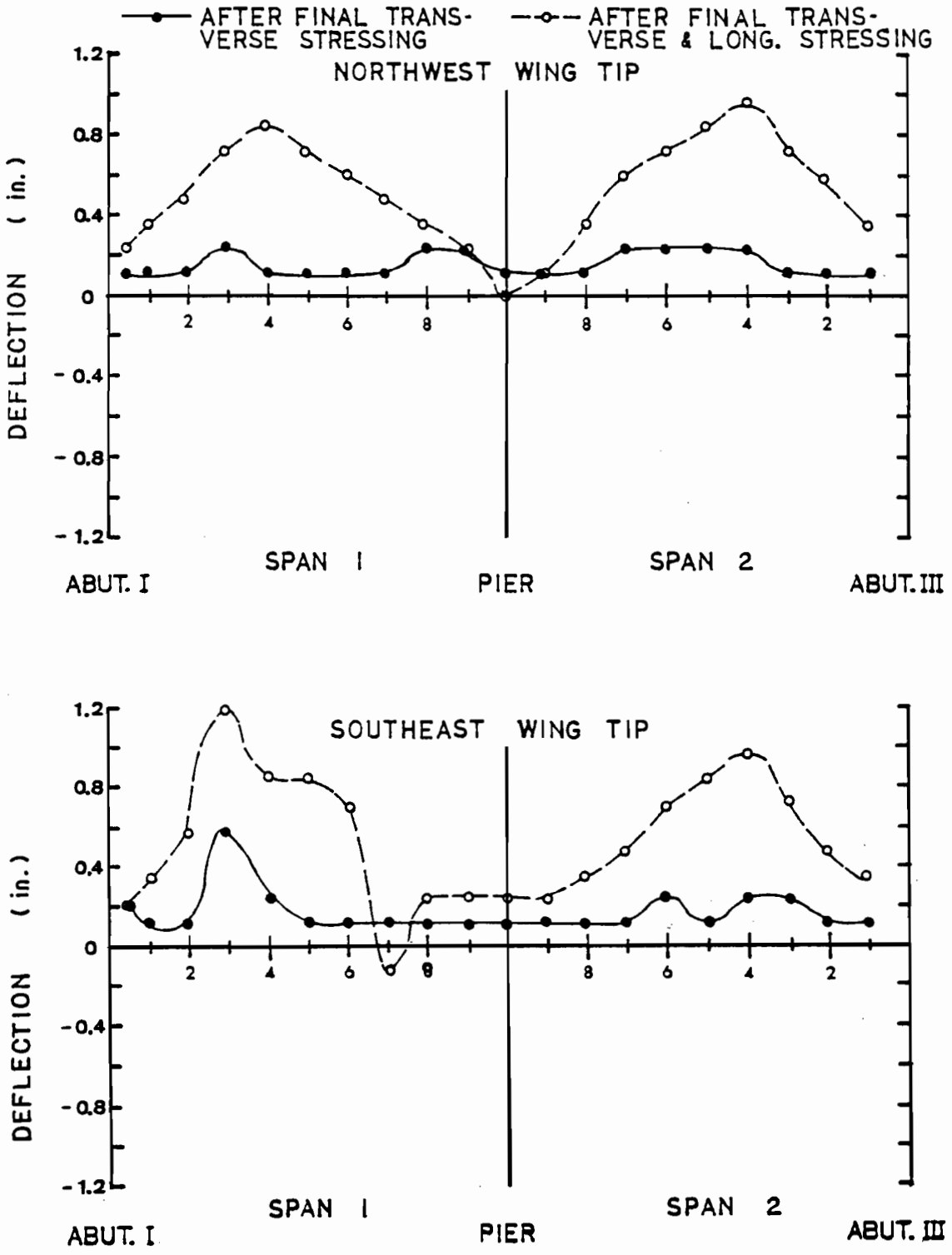

Fig. 4.6 Differential deflection profiles along the wing tips

plotted as changes in elevations measured prior to final transverse post-tensioning of the wings and those measured after final transverse stressing and after final longitudinal stressing of the spine beam. Thus, the displacement profiles are cumulative for the two load cases. Aside from local deviations at sections 3 and 7 on the southeast side of span 1, the profiles are consistent between spans and between the two sides of the bridge.

The effect of final transverse stressing on the wing tips was a consistent upward displacement of 0.01 ft to 0.02 ft along the entire length of the bridge. The displacement profiles after final longitudinal post-tensioning indicate nearly identical camber in both spans with peak values of 0.85 in. occurring at a distance of 0.4 L from each abutment.

4.1.3 Longitudinal Strains. Longitudinal concrete surface strains were measured on both the interior and exterior of the spine beam at the locations shown previously in Figs. 3.1 and 3.2. For simplicity, the locations of the cross sections are presented again in Fig. 4.7.

Sample results for sections 4 and 8 are presented as total strain gradients over the depth of the webs for the most critical load stages of construction. Plotted along with the measured strain gradients for are the strain gradients predicted by the conventional elastic analysis.

In Fig. 4.8 the completed spine beam has been subjected to its own dead weight plus the effect of first stage longitudinal post-

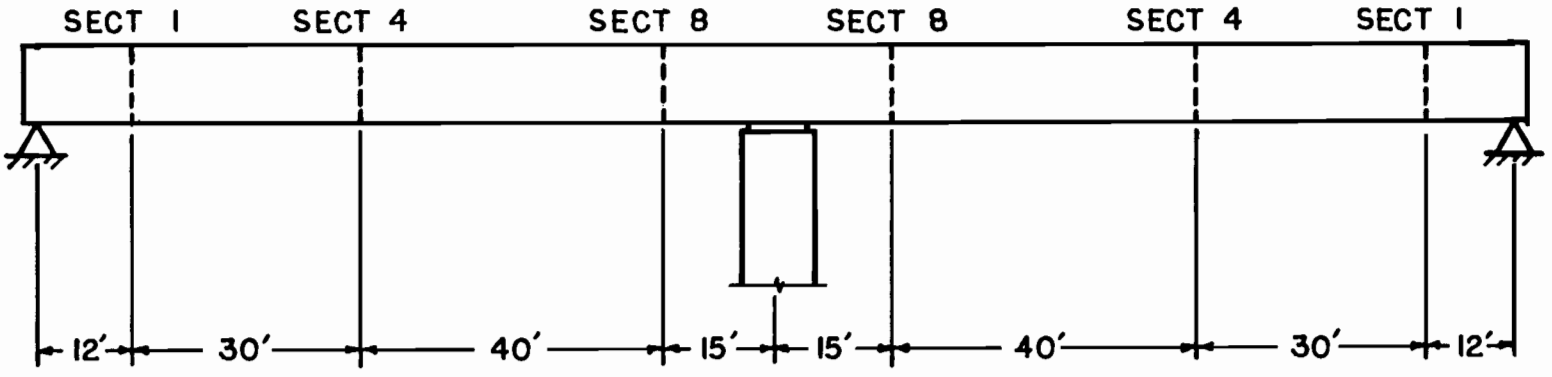

Fig. 4.7 Locations of instrumented sections for longitudinal concrete surface strain measurements

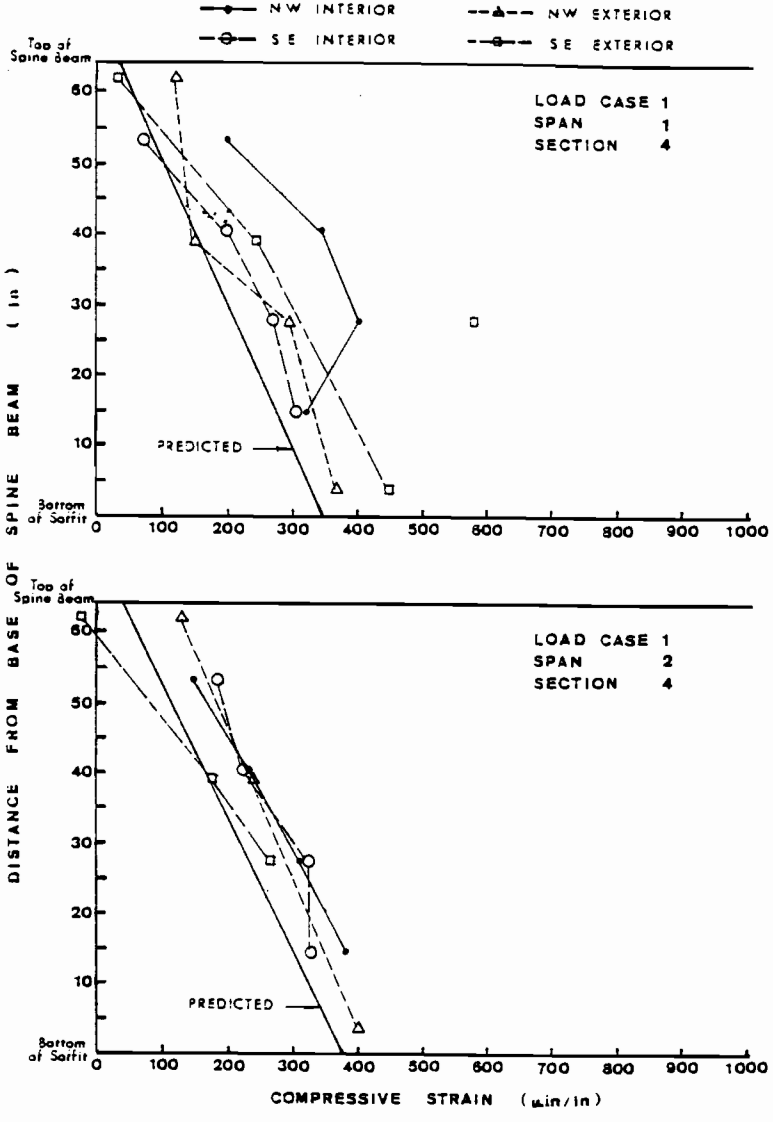

(a) Section 4 - Spans 1 and 2

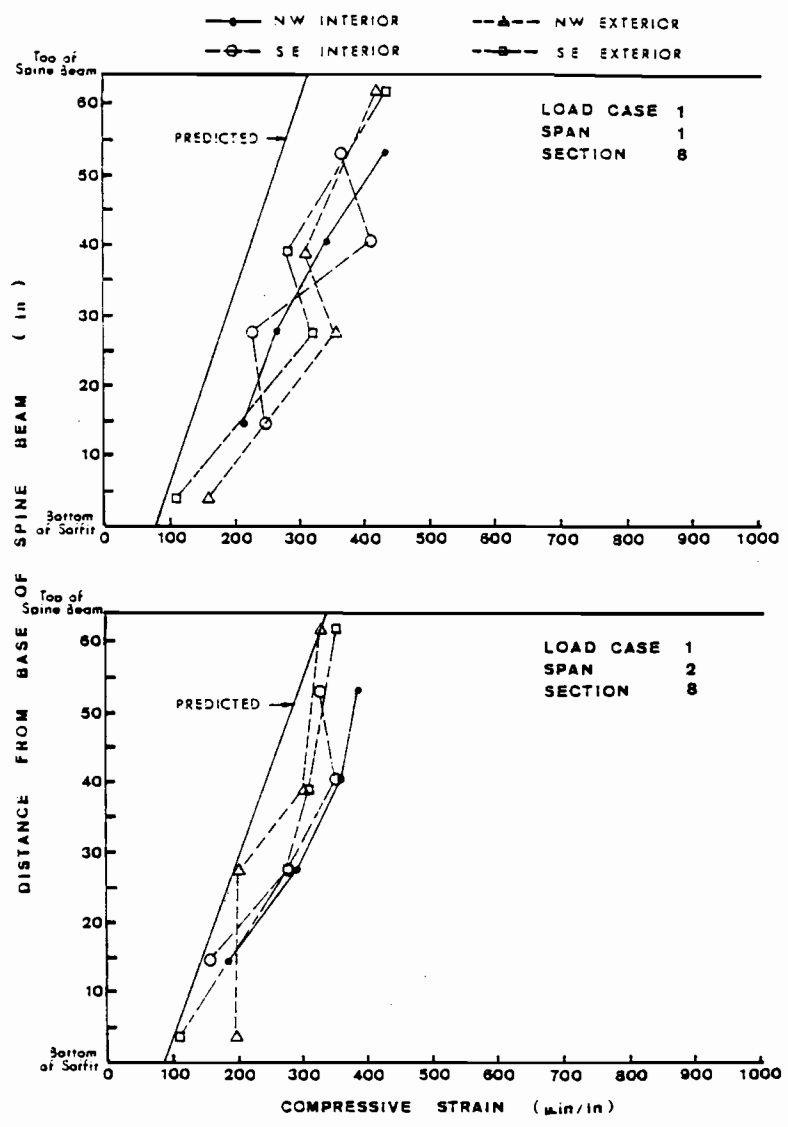

(b) Section 8 - Spans 1 and 2

Fig. 4.8 Total surface strains over spine beam depth for first-stage longitudinal post-tensioning and spine dead load

tensioning. Under these loads the measured results were in general agreement with predicted results. The shape of the strain profiles represents the measured gradients well qualitatively, but the analysis underestimates the average strains by roughly 15 to 25%.

The strain distribution at each section can be viewed as the superposition of three separate load effects (Fig. 4.9):

a) A large compressive strain over the entire cross section due to the axial component of prestress.

b) A linear change from compression at one extreme fiber to tension at the opposite extreme due to the eccentricity of prestress at a section.

c) A typical linear strain distribution with tension and compression at opposite extreme fibers due to the dead load moment at a section.

Since the flexural strains due to prestress eccentricity are larger than those due to dead load, one would expect the resulting strain distribution to resemble that of Fig. 4.9b with the entire distribution shifted towards the compression side. This can be seen in Fig. 4.8 where the compressive strains are larger at the bottom of the spine beam than at the top at section 4. The trend is reversed near the center pier at section 8.

Figure 4.10 shows strain readings taken 9 days after those in Fig. 4.8 under identical loading conditions (spine beam dead load and first-stage post-tensioning). The measured strain gradients have moved farther from the predicted strain distributions in the direction of

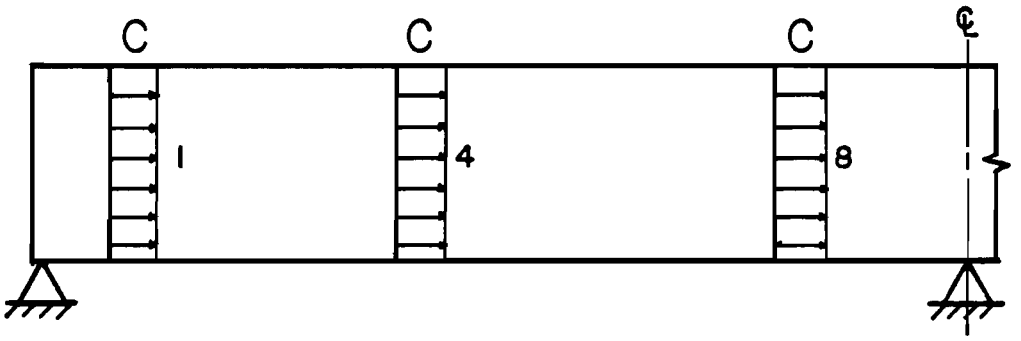

(a) Uniform strain distribution due to axial component of prestress

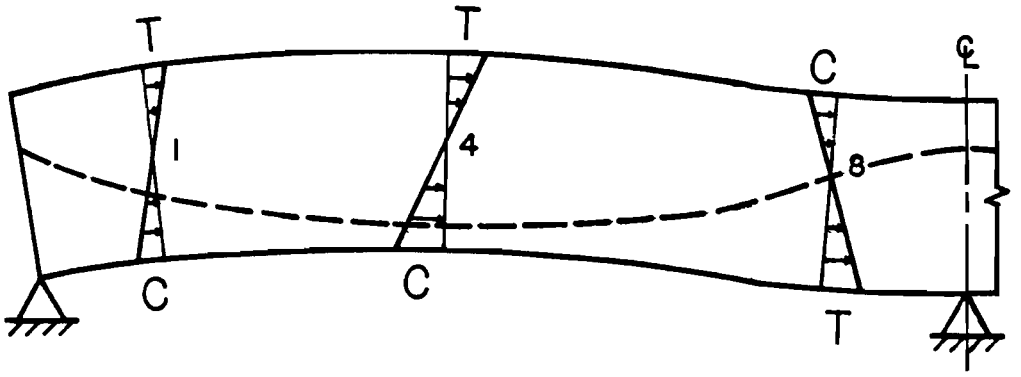

(b) Linear strain distribution due to eccentricity of prestress

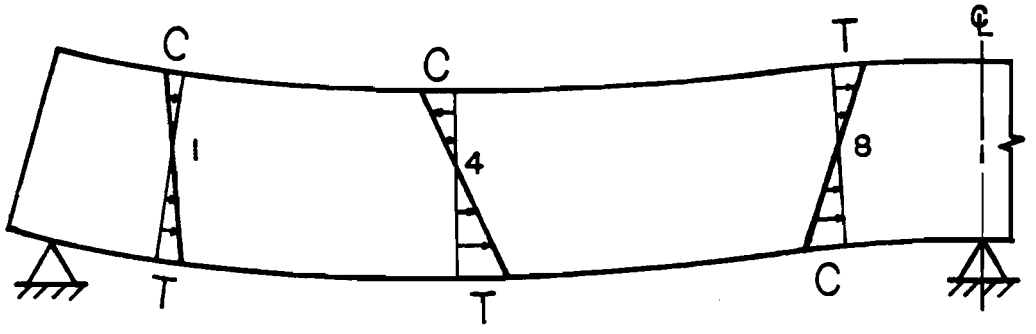

(c) Linear strain distribution due to gravity loads (i.e., dead load)

Fig. 4.9 Superposition of strain gradients from various load effects

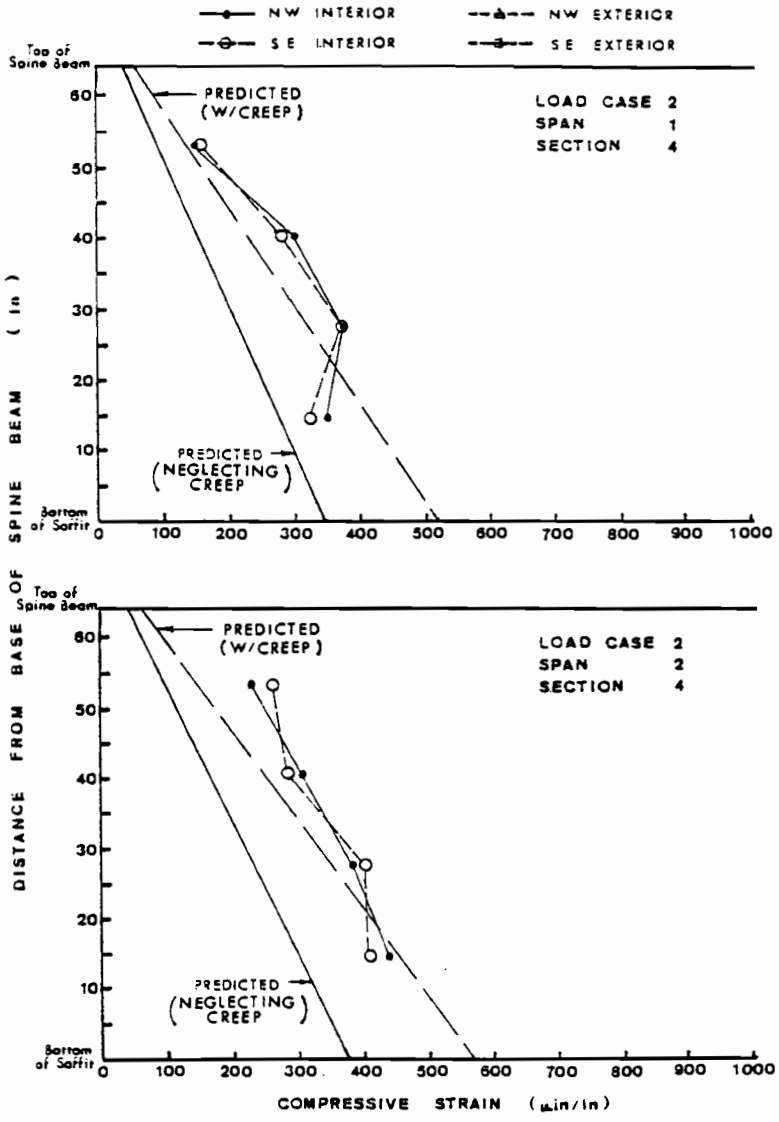

(a) Section 4 - Spans 1 and 2

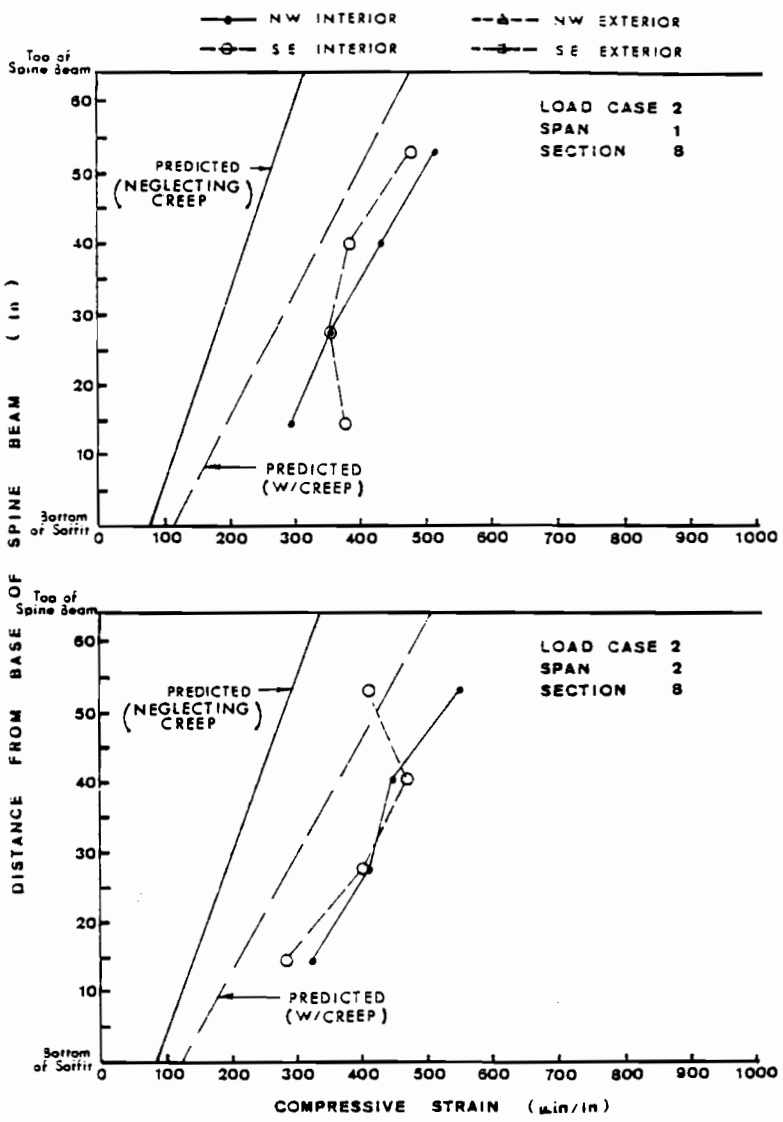

(b) Section 8 - Spans 1 and 2

Fig. 4.10 Total surface strains over spine beam depth 9 days after initial longitudinal stressing (same load as in Fig. 4.8)

increased compression reflecting creep. Due to the relatively young age of the concrete and the high compressive stresses involved, the ACI 209 Committee report [7] predicts time dependent effects of approximately 50% of the initial strains after 9 days, as shown on Fig. 4.10.

Figures 4.11 through 4.14 show measured and predicted total strain gradients after placement of all wing and wing panel sections (including the wing-spine closure strips), after casting the deck, after second-stage post-tensioning and after addition of rails and rail closure strips (completed bridge), respectively.

A comparison of the measured and predicted values shows agreement in the general shape of the gradients but large discrepancies in magnitude. Subsequent analyses [2] showed these are due to neglecting creep effects. The measured and predicted "changes" in strain at the time of second-stage post-tensioning were in good agreement [2].

4.1.4 Temperature Gradients. The temperatures at various points around the spine beam cross section were measured near midspan in span 1. Readings were taken throughout the construction sequence. In general, the temperature differential between any two points rarely exceeded 6-7°F at any given time. The one exception was a 10°F differential which is shown in Fig. 4.15 as a plot of temperature vs. depth of thermocouple over the cross section.

4.1.5 Transverse Tendon Strains. Transverse tendon strain readings were measured at stations indicated in Fig. 3.7. Readings were taken after post-tensioning and at subsequent critical loading stages during construction. Measured strains were total strains as referenced

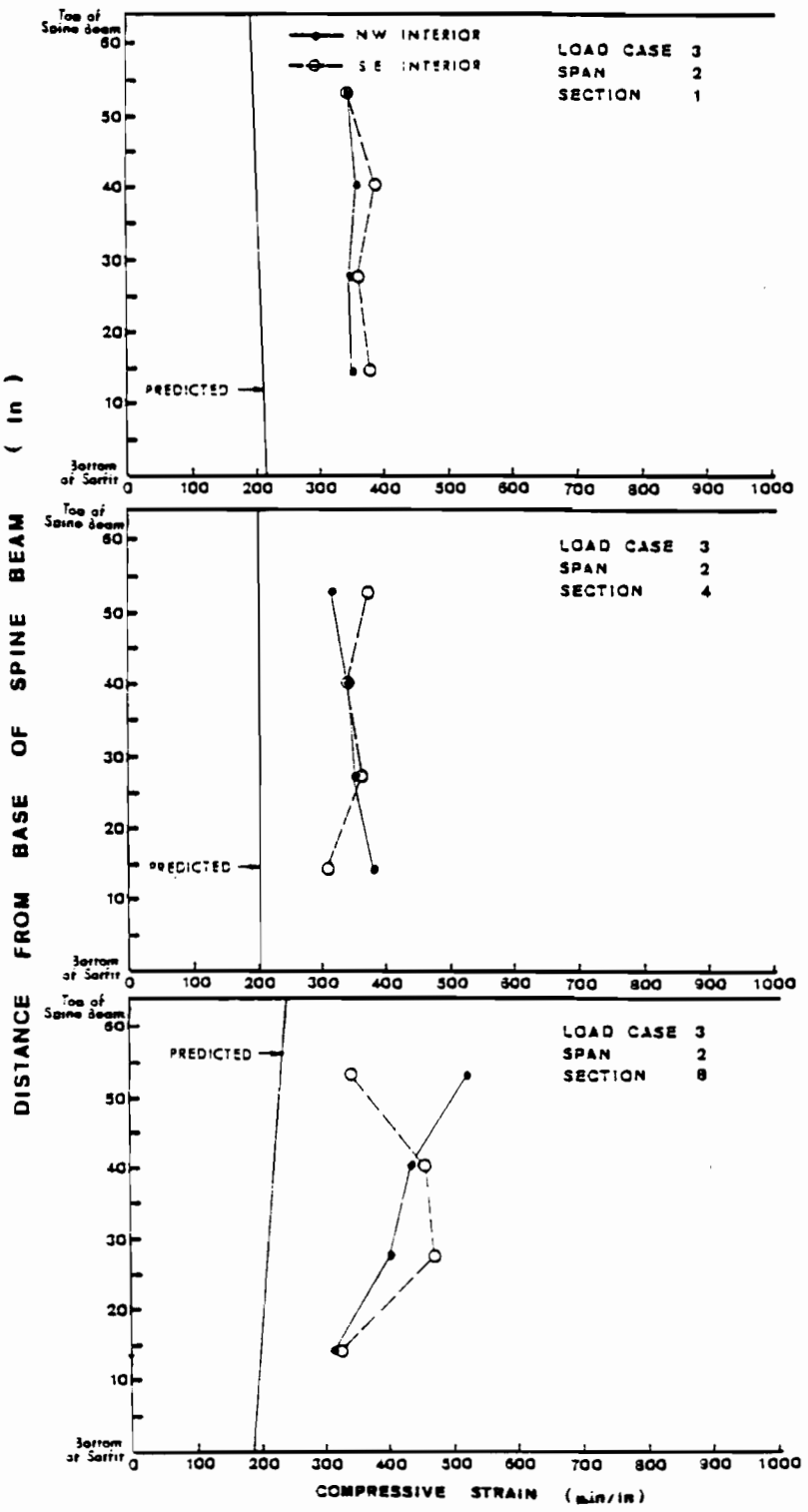

Fig. 4.11 Total strains over spine beam after wing and panel placement

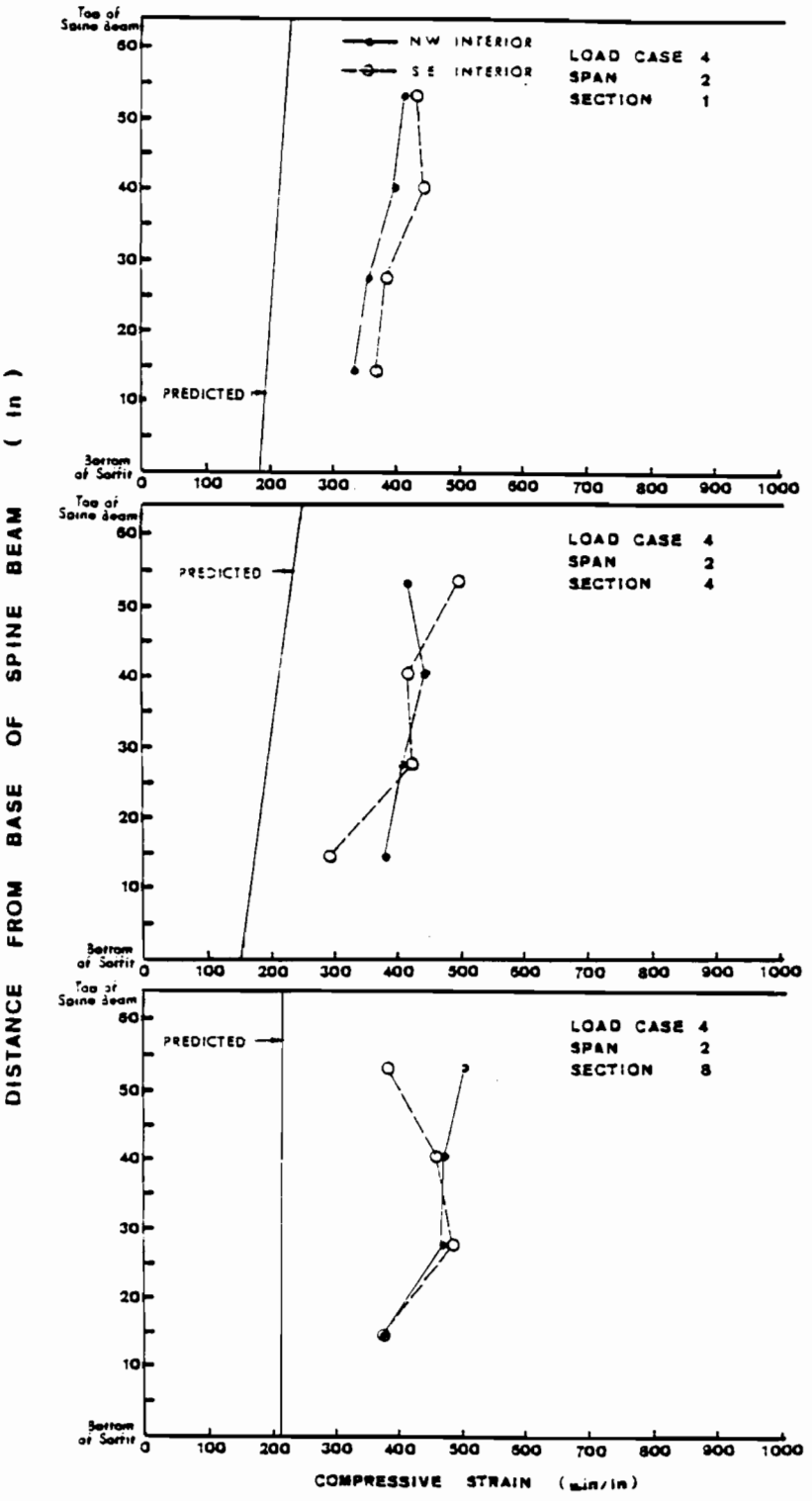

Fig. 4.12 Total strains over spine beam after deck placement

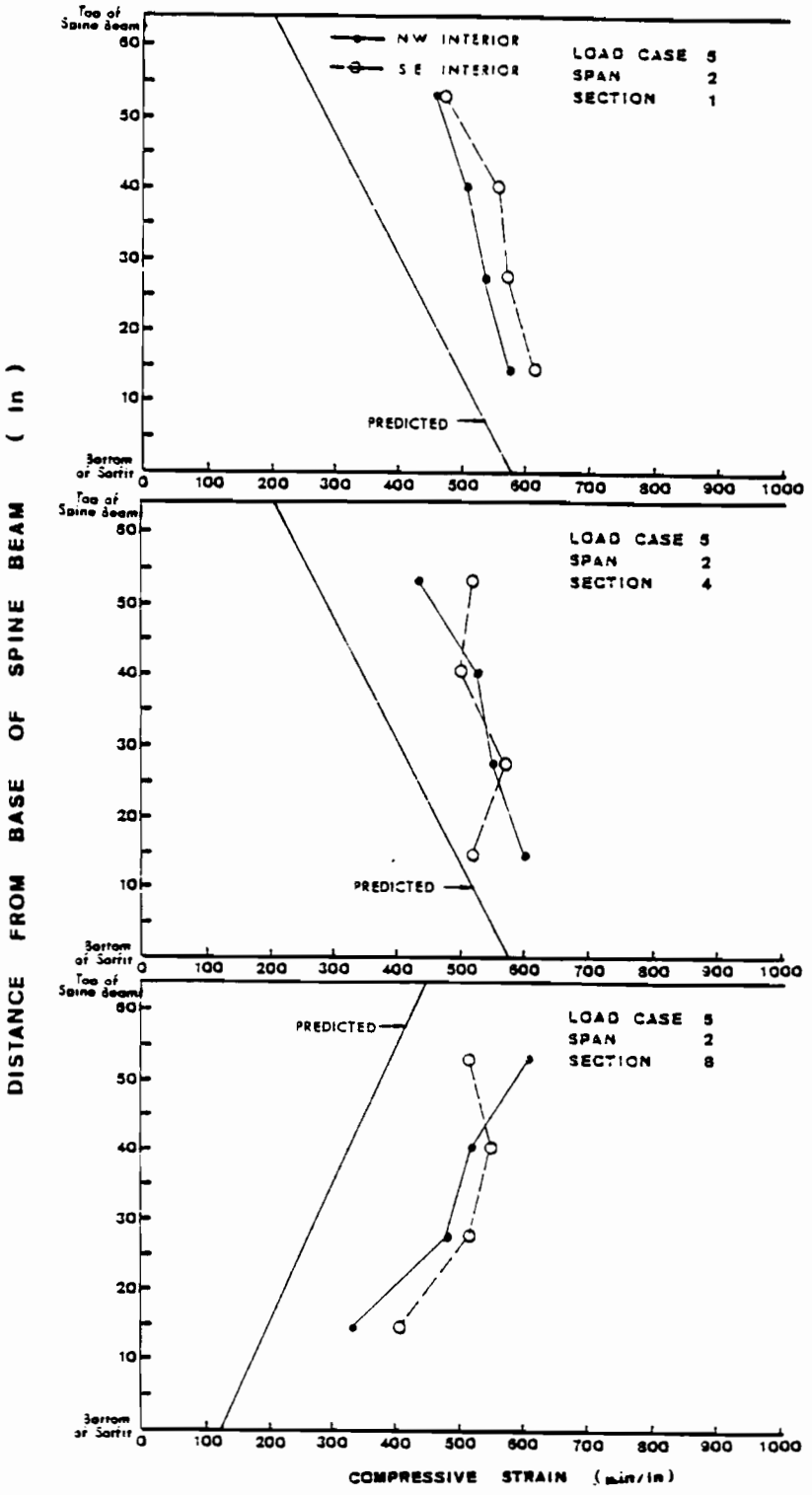

Fig. 4.13 Total strains over spine beam after second stage longitudinal post-tensioning

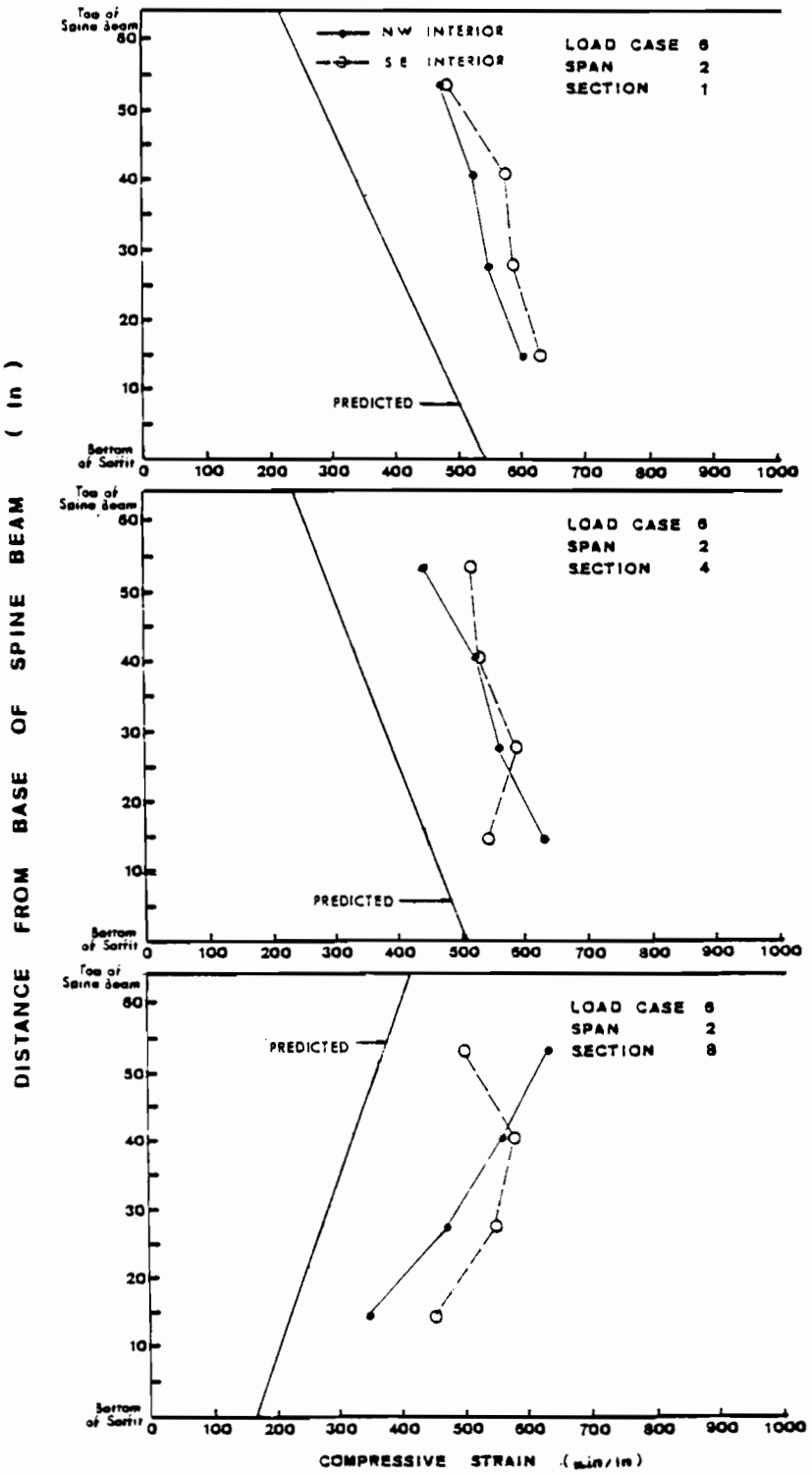

Fig. 4.14 Total strains over spine beam immediately after bridge completion

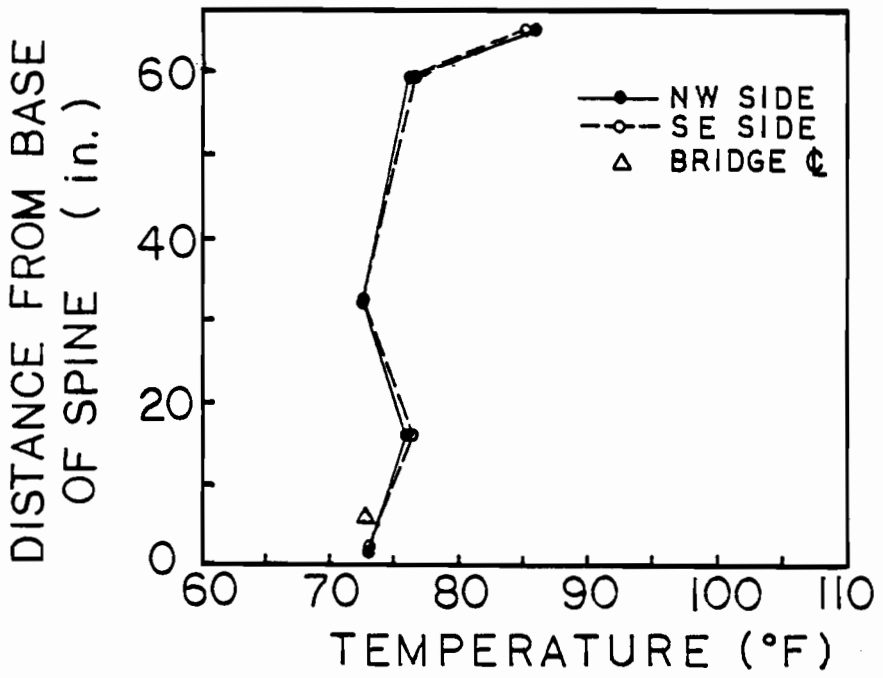

Fig. 4.15 Typical temperature distribution over depth of spine beam webs

to the tendons' unstressed condition. The measured tendon strains are presented in Table 4.1.

Most of the gages behaved erratically over the duration of the test period. Gage 6CW, which was on a center tendon, however, seemed to give reliable and consistent results. Upon initial stressing, it showed a strain of +5967 microstrains which, assuming a steel modulus of 27,500 ksi, corresponds to 164 ksi, or 0.61 F_{pu}. This is considerably lower than the $0.70f_{pu}$ level after seating specified in the original design drawings. Using Eq. (18-1) with K = 0.002 and L = 32 ft, the theoretical friction, or wobble, effect from the strain measurement location to the jacking end was calculated to be only 0.04 f_{pu}, or 11 ksi, which does not fully account for the difference. Throughout wing placement and completion of first-stage transverse post-tensioning, the strain level dropped off a very small amount. This was reasonable due to the effects of creep and shrinkage, etc. After casting the deck, the strain increased a small amount then subsequently decreased when the outer two tendons were stressed. Finally, the strain decreased substantially after placement of the parapet units on the wing tips. All of these trends were consistent with expected behavior although the strain loss due to parapet placement definitely appears excessive.

The remaining three tendons were at exterior locations in the three tendon groups in each wing. They were not stressed until second stage post-tensioning. These gages all exhibited a large amount of drift during multiple readings at the same load level, and the strain

TABLE 4.1 Results of transverse tendon strain measurements. [Tendon 6CW was stressed during first-stage post-tensioning (Column 1). Remaining tendons were stressed during second-stage operations (Column 5).]

TENDON LOCATION	STRAINS (μin/in) IMMEDIATELY AFTER FIRST STAGE WING STRESSING (CTR TENDONS) 5-13-83	PRIOR TO 1st STAGE STRESSING OF FINAL SET OF FIVE WINGS 5-18-83	ALL 1st STAGE STRESSING COMPLETED; PRIOR TO CASTING DECK 5-25-83	AFTER CASTING DECK; JUST PRIOR TO FINAL STAGE STRESSING 5-31-83	AFTER FINAL STAGE STRESSING AND GROUTING OF TENDONS 6-10-83	ALL RAIL UNITS IN PLACE; PRIOR TO CASTING CLOSURE STRIP 6-20-83
SOUTHEAST SIDE						
6CW	+ 5967	+ 5950	+ 5836	+ 5867	+ 5722	+ 5182
9LW	+ 8	+ 41	+ 27	+ 62	+ 5168 (DRIFTS)	+ 1429
NORTHWEST SIDE						
8LR	+ 496	+ 1284 (DRIFTS)	+ 976	+ 1159	+ 6714	+ 3056
9LR	- 18	- 2	- 24	- 76	+ 5042	+ 1524

readings fell off drastically between load cases. The results are not considered accurate and are presented only for completeness.

4.2 Service Load Tests

4.2.1 General. A service load testing commenced on Monday, July 11, 1983, and was completed the following Friday, July 15.

4.2.2 Analytical Model. Development of a finite element model computer analysis program capable of treating a wing girder bridge system like the Bear Creek bridge was undertaken by Professor C. P. Johnson and Mr. Pyong Soo Lee of The University of Texas at Austin in conjunction with the field testing program. An important verification of the analysis was obtained through comparison of the analytical results with those obtained from actual field measurements of service level live load effects. While it would be impractical to completely explain in detail the model and its operation herein, a brief description of its structure and underlying assumptions are presented.

The program, PUZF83, has a general capability which allows for the analysis of very complex bridge structures with arbitrary geometry and support conditions. The Bear Creek bridge was modeled using two-dimensional elements arranged in a three-dimensional global assemblage with six degrees-of-freedom (DOF) per node. The planar two-dimensional elements utilize both membrane and bending stiffness properties. The membrane stiffness types used were CLST (constrained linear strain triangle) and QM5 (quadrilateral membrane) while the bending stiffness type was HCT (Hseih, Clough, Tocher). These elements had been used

previously with success in analyzing the static and buckling behavior [8] and the thermal response [9] of highway bridges.

The program utilizes substructuring to a great degree whereby successive elements with similar properties are only analyzed once rather than on a separate basis. This results in vast savings in both computer and human resources. Fortran 66, a subset of Fortran 77, was used for all programming. All analyses were performed on the Cyber 750/170 system at The University of Texas at Austin.

Two detailed finite element meshes were developed for modeling the effects of bridge cross section, curvature, skew and torsion. The fine mesh contained 21 substructures, and the coarse mesh contained 19 substructures as shown in Fig. 4.16. Both had 8 repeated substructures. The former configuration resulted in 14,496 unknowns while the latter involved only 6,132. Comparison of results from both meshes showed good correlation, so the coarse mesh was normally used to improve computational efficiency. Further comparisons between computer results and hand calculations for a segment of a circular beam indicated that the small horizontal curvature in the actual bridge could possibly be neglected; however, it was included in the coarse mesh for design purposes. Primary consideration in modeling was given to maintaining moments of inertia comparable to those of the real structure and to limiting the element aspect ratios to 2:1.

Four load cases from the field tests were chosen for analysis. A modulus of elasticity, E_c, of 4810 ksi was used based on average cylinder strengths for the precast units and cast-in-place spine beam

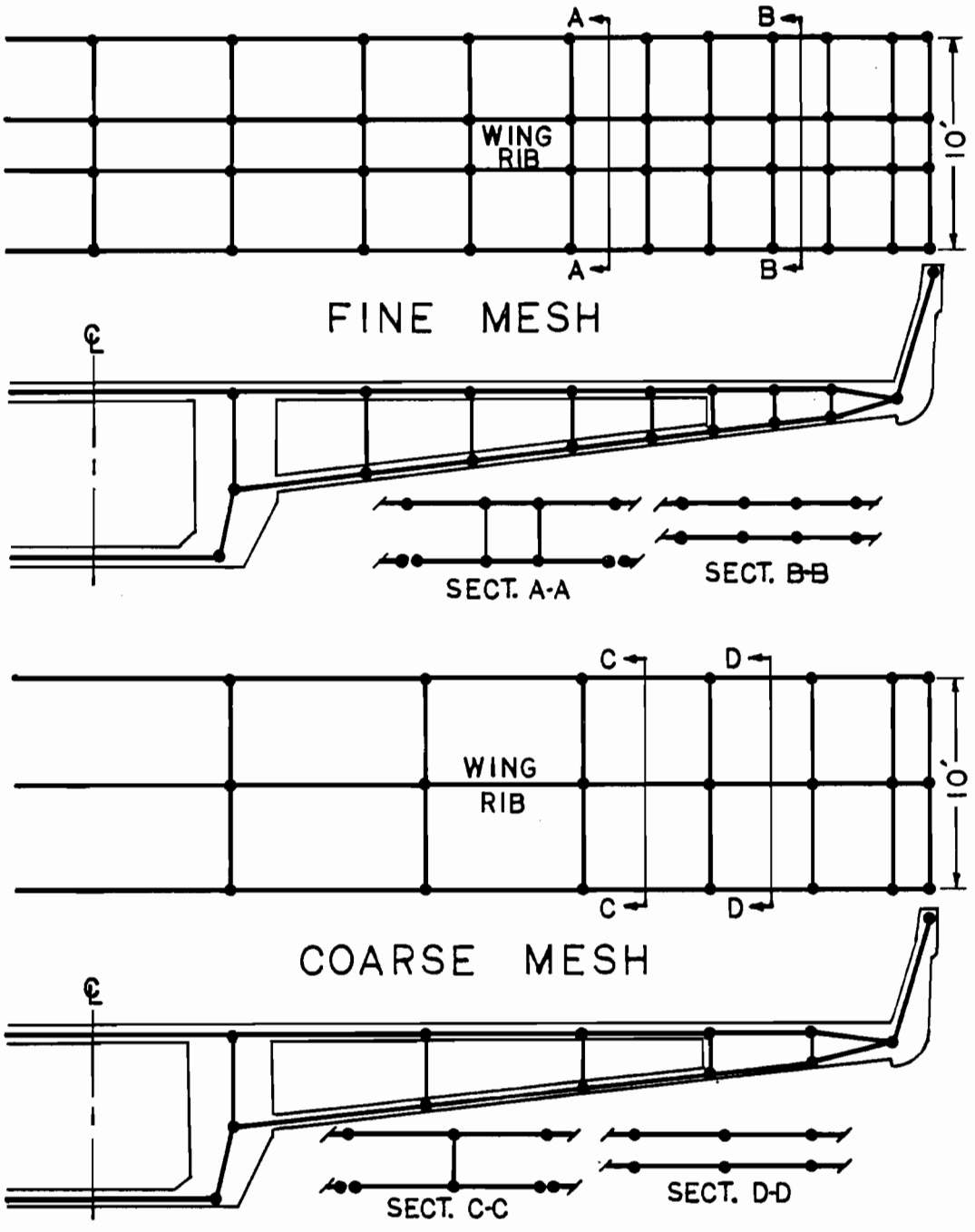

MESH	NO. OF GROUPS	NO. OF SUBSTRUCS.	NO. OF ELEMENTS	NO. OF NODES
FINE	7	21	3066	2416
COARSE	5	19	1246	1022

Fig. 4.16 Lee and Johnson finite element model of bridge

webs. The computed longitudinal deflections and slope profiles are compared later in this chapter with the measured profiles. Also included are the results from a coarse mesh finite element analysis furnished by the bridge designer, T. Y. Lin International. The load case used to compare measured results with the Lin model was 2N-22 which was similar with respect to the load location except that HS-20 rather than H-20 trucks were used by the designer. Also, an assumed concrete strength of 5000 psi was used by the designer. The Lin results have been factored by the truck load ratios and the concrete elastic modulus ratios for the purpose of comparison of both models and the test results.

4.2.3 Deflections. Sample longitudinal deflection profiles from the service load field tests are plotted in Figs. 4.17 through 4.22. The load case designations and corresponding truck locations are given in Fig. 3.11. Results of the finite element analysis are presented along with the test results. The bridge elevations were measured to 0.001 ft during service load testing using a vernier equipped rod and an automatic level. The maximum centerline deflection was 0.022 ft, or approximately 1/4 in., under a total load of 191.6 kips. The maximum wing tip deflection was 0.034 ft, or roughly 0.40 in., under an eccentric load of 126.6 kips. These deflection levels indicate that the bridge was quite stiff and displacements were relatively small compared to the load levels involved.

The measured deflection profiles suggest general trends which are consistent with predicted behavior. However, because deflections

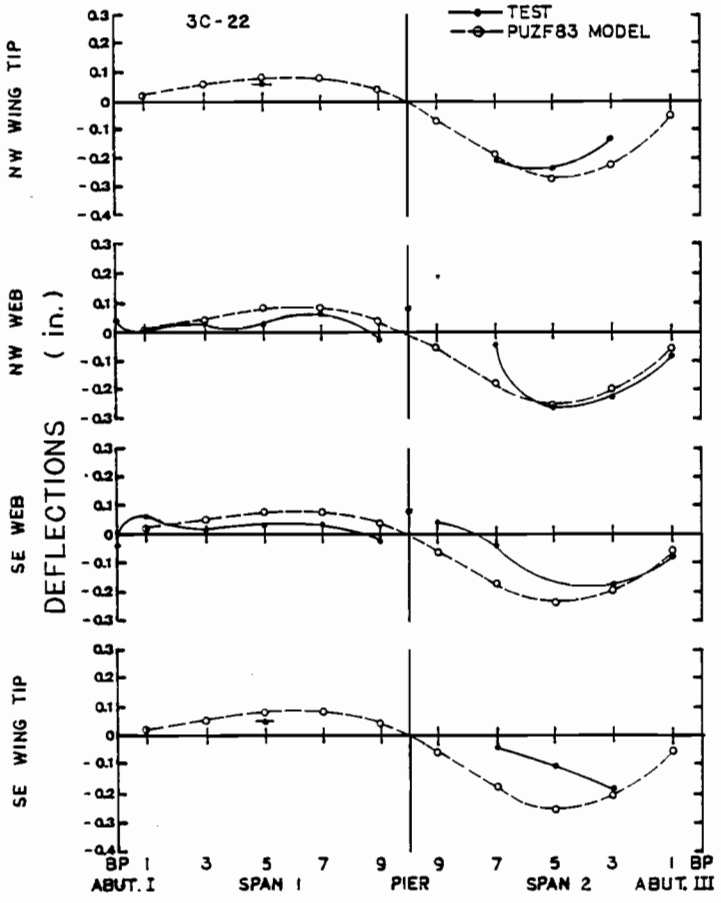

Load case 3C-22 (three trucks)

Fig. 4.17 Longitudinal deflection profiles resulting from trucks located at midspan of span 2

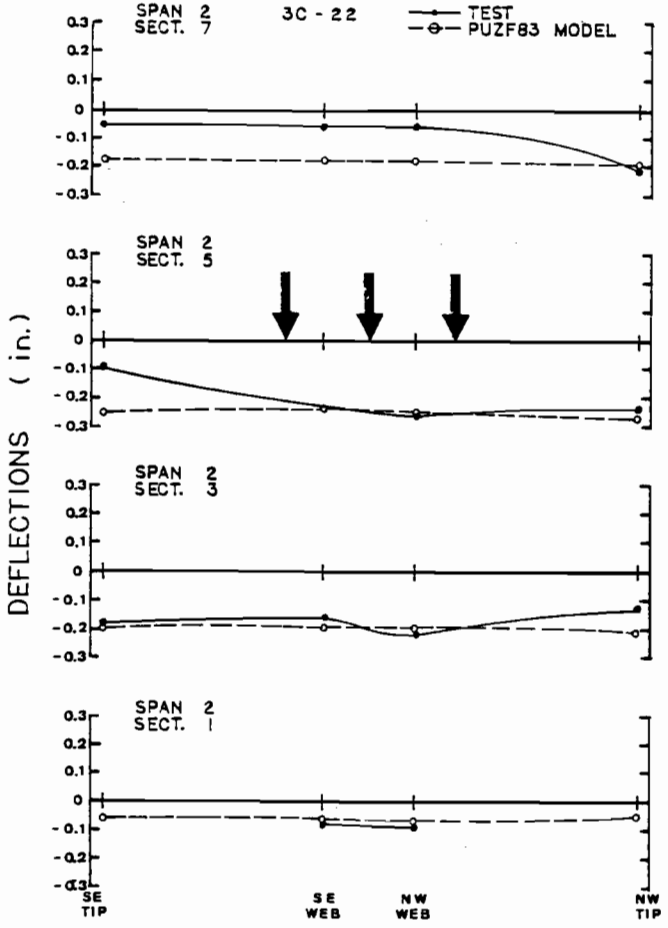

Fig. 4.18 Transverse deflection profiles resulting from load case 3C-22

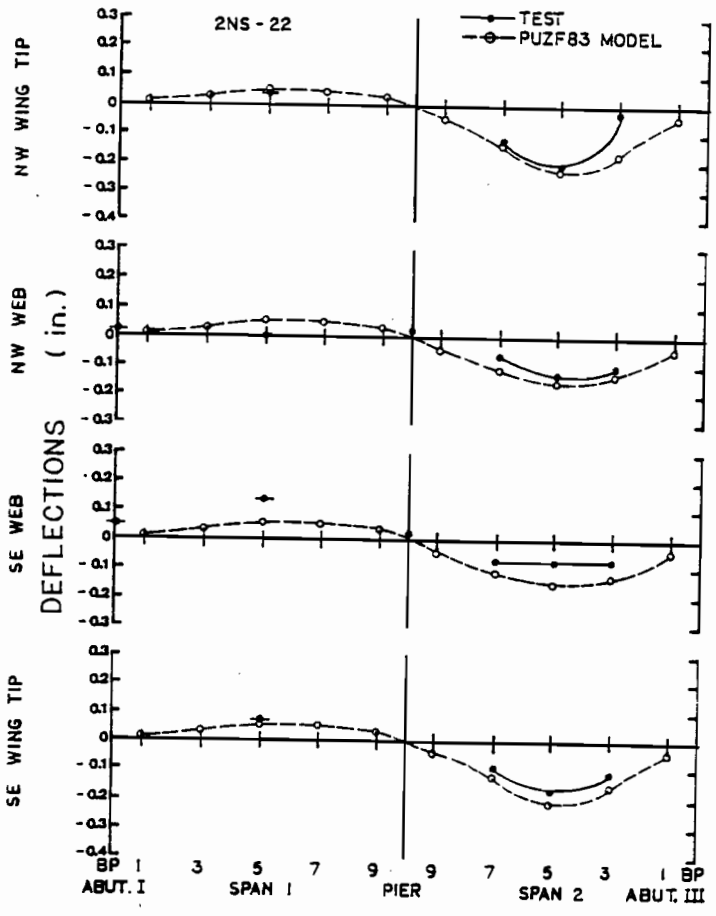

Fig. 4.19 Longitudinal deflection profiles resulting from load case 2NS-22

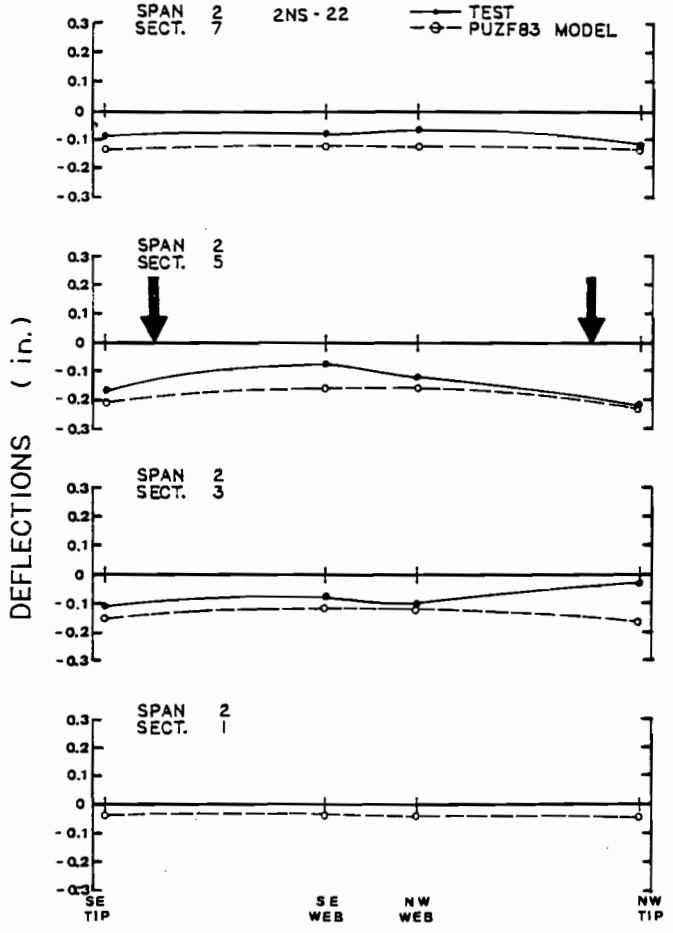

Fig. 4.20 Transverse deflection profiles resulting from load case 2NS-22

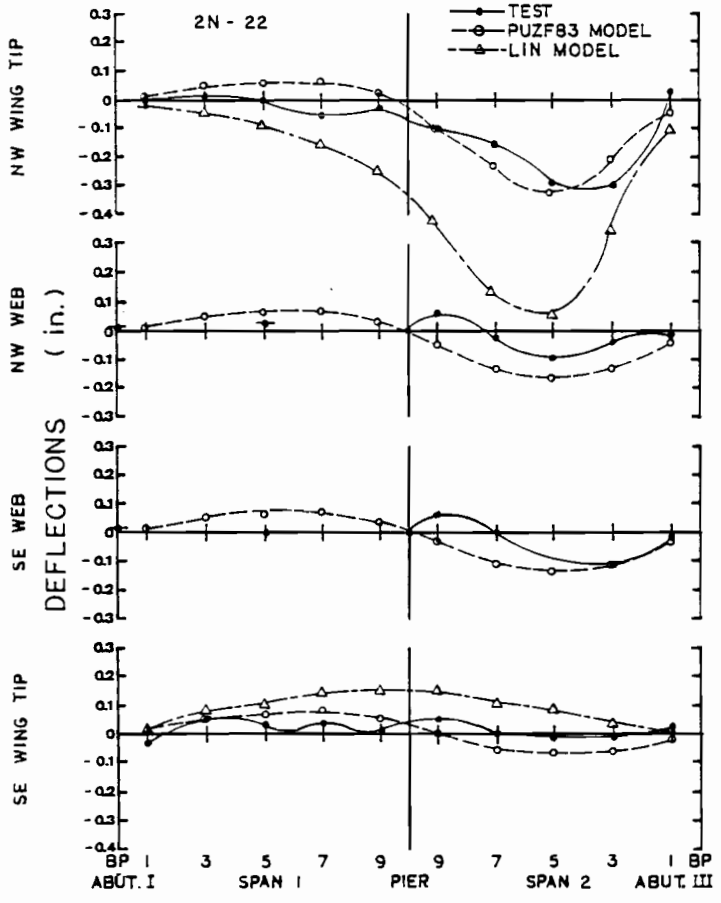

Fig. 4.21 Longitudinal deflection profiles resulting from load case 2N-22

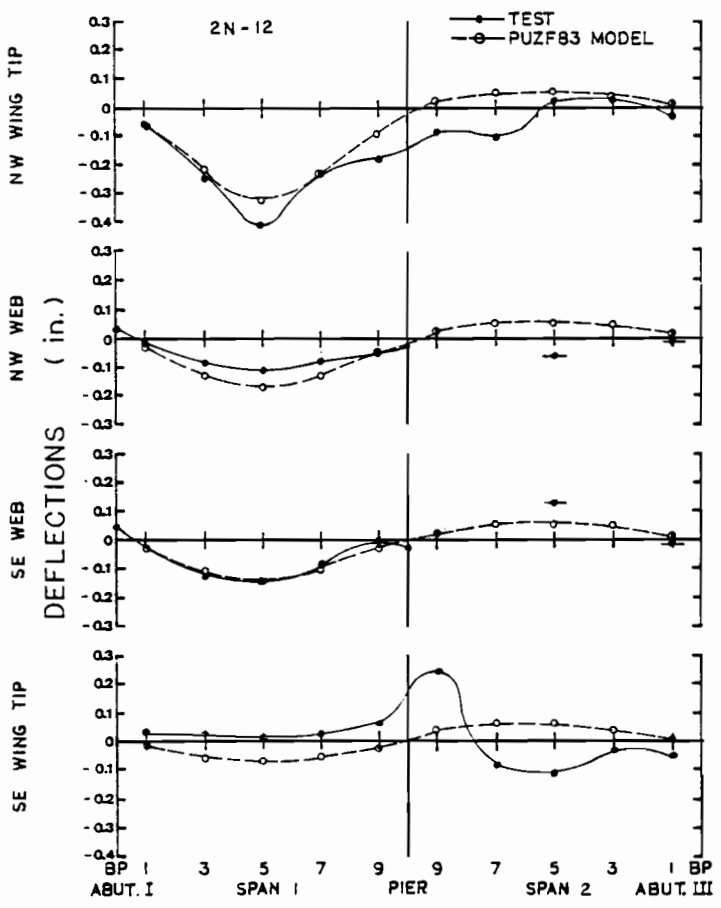

Fig. 4.22 Longitudinal deflection profiles resulting from load case 2N-12

were at such a low level relative to the precision of the measurement system used, there is a large degree of variability between some of the measurements. In many cases the profiles deviate sharply from a smooth curve. It should be kept in mind that the smallest division of 0.001 ft is approximately equal to 1/80 of an inch. Rod readings were taken from distances ranging between 20 ft and 110 ft, and even with the extreme care used, it was very difficult to read to the smallest division consistently. Thus, certain deviations in the deflection profiles should not be viewed as significant indicators of bridge behavior. The overall trends should be given more weight than peak values.

The deflection profile in Fig. 4.17, load type 3C, shows the results of these transversely symmetrically positioned trucks located at midspan of span 2 to produce maximum positive moment. The deflection profile for both wing tips and both spine beam webs are shown. Both the measured results and the results of the PUZF83 finite element analysis are presented. The maximum midspan deflection was measured as 0.26 in. over the northwest web. The results from the analysis predict generally larger deflections than were actually measured. The computed maximum deflection along the bridge centerline is approximately 30% greater than the measured value. As shown in Fig. 4.18, the model also predicts a fairly uniform transverse deflection profile with the wing tip displacements being 2% and 9% greater than the spine beam deflections on the northwest and southeast sides, respectively. The actual measured deflections across midspan of the loaded span show a large degree of twisting with greater displacements on the northwest side. Overall, the

PUZF83 model predicts a more flexible structure in the longitudinal direction than the test results indicate.

The results of load case 2NS-22 with a truck placed transversely symmetrically over either wing tip at midspan of span 2 is presented in Fig. 4.19. The deflection profile is consistent with those of the one and three truck load cases at midspan. Note that in load case 2NS-22 with trucks over the wing tips the wing tip deflections are substantially larger than the respective web deflections for either side of the bridge.

The deflection profiles for load case 2NS-22 calculated using PUZF83 are presented along with the measured profiles in both Fig. 4.19 and Fig. 4.20. Again, the computed deflections do not indicate twisting of the cross section and are substantially greater than the measured values. The computed maximum deflection of the spine beam exceeds the measured value by approximately 65%.

Figures 4.21 and 4.22 sample the results for load type 2N with two trucks located eccentrically along the northwest parapet. In these figures the loads are at midspan in spans 2 and 1. While generally good agreement exist6s between the measured and the PUZF83 Model, the predictions from the Lin analysis show substantial disagreement.

The deflected shape of the cross section under eccentric loads can be viewed as the superposition of two separate load effects for the spine beam webs plus a third effect for displacements at the wing tips. As shown in Fig. 4.23, the spine beam is subject to uniform cross-sectional displacements as calculated from an elastic analysis of a two

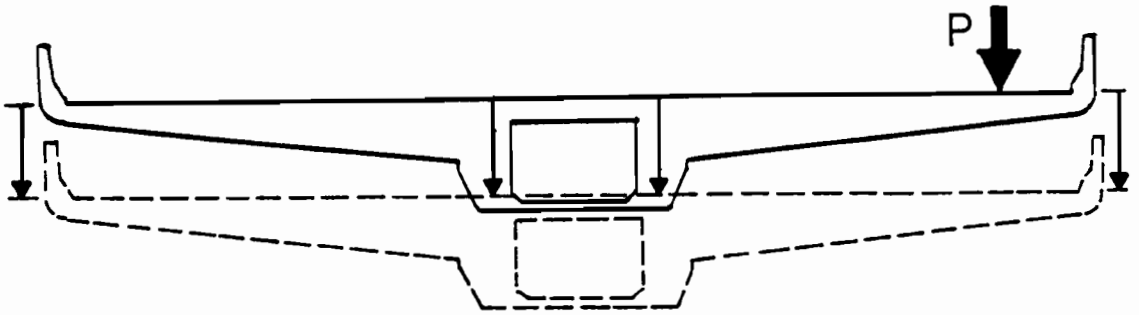

(a) Uniform cross-sectional deflection

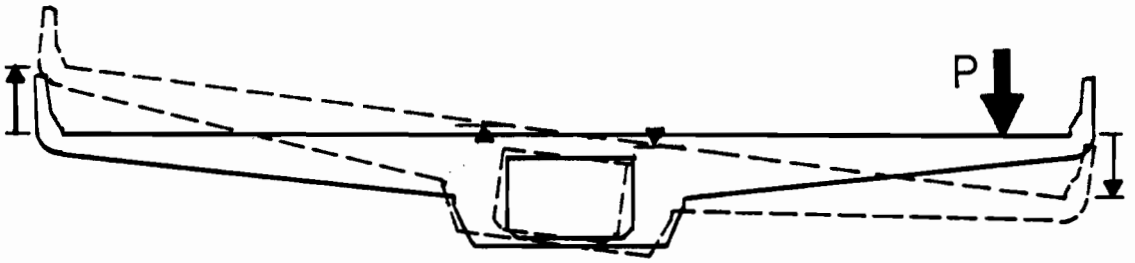

(b) Rotation due to eccentricity of loading and curved beam effects

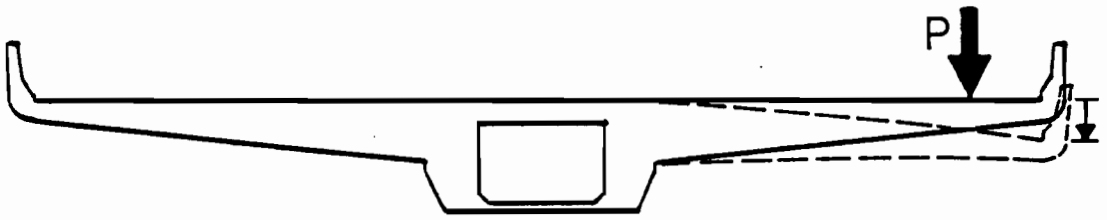

(c) Cantilever deflection of wing

Fig. 4.23 Total deflection resulting from the superposition of load effects

span continuous beam and displacements caused by rotation of the cross section due to eccentricity of load or curved beam effects. In addition to the above, the wing tips are also subject to displacements resulting from cantilever action. The transverse deflection profiles for the midspan and three-quarter point load cases in spans 1 and 2 are shown in Figs. 4.24 and 4.25. The rotation effect (Fig. 4.25) of the spine beam itself is evidenced by the greater deflection of the web on the loaded side than on the nonloaded side. However, due to the small distance of the measurement point from the bridge centerline (4'-2") and the relatively small displacement levels, the results are not always consistent. Because the wing tip measurement locations were approximately 26 ft out from the bridge centerline, the rotation effect is much more pronounced and consistent when viewing the entire profile from one wing tip to the other.

The transverse deflection profiles in Figs. 4.24 and 4.25 also show that measured deflections were generally larger in span 1 than span 2. This is particularly true at the loaded wing edge near the abutment due to the smaller bearing spacing at abutment I and the greater stiffness of the diaphragm beam at abutment III. The relatively short spacing of the bearing pads at abutment I allows greater rotation while the smaller transverse bending stiffness allows greater cantilever deflection. These effects are reduced as the load advances toward the center pier, and the difference in displacement levels between spans 1 and 2 is reduced. It also appears that as the load approaches the center pier, the nonloaded wing edge displaces upward more indicating

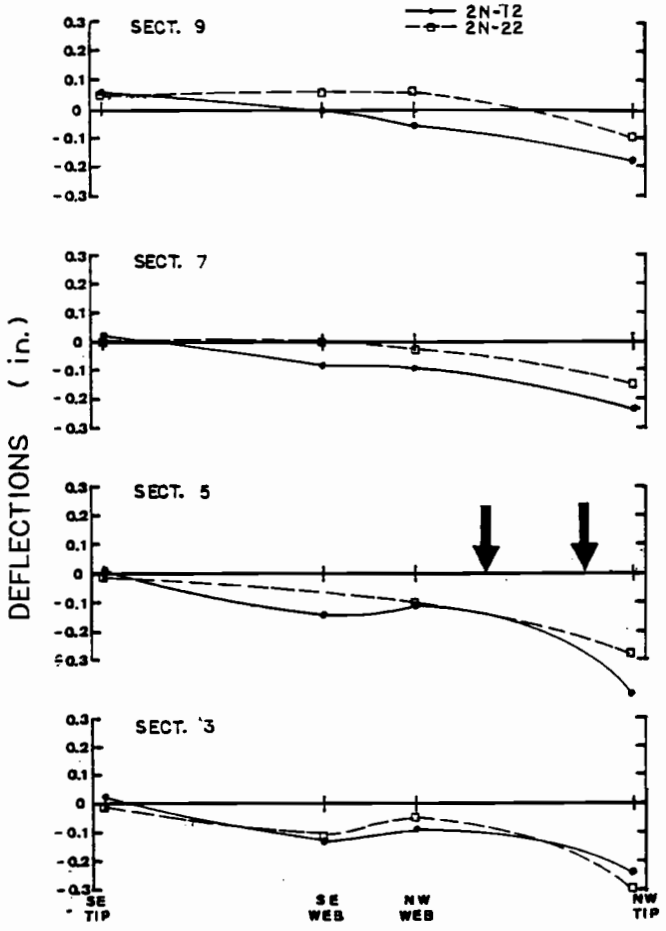

Fig. 4.24 Transverse deflection profiles resulting from eccentric, two truck loads at midspan

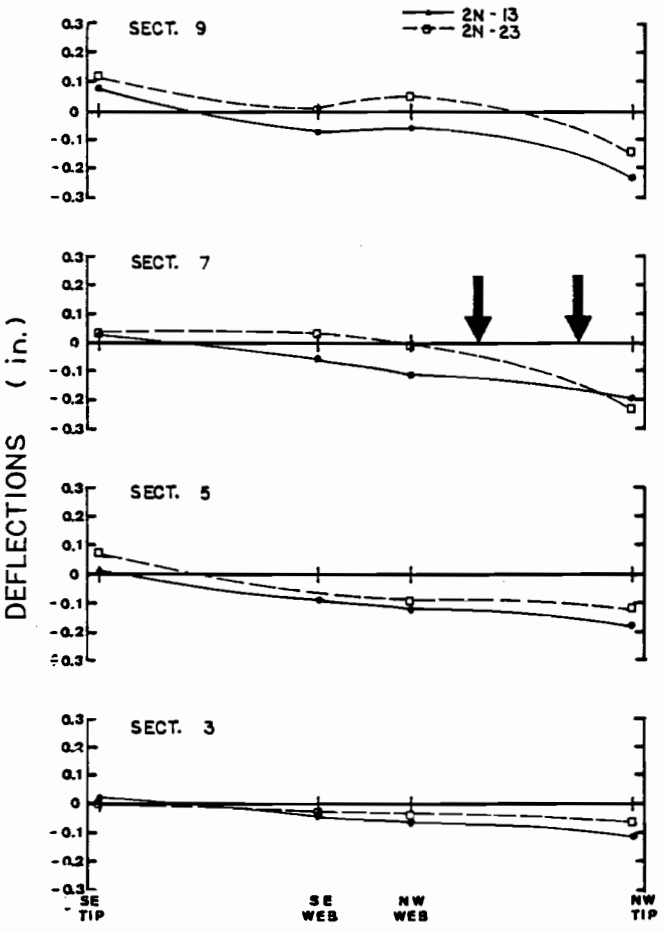

Fig. 4.25 Transverse deflection profiles resulting from eccentric, two truck loads at three-quarters span

increased rotation of the section. However, due to the inconsistencies in the span 1 plots along the nonloaded edge, this cannot be verified.

The deflection profiles predicted by the Lee and Johnson model, PUZF83, are presented with the measured results in Figs. 4.21 and 4.22 for the midspan loadings 2N-22 and 2N-12. In general, the FEM model overestimates deflections of the cross section by anywhere from 25% to 60% in the loaded span. This can also be seen in the transverse deflection profiles presented in Figs. 4.26 and 4.27. For the span 1 case, the predicted maximum deflection is approximately 25% greater than the measured value. In span 2 the predicted maximum is 50-60% greater. The PUZF83 model thus predicts a less stiff structure than actually exists in the longitudinal direction with regard to bending.

A comparison of the bending and rotational stiffnesses of the actual structure and the model seem to differ depending on which span is being considered. In span 2 (Fig. 4.26) the transverse deflection profiles are similar in shape which would indicate general agreement between the two sets of results regarding transverse bending and rotational stiffness. With the trucks loaded at midspan of span 1, however, the measured deflections over the loaded wing edge are greater than those predicted by the model (Fig. 4.27). The measured results for the nonloaded wing edge indicate less displacement than that predicted by the model. Thus, it appears that in span 1 the model predicts greater transverse rotational and wing bending stiffnesses than the actual behavior indicates. The larger measured values of the loaded

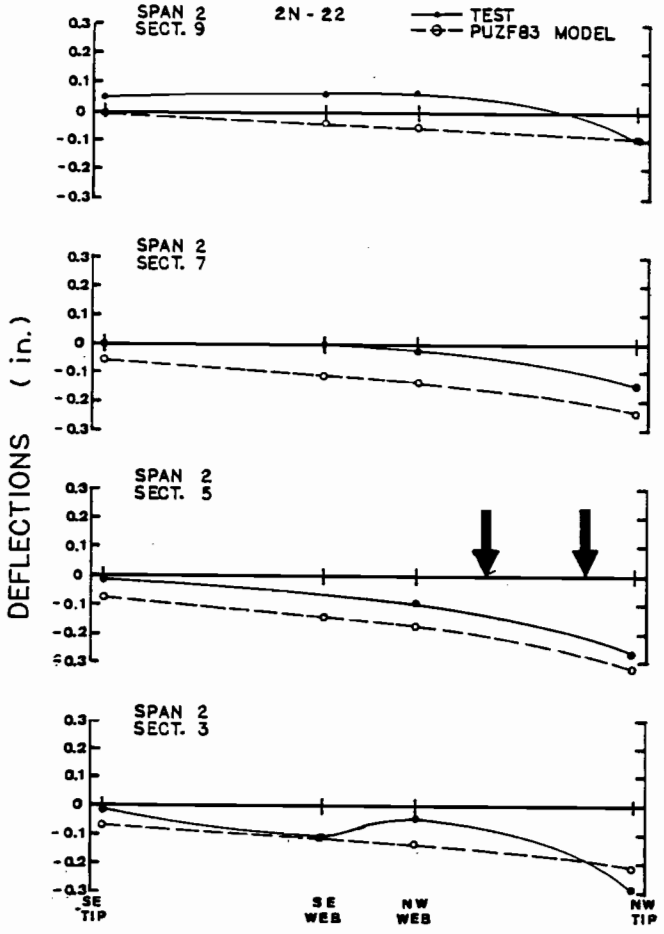

Fig. 4.26 Transverse deflection profiles resulting from load case 2N-22

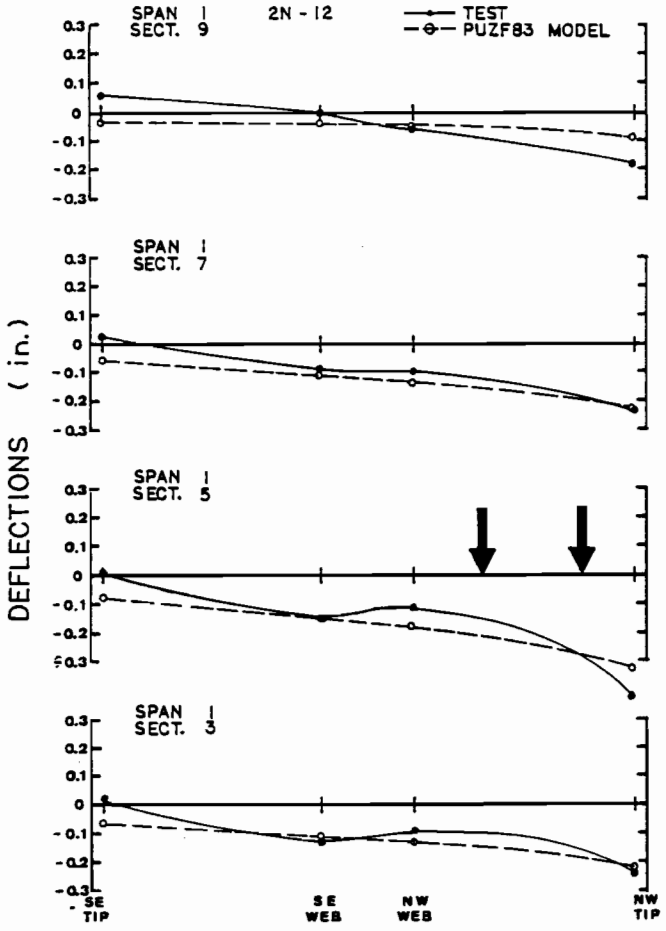

Fig. 4.27 Transverse deflection profiles resulting from load case 2N-12

wing edge deflections near abutment I show the effect of the closely spaced bearing pads at that location.

Also shown in Fig. 4.21 are the results of a finite element analysis provided by the designer, T. Y. Lin International. Their profiles have been scaled down to account for the different truck weights and the different moduli of elasticity between the design and measured concrete strengths. The difference in truck type and loading position between the Lin model and the field tests are shown in Fig. 4.28. Two trends are apparent in the Lin analysis: (1) The analysis greatly underestimates the stiffness of the bridge, and (2) this underestimation of stiffness is particularly evident in the transverse direction where the wing tip deflection profiles are positive or negative along the entire length of the bridge. The Lin analysis results indicate substantially less torsional and transverse bending stiffness than seems present in the actual structure and possibly a very large misestimate of the overall centerline deflection. Only wing tip deflections were furnished.

4.2.4 Longitudinal Strains. Longitudinal strains were measured only during the noneccentric, flexural loading cases where trucks were placed symmetrically about the longitudinal centerline. Strains were measured around the spine beam cross section at the locations indicated previously in Fig. 3.1. Gage readings were referenced to frequent "no load" readings then converted to differential strains. This helped eliminate any effects due to temperature or other environmental factors.

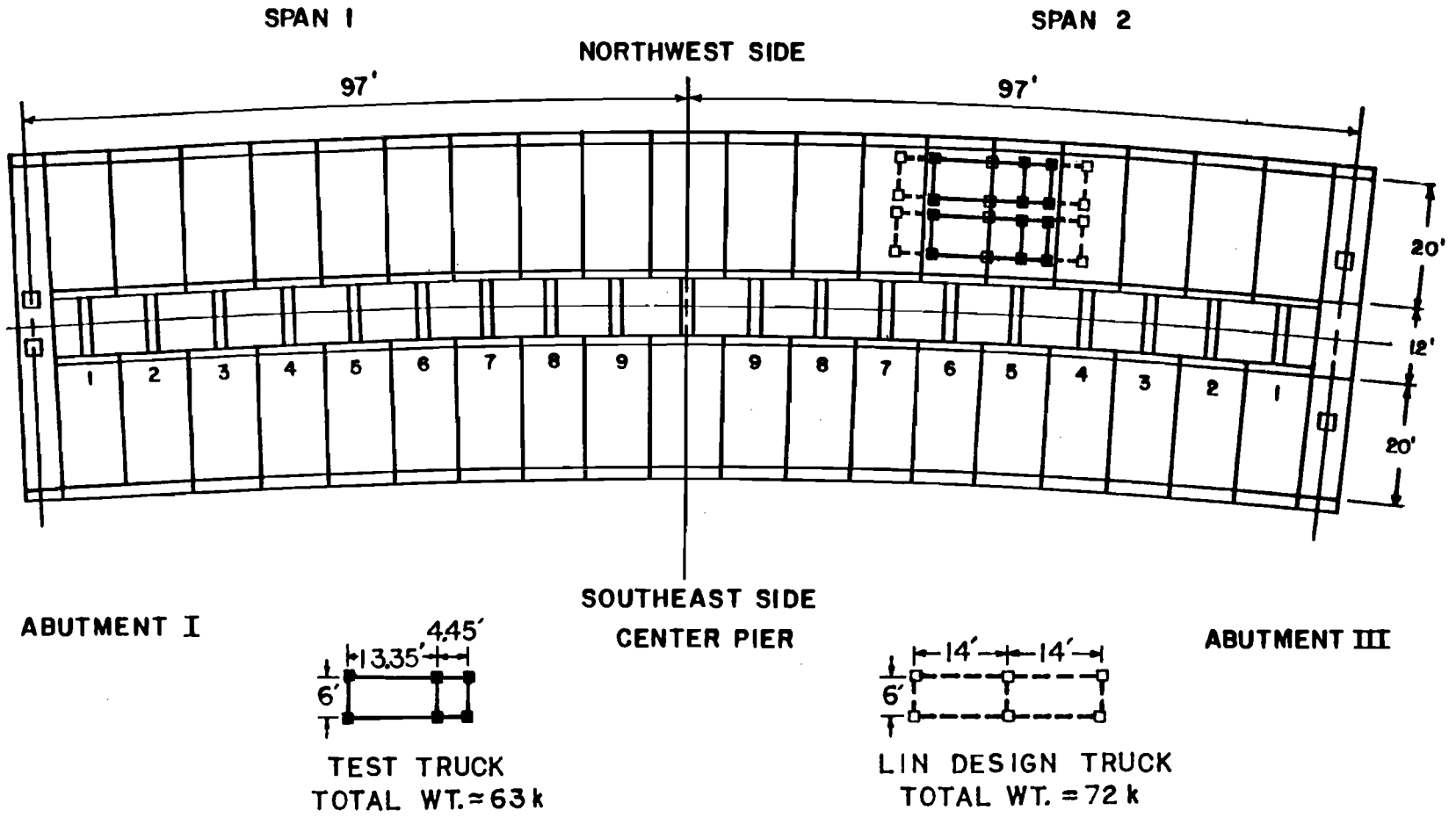

Fig. 4.28 Comparison of loading patterns between test program and Lin analytical model for load case 2N-22

Sample live load strains for the three truck loading cases are plotted in Figs. 4.29 and 4.30 as distributions over the depth of the spine beam. Other load case results are given in Ref. 2. All strains were measured on the interior surface of the box. The live load strains are all small, indicating a relatively stiff structure in regard to longitudinal bending. Also plotted in Figs. 4.27 and 4.30 are the M_y/I strain distributions calculated from a simple elastic analysis based on the cross section in Fig. 4.2c.

Figures 4.29 and 4.30 show strains resulting from three truck loadings placed symmetrically about the longitudinal axis. The measured strains appear to be somewhat smaller in general than the calculated strains. This can best be seen at section 4 where the measured strain distributions lie within the calculated strain profile (i.e., less rotation away from the vertical axis in the measured profile). This result, however, is partially masked by the inherent scatter in the measurements, so the comparison is not really quantifiable.

4.2.5 Temperature Gradients. Temperatures were measured in conjunction with each load case at the location indicated in Fig. 3.3 near the middle of span 1. Aside from temperatures on the top surface of the deck, the temperature distributions were approximately linear with the top of the spine beam 5° to 7° warmer than the bottom. The deck surface itself gradually warmed up as the day progressed. The temperatures there changed substantially over the length of the day, but the remainder of the temperatures over the depth changed less and at a more even rate between them. The maximum deck temperature measured was

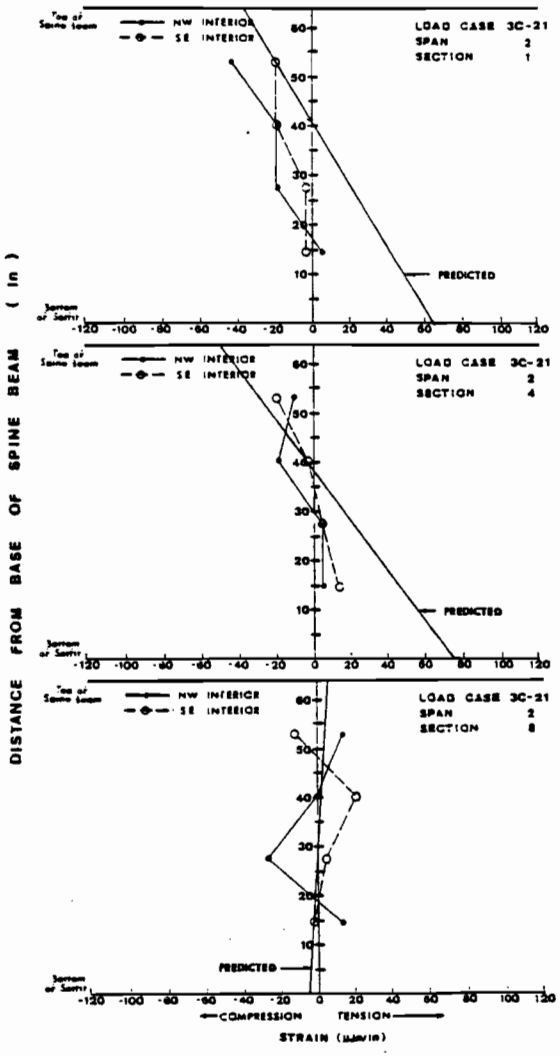

Fig. 4.29 Strains over spine beam resulting from load case 3C-21

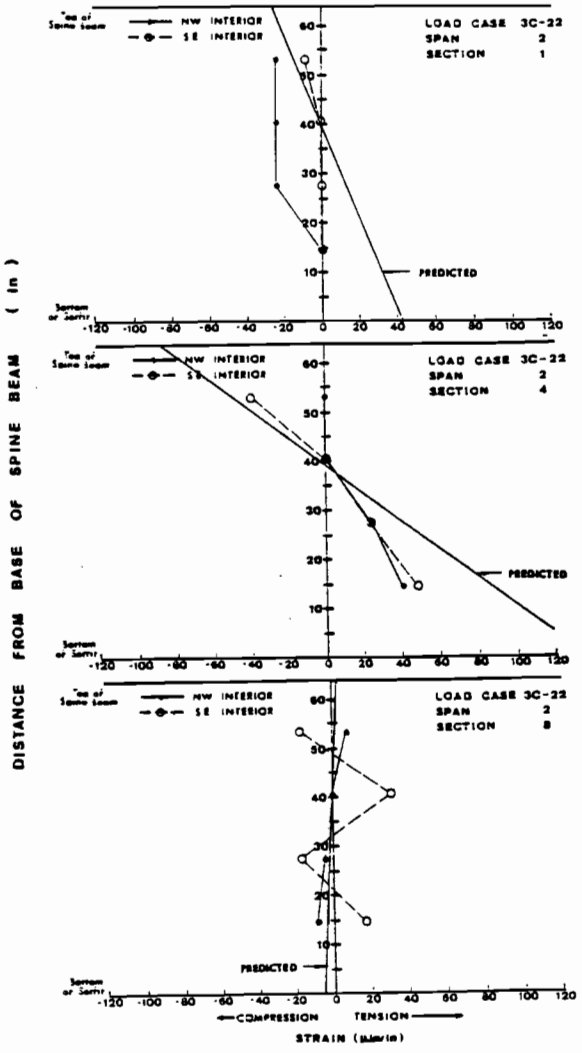

Fig. 4.30 Strains over spine beam resulting from load case 3C-22

112° under direct sunlight on the first day of testing. Temperatures on the southeast side of the bridge were generally slightly higher due to direct radiation from the sun. Figure 4.31 shows the evolution of temperature over the cross section for the second day of testing.

Based on the observed temperature variations during construction and during the service load testing program, it appears that the effect of a 9°F temperature gradient between top and bottom surfaces as proposed in Ref. 10 would be adequate for design purposes. An additional 15°F gradient between the top of the deck and the bottom surface of the top flange should be sufficient to account for the temperature variations resulting from the direction radiation on the deck surface.

4.2.6 Differential Slip. Slip between cast-in-place and precast sections was measured using the slip wire techniques described in Chapter 3. The dial gages used had a sensitivity of 0.001 in. The only movement registered on the dial gages during the test program were an occasional 0.0005 to 0.001 in., or 1/2 to 1 dial division. This is not significant, and it is believed that no actual slip occurred between any elements under design service loads. The results indicate no change between readings, and thus it was not necessary to include the actual data in this report.

4.2.7 Cross-Sectional Distortions. Cross-sectional distortions of the spine beam diagonals were measured under eccentric loads at the locations shown in Fig. 3.7. Displacements were measured using dial gages with a 0.0001 in. sensitivity. The results are

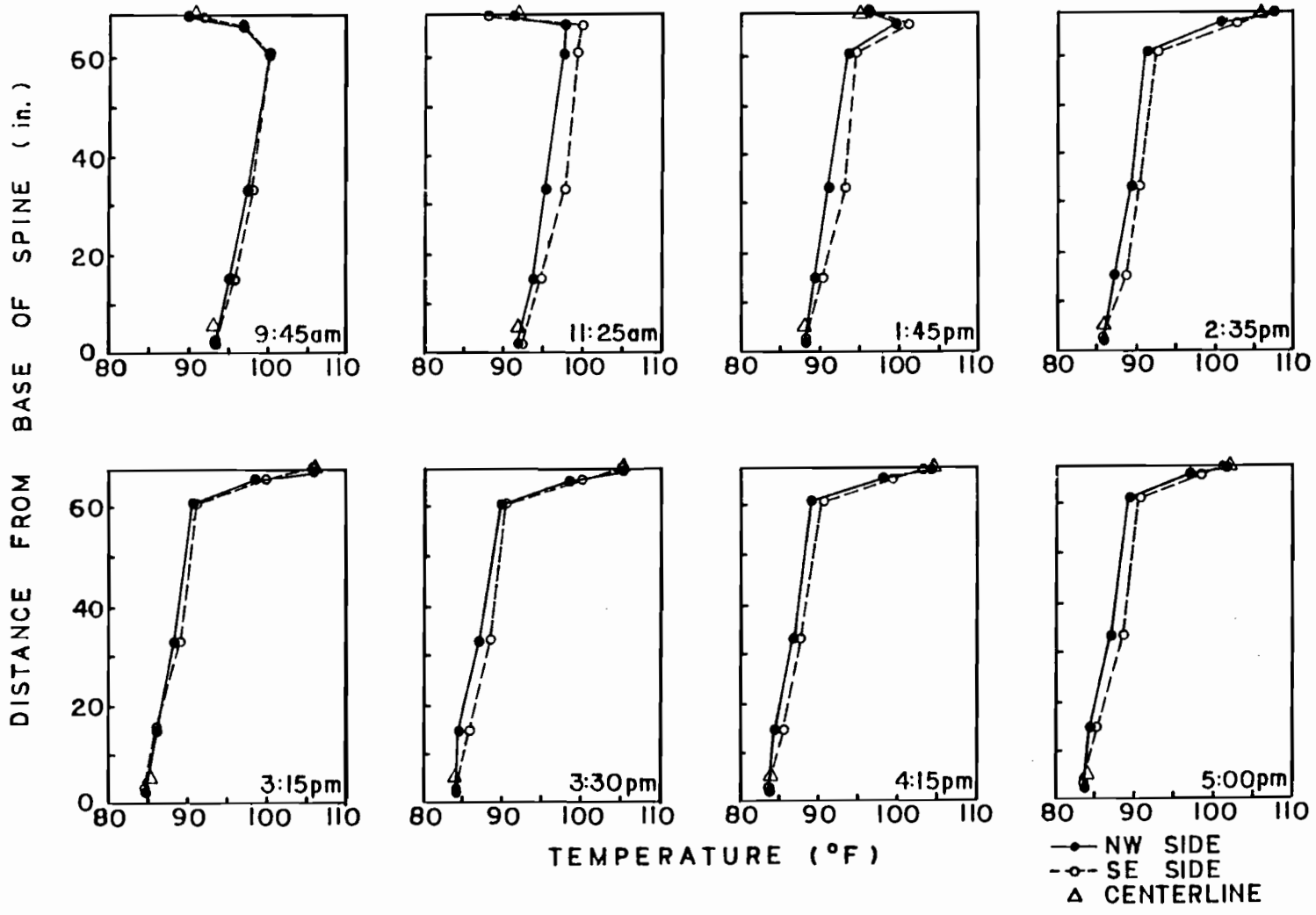

Fig. 4.31 Progression of temperature gradient over spine beam webs for typical testing day

presented in Figs. 4.32 and 4.33 as diagonal displacements vs. gage location for a particular load case. They are also shown as diagonal displacements vs. load position for a particular gage in Figs. 4.34 and 4.35. In both cases displacements are plotted relative to a "no load" reading taken both prior to a particular set of load measurements and upon completion of that same set of measurements. Theoretically, the two sets of "no load" readings should be the same for displacements in the elastic range. However, as can be seen from the plots, there is some variation between the two sets of readings, particularly in span 1. This may have been due to extra play in the distortion meter or perhaps to some friction in allowing the dial gage to return to its original configuration after unloading. At any rate, the displacements were at such low levels as to be of little consequence in determining the exact distribution of twist. A positive reading on the displacement plot indicates compression of the dial gage tip, or a shortening along the diagonal along which the gage is located. A negative reading indicates a lengthening of that same diagonal.

The plots of displacement versus gage position (Figs. 4.32 and 4.33) show that the largest movement occurred near the abutment in span 1. This is logical since the loaded wing side is allowed to deflect a great deal due to the torsionally simple support condition. This causes a greater degree of cross-sectional distortion near this end of the bridge. The displacement is such that the diagonal with its upper corner on the loaded side is elongated (shearing deformation resulting from twist). This displacement is a maximum with the truck directly

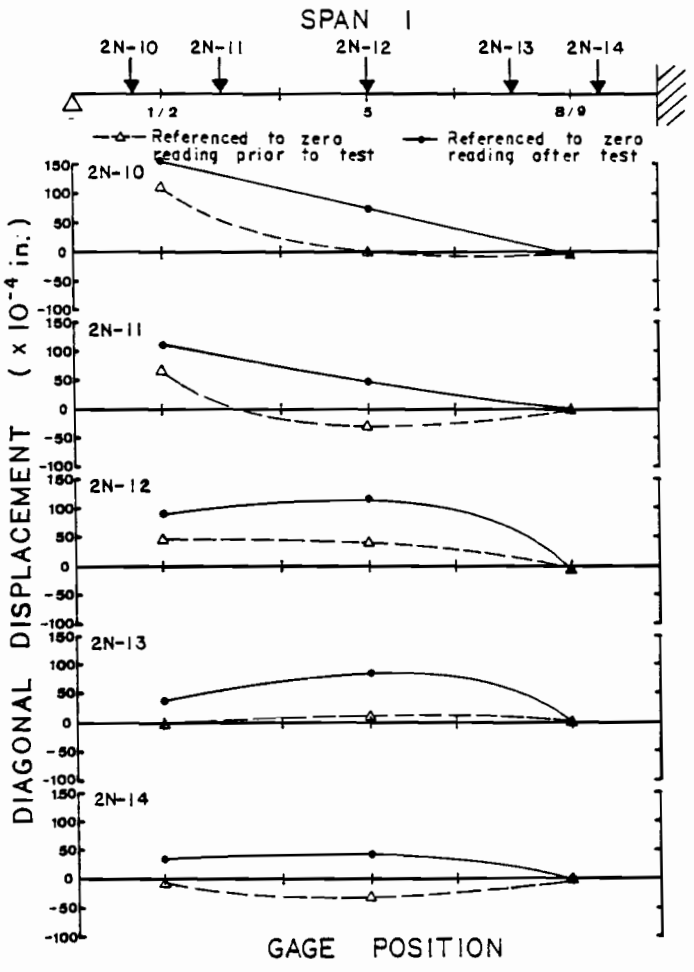

Fig. 4.32 Diagonal displacement of spine beam cross section along span 1 for various two truck eccentric load cases

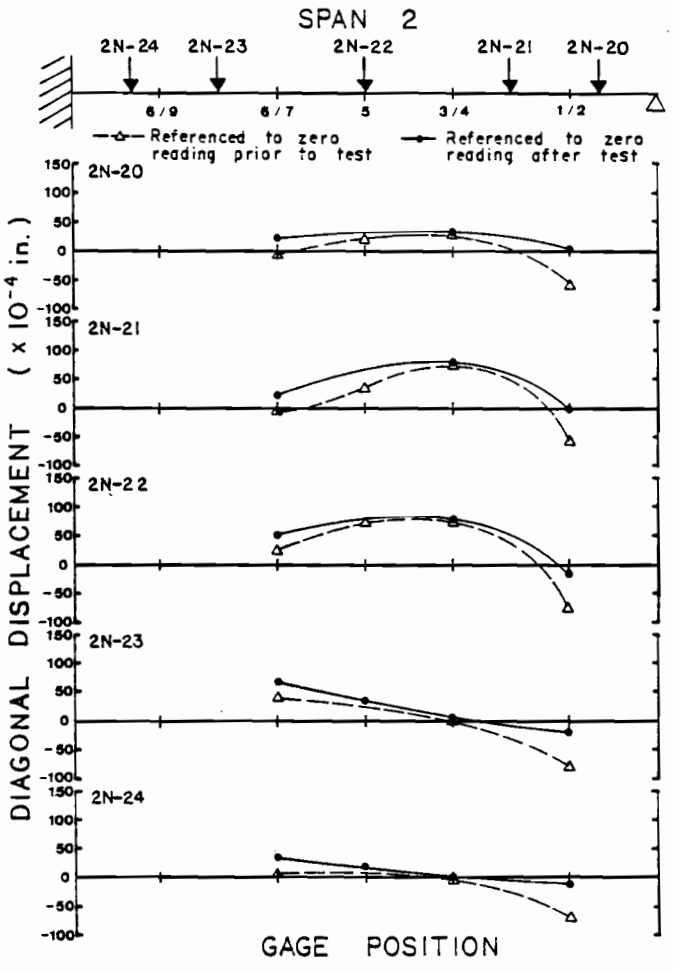

Fig. 4.33 Diagonal displacement of spine beam cross section along span 2 for various two truck eccentric load cases

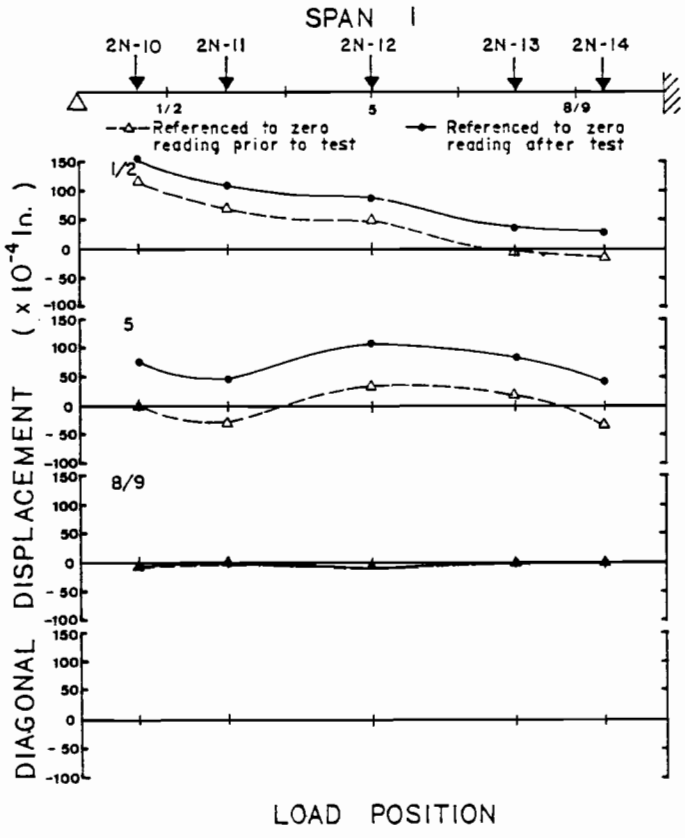

Fig. 4.34 Variation in diagonal displacement of spine beam cross section with load position for each instrumented section of span 1

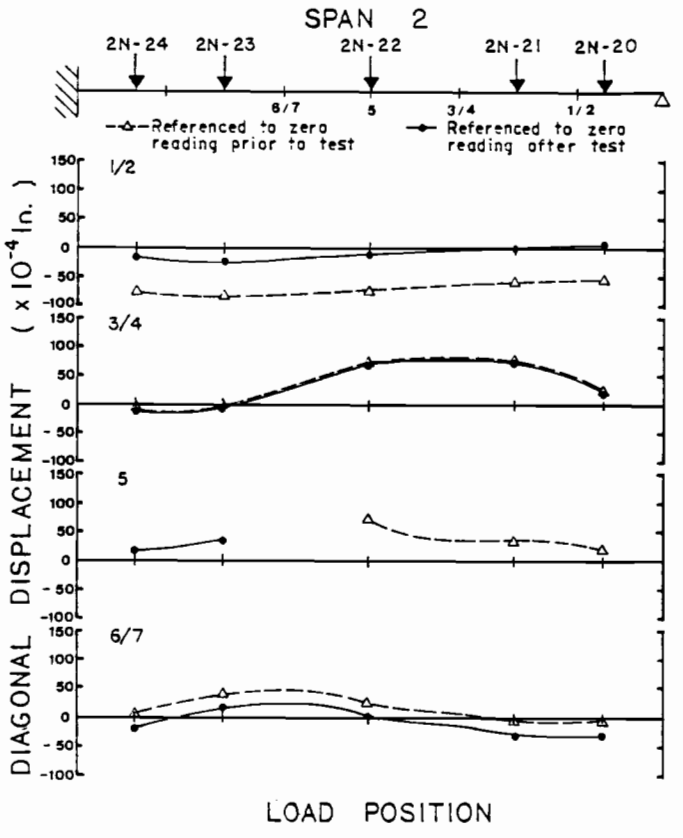

Fig. 4.35 Variation in diagonal displacement of spine beam cross section with load position for each instrumented section of span 2

over the gage and decreases as the truck moves toward the center pier. In fact, as Figs. 4.34 and 4.35 indicate, the maximum displacement for a particular gage in either span occurs with the truck located over that gage.

At the abutment III end of the bridge, rotation was restricted by the heavy diaphragm beam and the wide spacing of the bearing pads. The measured results indicate a cross-sectional distortion opposite that ordinarily caused by torsion (opposite that at abutment I). This diagonal displacement gets somewhat larger as the truck is moved toward the center pier. For the gages near midspan, Fig. 4.35 indicates twist induced distortions as expected.

The gage located near the center pier in span 1 indicates very little distortion. This was due to the increased stiffness of the pier and the solid pier cap. Although no gage was located adjacent to the pier in span 2, extrapolation from Fig. 4.33 indicates similar behavior there as well.

4.2.8 Differential Slopes. Differential slopes were measured for each load case at the locations indicated in Fig. 3.7. The slope at each of these locations was measured prior to and during each particular load case. The difference between the two readings gives the change in elevation between the two bearing points over an 8 in. gage length. This change in elevation is then converted to a change in slope at the particular measurement location. Sample results are presented as differential slope versus the gage location along the direction of measurement in Figs. 4.37 through 4.40. Plotted along with these

results are the results of the PUZF83 finite element analysis. Complete measurement results are given in Ref. 2.

The sign convention used in plotting the differential slope profile is shown in Fig. 4.36 and is that used in an ordinary mathematical treatment. That is, sloping upward to the right is positive and downward to the right is negative. As a further aid, the slope measurements are plotted as qualitative deflection curves along with the slope profiles in Figs. 4.37 through 4.40. In viewing these curves, it should be remembered that the magnitudes of the deflection profiles themselves are not accurate and that the relative values of the slopes at the measured points are what is important.

Figures 4.37 and 4.38 present both the longitudinal and transverse slope profiles for load type 2N with two trucks placed eccentrically along the northwest wing of the bridge. The transverse slopes were measured on the loaded side of the bridge. The longitudinal slope profiles are in general qualitative agreement with expected results. Zero slope readings occur in the near vicinity of the loaded regions which indicates maximum deflections at these locations. This, too, is logical on the basis of elastic beam theory. Maximums and minimums on the slope profile (zero slope on the slope curve) indicate points of inflection on the curve of deflected shape.

The results of the PUZF83 model analysis are presented along with the measured results in Figs. 4.37 through 4.40. In general, the computer results predict larger slope changes in the longitudinal direction than were actually measured. This would indicate that the

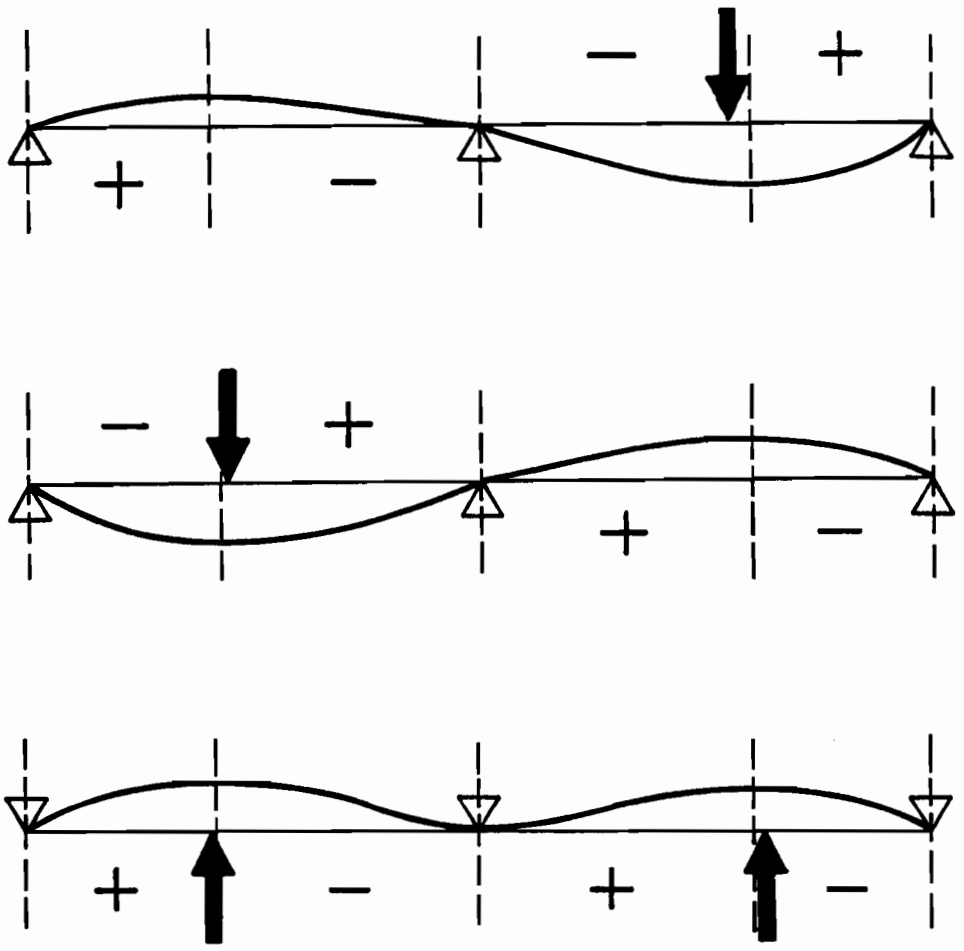

Fig. 4.36 Sign conventions for slope measurements under typical loading conditions

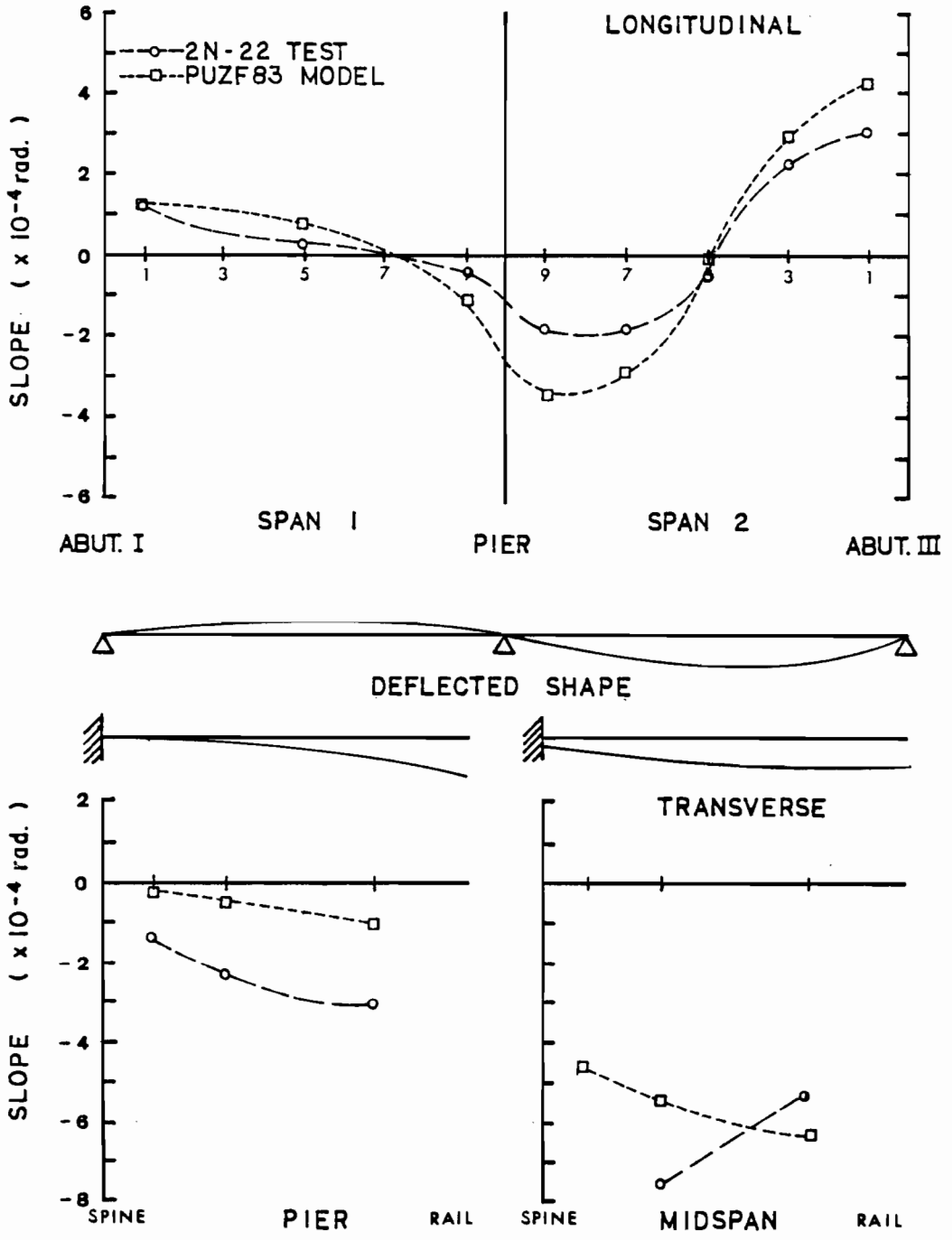

Fig. 4.37 Differential slope profiles resulting from load case 2N-22

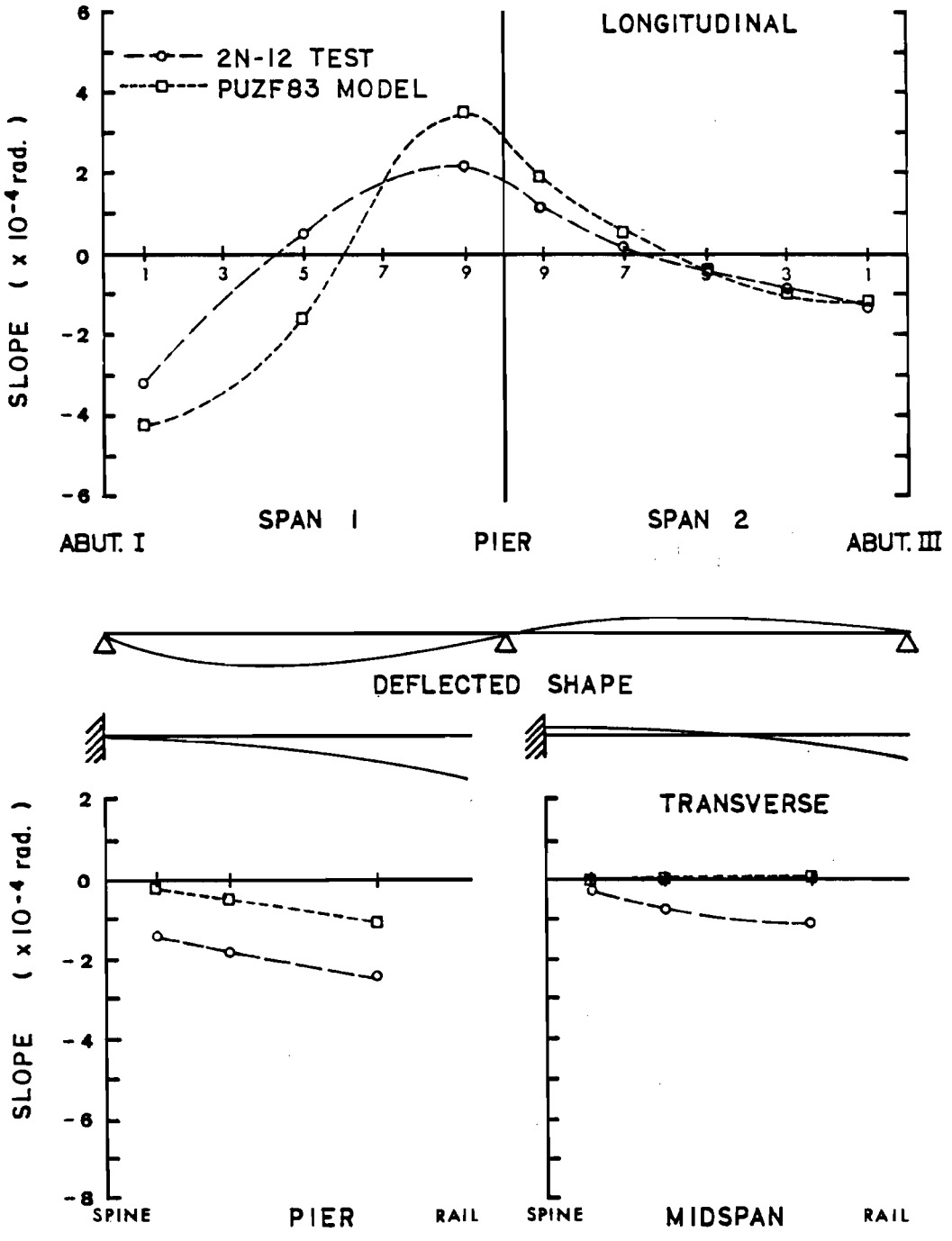

Fig. 4.38 Differential slope profiles resulting from load case 2N-12

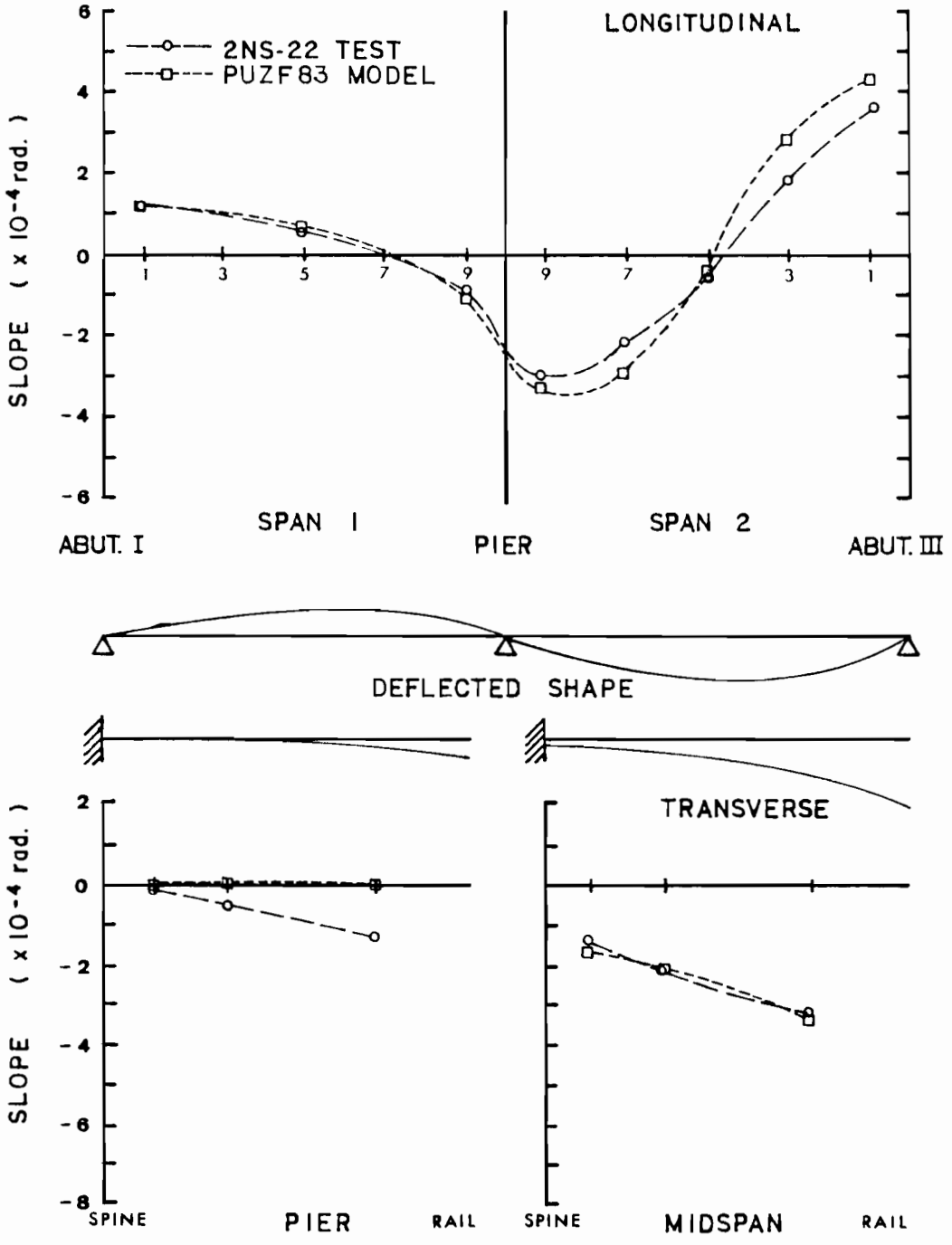

Fig. 4.39 Differential slope profiles resulting from load case 2NS-22

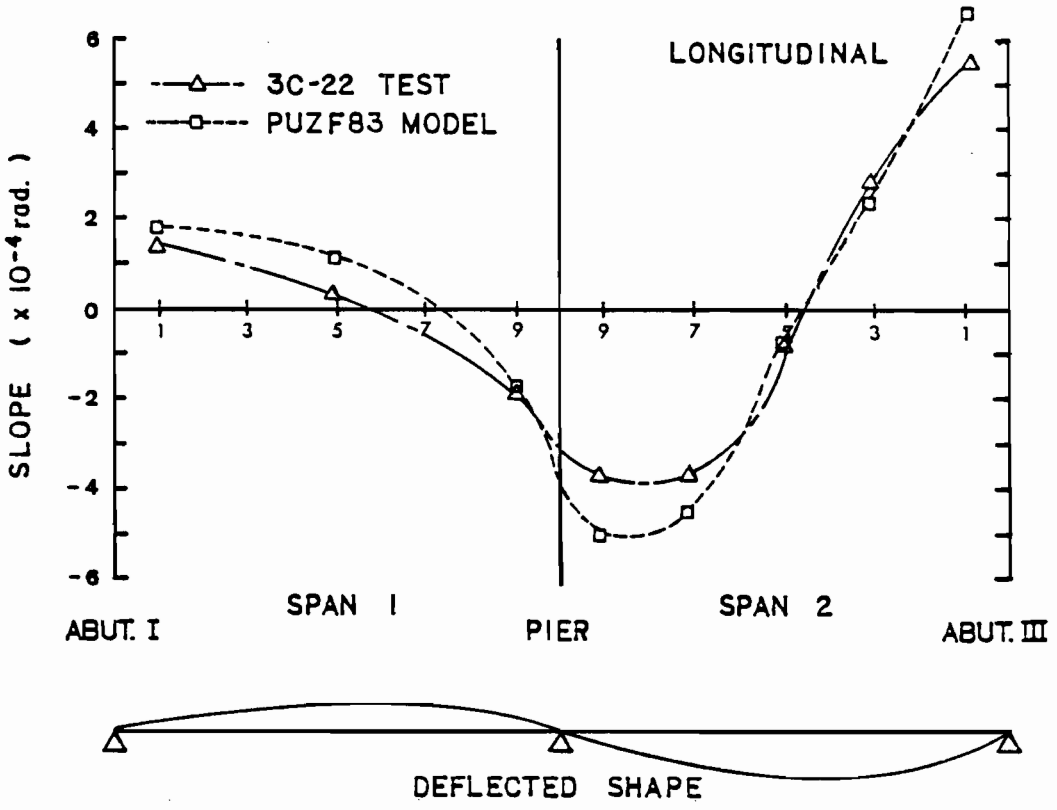

Fig. 4.40 Differential slope profiles resulting from load case 3C-22

bending stiffness of the actual structure is greater in the longitudinal direction than that assumed by the model. The degree of slope change overestimation is dependent on the location along the bridge. In the loaded region the calculated maximum slopes are anywhere from 30% to 85% greater than those measured. Near the abutment end of the loaded span, the calculated slope changes are 15% to 30% greater, and near the abutment end of the unloaded span, the calculated slope changes are 2% to 5% smaller than those actually measured. In the transverse direction the predicted slope changes are for the most part smaller than the measured changes. This indicates an opposite trend from that apparent in the longitudinal direction. Namely, the model is stiffer in regards to torsional and transverse bending stiffness than the actual structure. Similar trends were noted previously with regard to deflections.

The sensitivity of the slope measuring instrumentation was much greater than that of the deflection measuring equipment. Deflection measurements were taken to 0.001 ft using an optical instrument and rod over large distances. They were thus subject to variability due to judgment and measurement techniques. In addition, the maximum change in elevation recorded was only 0.034 so the smallest division was always less than 1/34 of the value measured. With the slope measurements, on the other hand, the smallest division was 0.0001 in. and the maximum difference between readings was 0.0252 in. Thus, the smallest division approached 1/250 of the difference between readings. Also, the error inherent in leveling a 20-second level bubble was much less than that involved in reading deflections to 0.001 ft from a distance of 100 ft.

The difference in precision of the two measurement systems can be seen by comparing the smooth curves of the slope profiles with the irregular deflection curves.

4.2.9 Crack Mapping. A visual inspection and the mapping of cracks was carried out during the service load testing program. Although very little cracking was observed during service load tests themselves, the results of cracking during all phases of construction and testing are presented in this section. The areas in which cracking was observed can be divided into three categories based on the construction operation or structural component involved:

1. Cracking in the post-tensioning anchorage zones
2. Cracking in the wings or at the wing-spine connection
3. Cracking along the deck panels and deck

Cracking along anchorage zones occurred at both the wing stressing pockets and along the transverse diaphragm beam at abutment III. The cracking in the wing areas was observed immediately after first-stage post-tensioning when only the center tendon of the three tendon group in each wing was stressed. This was mainly observed in span 2, the first span on which wing units were placed and stressed. Cracking was noticed only on the side of the bridge from which the tendons were post-tensioned (northwest side). No similar cracking was noted at the opposite dead end anchorages. Some of the cracking is shown in Fig. 4.41. The cracks in the photograph have been marked with a black marker for experimental purposes. The actual cracks were hairline cracks. Most of the cracks closed appreciably upon second-

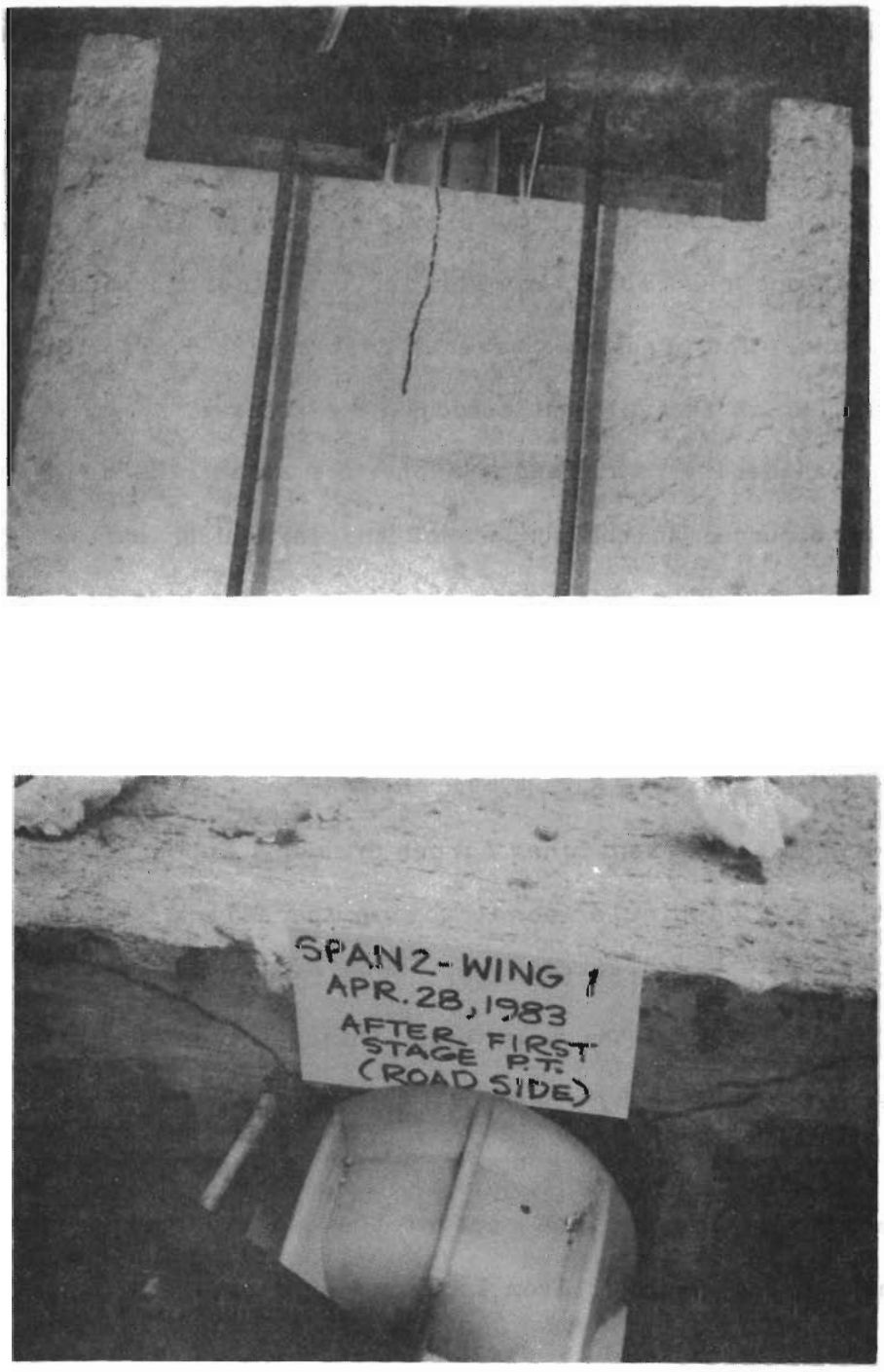

Fig. 4.41 Cracking in wing anchorage zones after first stage wing post-tensioning (cracks highlighted with black marker for better visibility)

stage stressing of the remaining two tendons in each wing. While other cracks may have occurred along the wings in span 1 or on the dead end anchorage side of the bridge, none were readily observable.

The cracking along the diaphragm beam, as seen in Fig. 4.42, was not noticed until near completion of the bridge. However, it may well have occurred some time earlier, particularly during stressing operations. The crack was several feet long and also occurred on the side from which the adjacent tendons were stressed.

Aside from the tendon anchorage zones, the majority of wing cracking occurred at the corners of the individual units. Figure 4.43 shows one particular unit where this type of cracking was observed. In many of the units cracking was noticeable from the ground 20 ft below. This was especially true after a rain when capillary action highlighted the cracks as shown in Fig. 4.43.

The above-mentioned corner cracking appeared to occur as the result of two particular construction operations. Some of the units were cracked during the transport when the entire bottom slab of the wing was supported on the truck bed. This was corrected after the first cracked units arrived by supporting the remaining units under the center rib only. This type of support seemed to eliminate the transport cracking. Cracking in the rest of the units occurred either during placement of the wings or from localized bearing of the corners upon the spine beam ledge. This accidental localized bearing is further evidenced by spalling of the ledge corner, as seen in Fig. 4.44. Figure 4.45 shows a schematic of the planned wing support mechanism and what

Fig. 4.42 Cracking in anchorage zone of abutment III diaphragm beam (cracks highlighted with black marker)

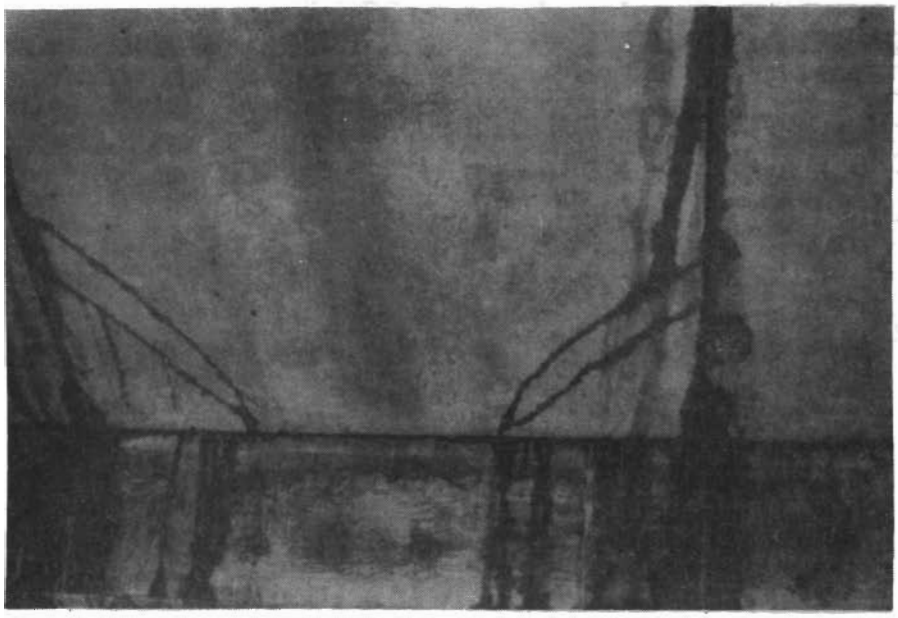

Fig. 4.43 Cracking at the corners of a wing unit

Fig. 4.44 Spalling of the spine beam ledge under the wing closure joint interface

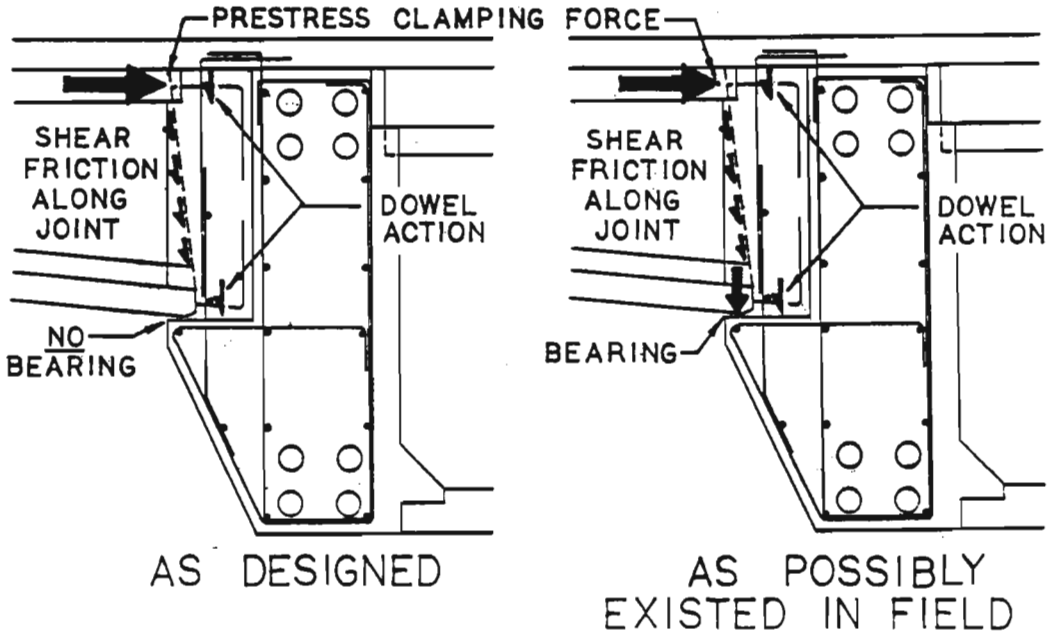

Fig. 4.45 Conceptual view of wing-spine load transfer as originally planned and as it may have actually existed when built

may have actually existed in the finished bridge. Recommendations for eliminating both types of wing cracking are presented later in Chapter 5.

Figure 4.46 maps the crack locations on the underside of the bridge. A visual inspection was made both before and after testing by observers moved into close proximity using a bucket truck. All cracks shown occurred prior to testing. No new cracking was discovered during a similar post-test inspection on the underside of the bridge and in the interior of the spine beam. The crack map presented is basically complete except for a few wing units near either abutment where it was not always possible to gain access for a close visual inspection.

The only other significant cracking observed was between the top precast deck panels and the closure pours and in the cast-in-place deck itself. Cracking in the longitudinal direction between the C1 and S3 precast units and the cast-in-place webs and between the C1 and S3 units themselves in the transverse direction (Fig. 4.47) was noticed during transport of the wings over the spine beam. The longitudinal cracking extended nearly the entire length of the bridge. Final post-tensioning tended to significantly close the cracks in both directions.

Cracks on the deck were also observed during the final day of service load testing. The cracks were located in the transverse direction along the wing ribs over several of the units. These cracks were only discovered after rains provided the necessary capillary action to make them visible (Fig. 4.48).

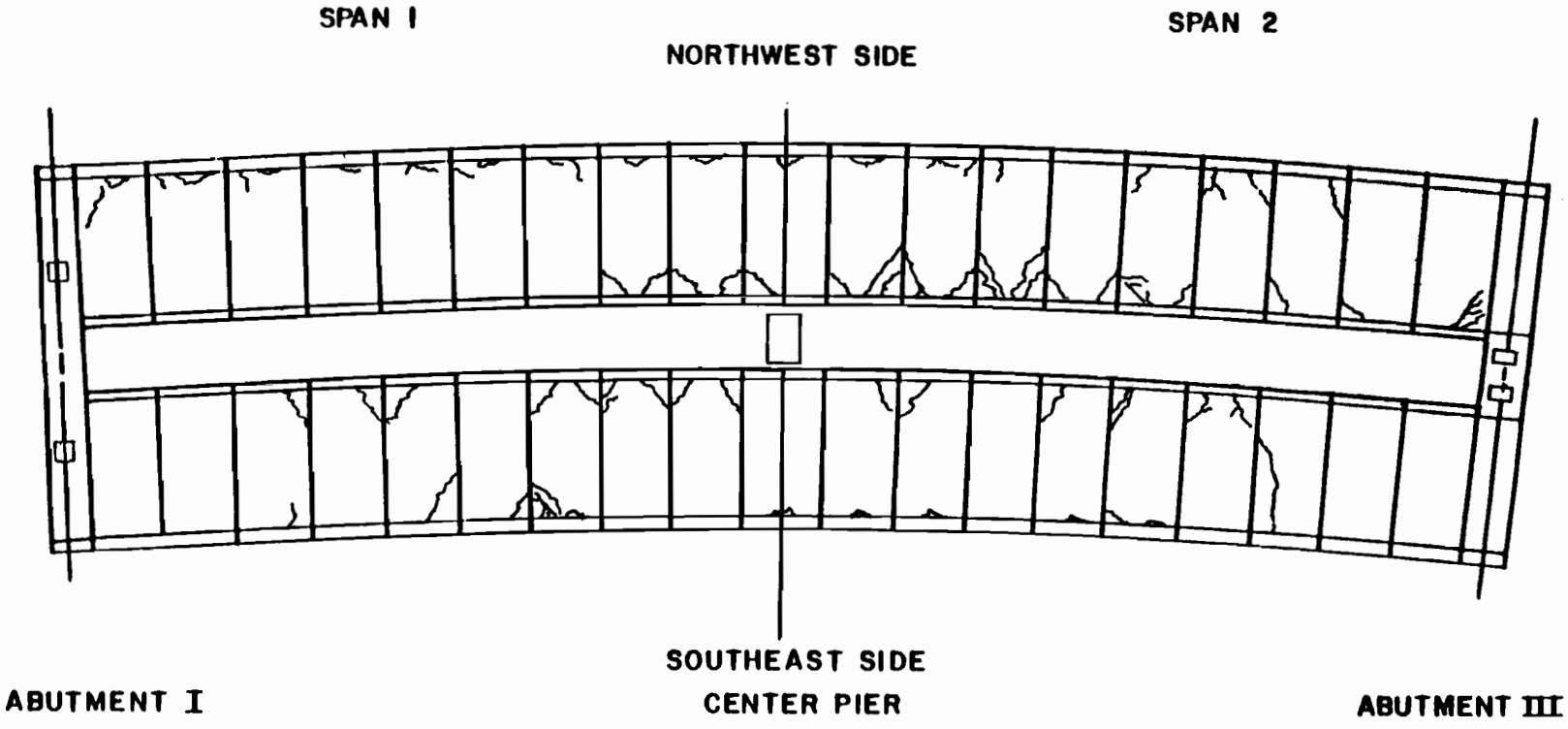

Fig. 4.46 Map of wing cracking on underside of bridge

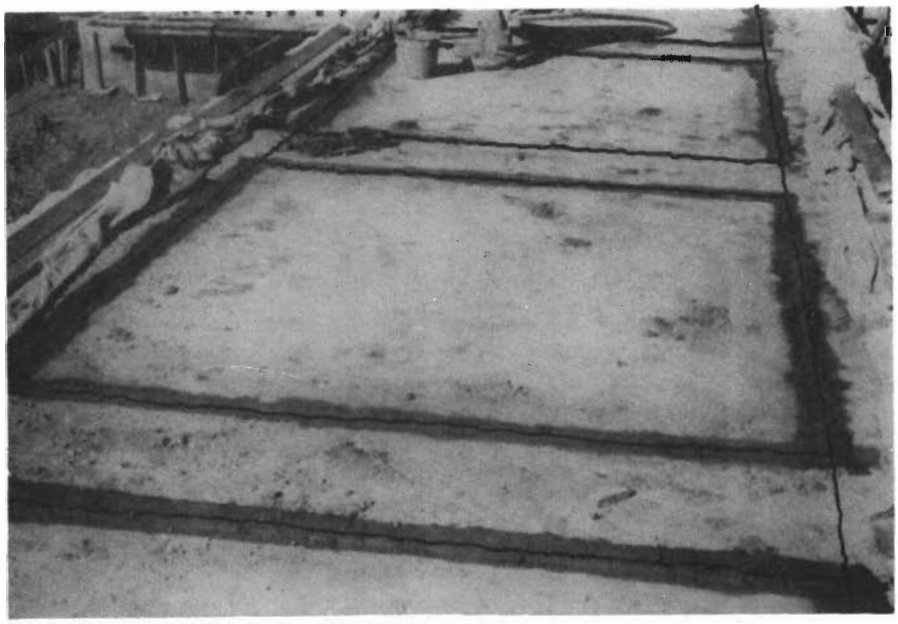

Fig. 4.47 Location of spine cracking between precast units and cast-in-place construction upon spine completion

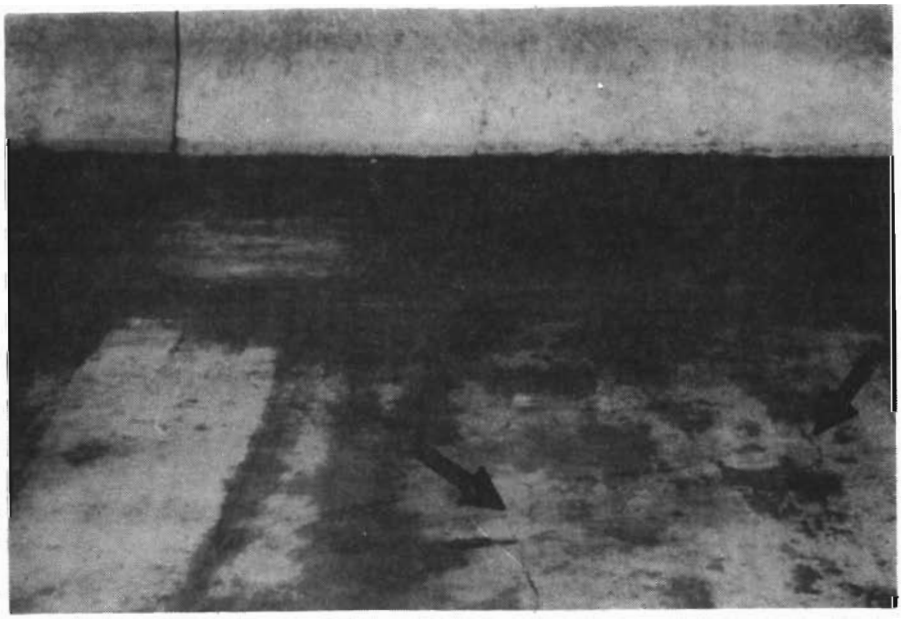

Fig. 4.48 Transverse deck cracking over the wing rib edges (pocket knife shown for scale purposes)

CHAPTER 5

RECOMMENDATIONS

5.1 General

Recommendations for improvements in the loose-fit composite wing girder method of design and construction are separated into three categories: (1) Design, (2) Construction, and (3) General.

5.2 Design

Design recommendations for the "loose-fit" composite wing girder concept can be subdivided into two categories: (1) Those that modify the existing design to facilitate construction and improve performance without changing the basic concept, and (2) Those that significantly alter components of the current design to create a more competitive alternative for selection.

5.2.1 Design Recommendations Which Do Not Significantly Alter the Present Wing Girder Concept. These recommended changes for constructability purposes are meant to facilitate casting and precast placement operations without overall changes in the loose-fit concept. The wing placement operation represents a critical stage in the construction sequence. Thus, it is important that it be executed with maximum speed and minimum difficulty. As shown in Fig. 5.1, the presence of protruding hooks along the top of the spine beam (bar labeled P25, P27, P29, P31 in the plans, [2,3]) and protruding vertical bars on the spine beam ledge seat (labeled Bar P9) in the wing closure area make wing transport and placement slow and cumbersome. At least

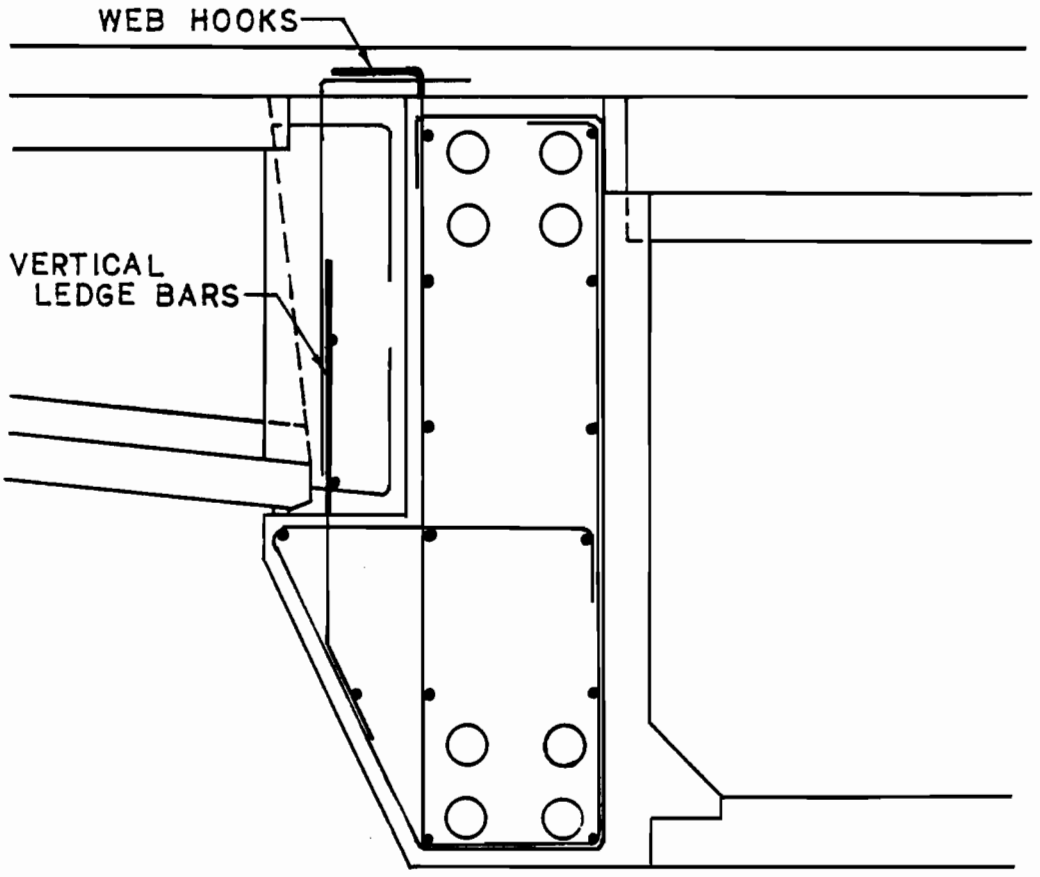

Fig. 5.1 Spine beam reinforcement in wing-spine area, which made wing transport and placement difficult

one, or preferably both, of these details should be altered or eliminated if possible.

Turning the top hooks inward over the web rather than outward over the closure area and lengthening the horizontal extension of the hook bar would facilitate both wing transport and spine beam form removal. This change would still allow another hooked bar to be spliced to the web hooks to enclose the top of the cast-in-place joint as in the existing design. Longer hook extensions would provide a more adequate splice development length. This proposed change is shown in Fig. 5.2a.

The vertical spine beam ledge/closure bars (bar labeled P9) should be completely redesigned to facilitate form removal and wing transport. From Fig. 5.1, it can be seen that the bars would have to be moved in very close to the web face if this means was chosen to permit clearance for the bottom wing hooks when moving the wings longitudinally along the bridge. This would greatly reduce the overall confinement in the closure joint and is undesirable from a structural efficiency and integrity viewpoint. However, if the top web hooks were bent inward as suggested previously, the wing units could be carried in a higher position and finally lowered into place without altering the vertical ledge closure bars. Another alternative would be to couple the ledge bars into embedded threaded anchors as shown in Fig. 5.2b. This could be done just prior to casting the closure joint to eliminate interference with the wings during transport and placement. An added advantage to coupling the bars would be the increased ease with which the spine beam wing ledge could be finished and the exterior spine forms

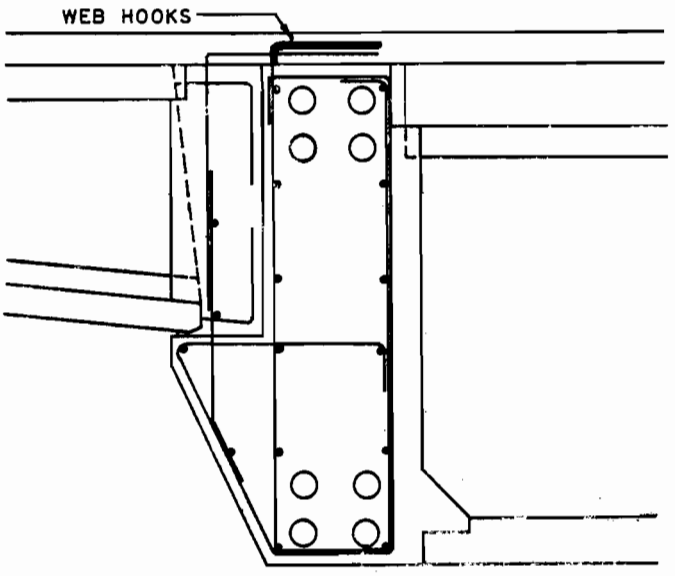

(a) Longer web-deck hooks with inward bend to improve splice length and facilitate spine beam form removal and transport of wings over spine

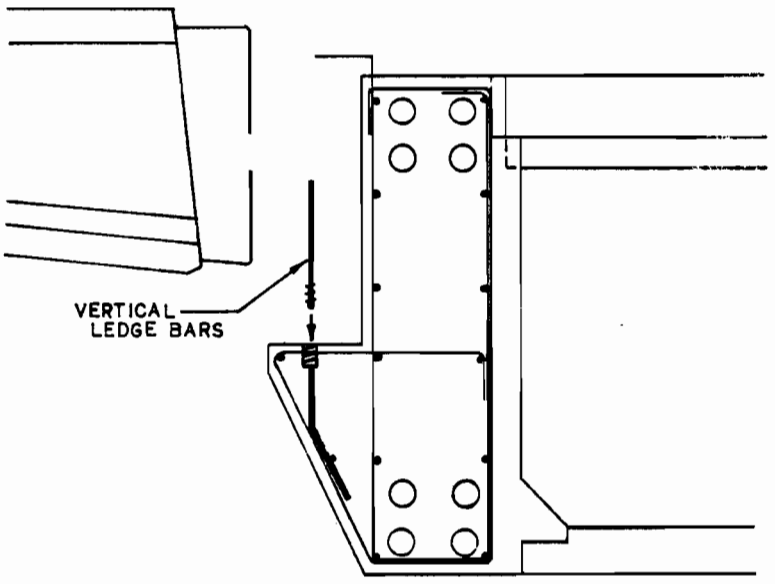

(b) Coupling system for vertical ledge bars

Fig. 5.2 Proposed alternatives for web reinforcement details

removed. A leveler and smoother ledge surface would possibly lessen some of the accidental wing bearing on the ledge and reduce the cracking and spalling shown in Fig. 4.44. An even better way of controlling the wing bearing along the spine beam ledge would be to provide neoprene pads located under the wing center ribs. Such pads would provide controlled bearing along the ledge and eliminate damage to any inadvertent contact between the two surfaces. The steel reinforcement in the spine beam ledge should also be redetailed to extend out fully under the contact area. With the above modifications, the compression struts in the spine beam ledge would deliver the wing forces to the spine beam web where tension hanger bars would then transfer the forces vertically to the spine beam top chord (Fig. 5.7). In order to eliminate corner cracking in the wing flange slabs, it would be advisable to add special reinforcement consistent with Sec. 13.4.6 of ACI 318-83. In fact, it may be desirable to use this practice at the corners of all the precast slab units. This would minimize transport damage as well as damage due to final support conditions.

There is also some question as to whether the specified 1/2-in. longitudinal gap between adjacent wing units is sufficient to allow proper positioning of the wings. Over a 100 ft. span length this limited gap width could make it difficult to align the transverse tendon ducts between the wing and spine beam. Figure 5.3 shows the difficulty involved in lining up the transverse wing ducts with the spin beam ducts. This becomes the most critical alignment in the present "loose-fit" concept. Aside from allowing a slightly wider gap on the order of

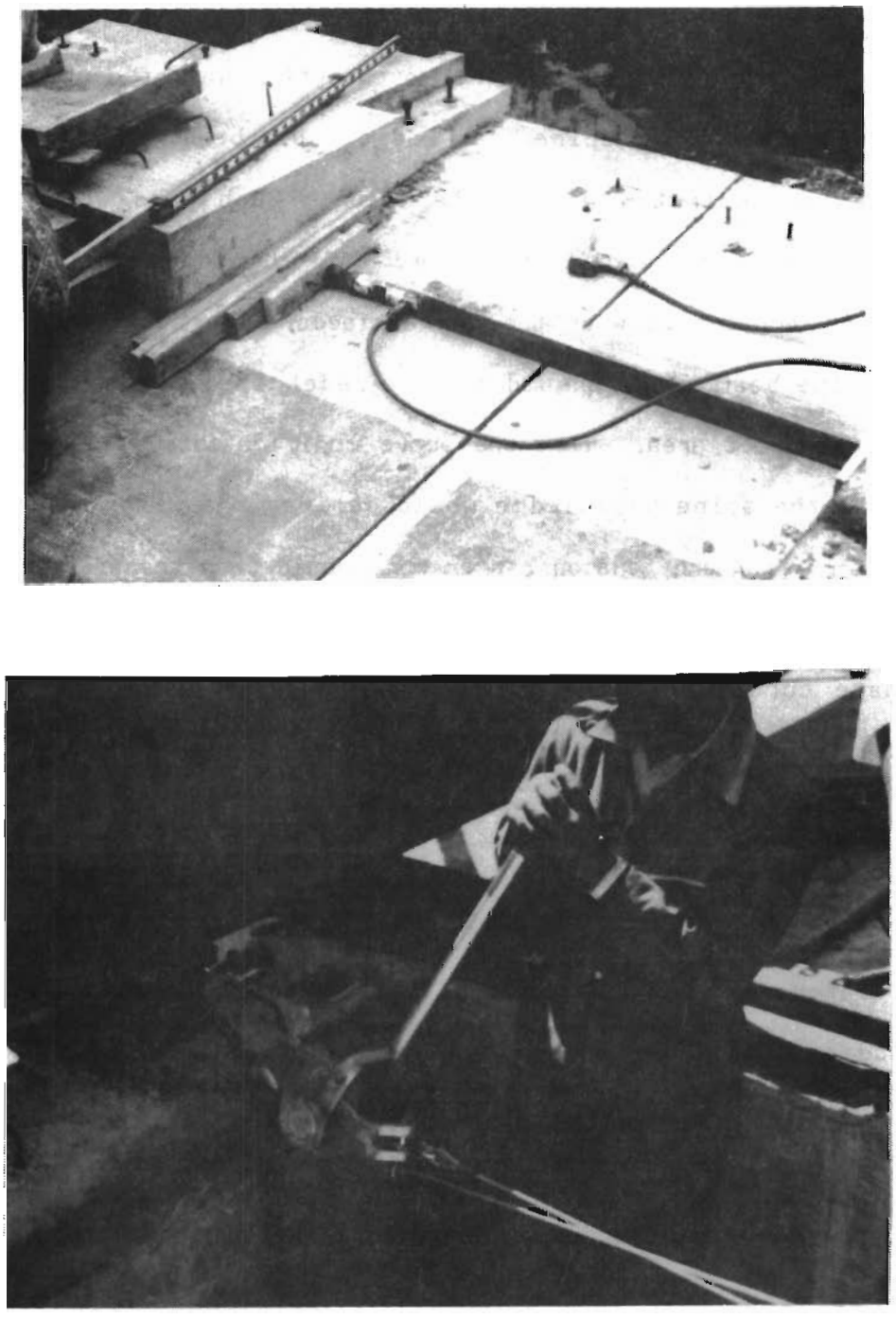

Fig. 5.3 Difficulty involved in exact positioning of wings and coupling of transverse tendon ducts

3/4 to 1 in., a possible alternative might be to use a more flexible coupler for the conduit connections. This would allow for any minor duct alignment in either the horizontal or vertical directions. In either case, when casting the wings, it is critical to maintain tight control over tolerances to promote the loose-fit concept upon which the design is based. The present transverse tendon alignment detail is in conflict with the concept of "loose-fit." Careful control was required in all phases of construction to ensure proper alignment of the tendon ducts. When setting the C1 compression struts in place, it was necessary to use optical instruments located off the bridge to achieve proper positioning. This may not be as easily facilitated in an urban environment like San Antonio.

Constructing the spine beam is the other time-determining step in construction involving the current wing-girder design concept. It was previously suggested that eliminating the protrusion of vertical reinforcement at the spine beam ledge would facilitate finishing of the ledge surface and the wrecking of forms. Some questions have also been raised as to the need for setting the C1 compression struts in place prior to casting the spine beam webs. If the spine beam were to be cast without these overhead obstructions, the interior forms could be made up of longer sections which are more easily lifted out after casting. Since the strut elements do not utilize reinforcement to tie into the web, it seems they could just as easily be dropped into place after the webs are cast. It may even be possible to combine the C1 and S3 panel units into a single element.

Another item concerning forming and casting operations, as well as the control of concrete cracking, deals with the bursting reinforcement in the post-tensioning anchorage zones. The Bear Creek design utilized W-bars, as shown in Fig. 5.4, to provide bursting resistance in the wing anchorage regions. The W-bars are difficult to install in congested regions and are not nearly as effective as spirals in preventing cracking due to bursting stresses. The use of spirals might have eliminated some of the anchorage zone cracking shown in Chapter 4.

A few other areas which may benefit from minor modifications are the pier erection and guard-rail placement operations. Precast piers, or pier segments, could easily be designed and would speed up substructure operations. By post-tensioning, steel congestion would be reduced and the need for splicing long column bars and tying long column cages would be eliminated. Such precast piers have ben widely used on recent trestle type projects in other states. With regard to the parapet placement procedure, there was some discussion as to the minor inconvenience of leveling the units with such a short distance between connection channels. If the channels were moved out from the center rib, as shown in Fig. 5.5, they would afford a greater working distance with which to adjust and level the rail units. Also, providing more concrete clearance over the top of the channels would permit the contractor to install a nut both above and below the channel to allow grading in either direction vertically.

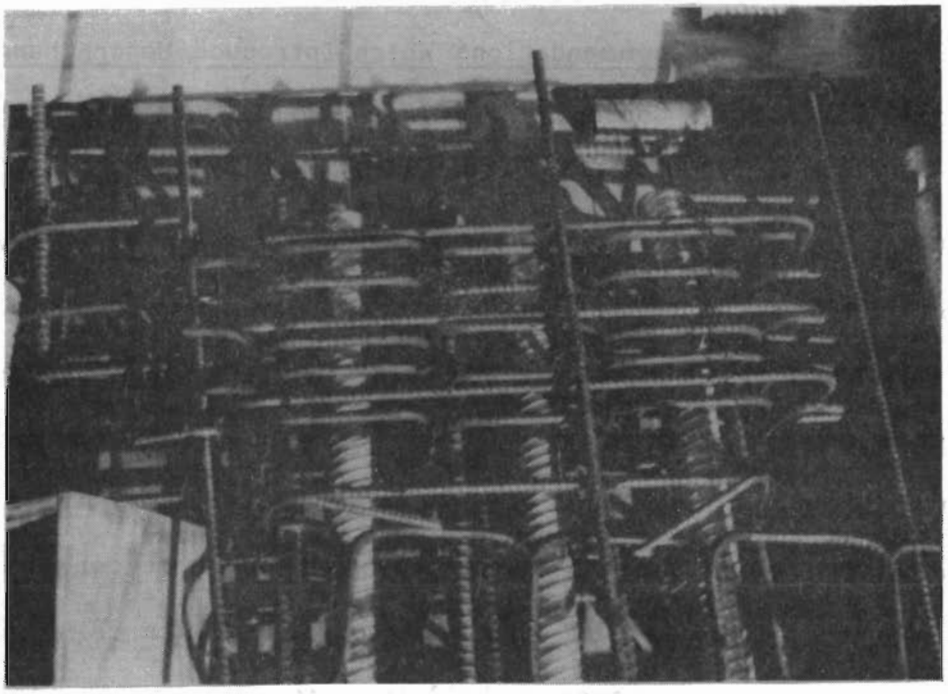

Fig. 5.4 W-bar bursting reinforcement and rebar congestion in wing anchorage zone

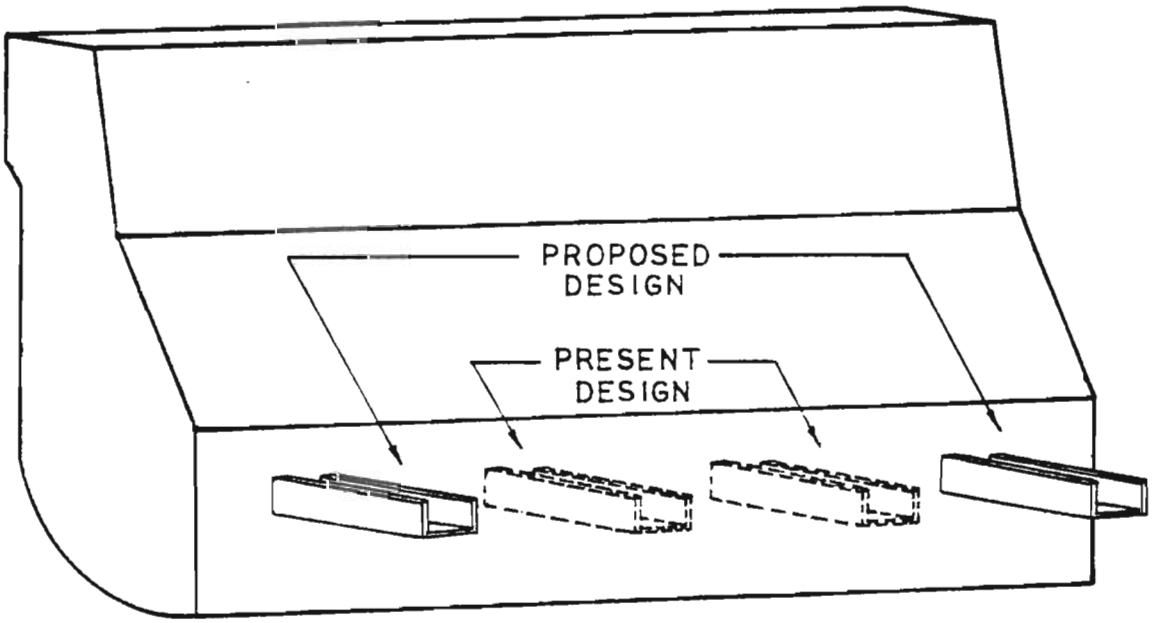

Fig. 5.5 Proposed change in spacing of connection channels would facilitate adjustment and leveling of the parapet units

5.2.2 Design Recommendations Which Introduce Major Changes in the Present Wing Girder Concept. There are several substantive changes to the wing-girder concept which should be viewed as possible alternatives to the present method of construction. The first involves erection of the spine beam. Because the two critical stages in the present method of construction are the spine beam erection and the wing placement operation, both procedures should be designed to ensure the minimum completion time. The present method of fabricating and casting the spine beam webs in place is too awkward and time-consuming to achieve any significant rate of construction speed. Even using pretied web cages, the erection sequence still involves setting the cages and precast slab units in place, erecting the forms, installing the tendon ducts and anchorage hardware, casting, curing, setting additional slab units and post-tensioning. This is not to mention the excessive amount of formwork involved (hopefully steel forms will be used), the limited access space allowed for workmen to carry out a myriad of tasks, and the increased possibility of debris from extensive construction efforts being knocked off into the path of traffic below. The wing-girder concept does merit special consideration, however, in that it allows for the transport of smaller and lighter precast units than those used in conventional segmental construction. Also, with the limited right-of-way available in San Antonio, the narrow spine beam might be preferable to precast units which span the entire width. For instance, during early stages of construction, the 12-ft wide spine beam may permit the

use of a small crane below which would not be possible with the entire 52-ft width in place.

A more desirable means of constructing the spine beam while still maintaining the positive aspects of wing-girder construction would be to precast the entire spine beam cross section in approximately 10-ft lengths. As shown in Fig. 5.6, the weight of a 10-ft section of spine beam is approximately the same as that of a pair of wings. Thus, the same equipment could be used for lifting either unit in place. Some type of erection truss or shoring is required in both instances, but with precast segments the spine could be erected much more quickly than with in situ spine fabrication. Tighter control over casting could also be maintained, and the spine beam could be post-tensioned immediately. The general geometry could be easily controlled by using the long line method for the spine beam with match cast segments employing multiple shear keys. When erected, epoxy or grout between units would seal tendon joints, and threaded bars could be used for both connections and continuity. Precasting the spine beam in this way would also allow most of the ultimate shrinkage to occur before post-tensioning, reduce creep significantly due to the greater age at time of stressing, and thus ensure much more favorable behavior of the post-tensioning system over the bridge life.

The wing-spine connection and the cast-in-place closure area has prompted considerable concern from the earliest stages of the project. From Fig. 5.7 it can be seen that the as-designed load paths in transferring load from the wings to the spine beam are not clearly

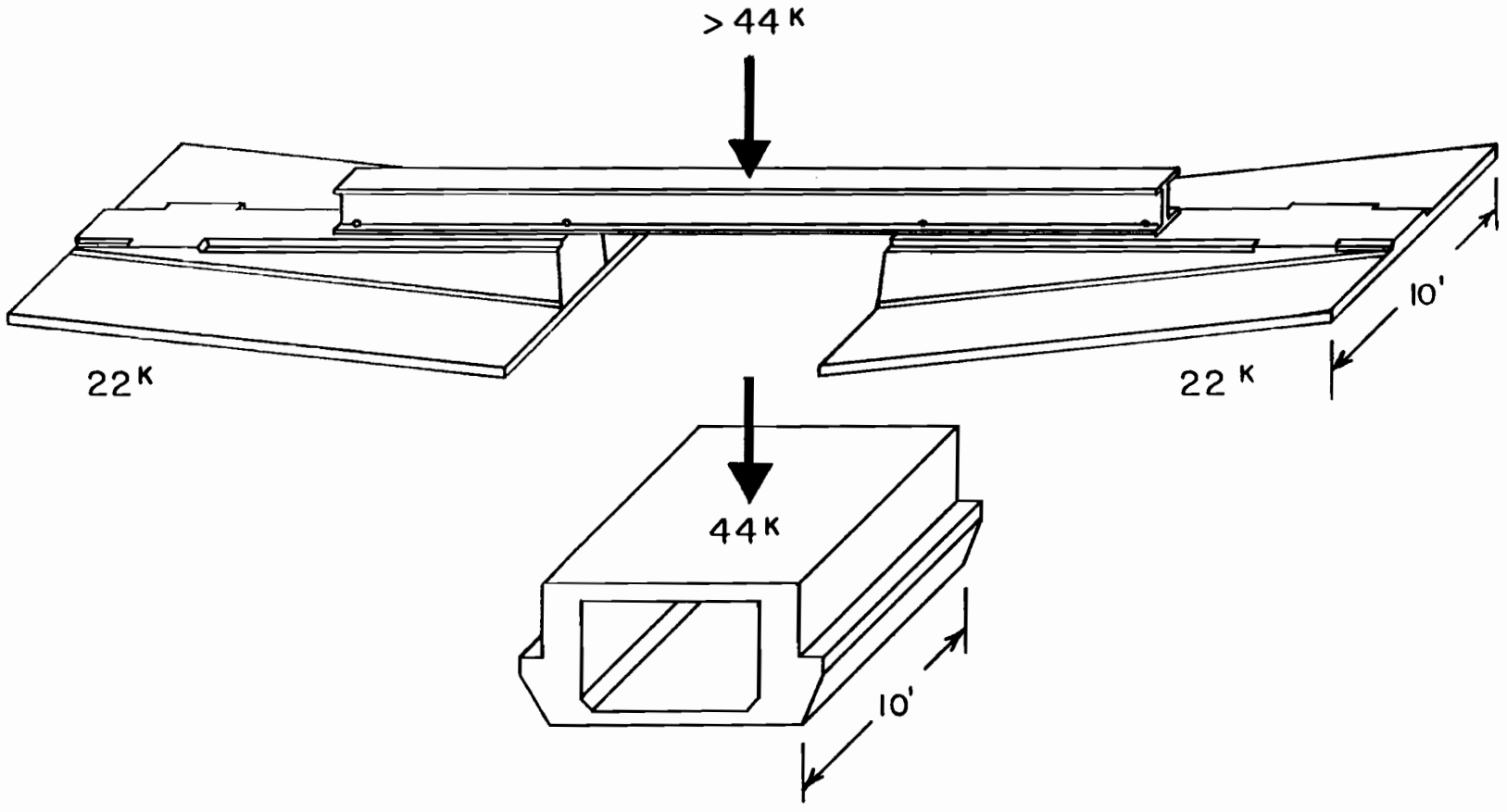

Fig. 5.6 Comparison of the lifting weights of a 10-ft section of precast spine beam and a pair of precast wing units

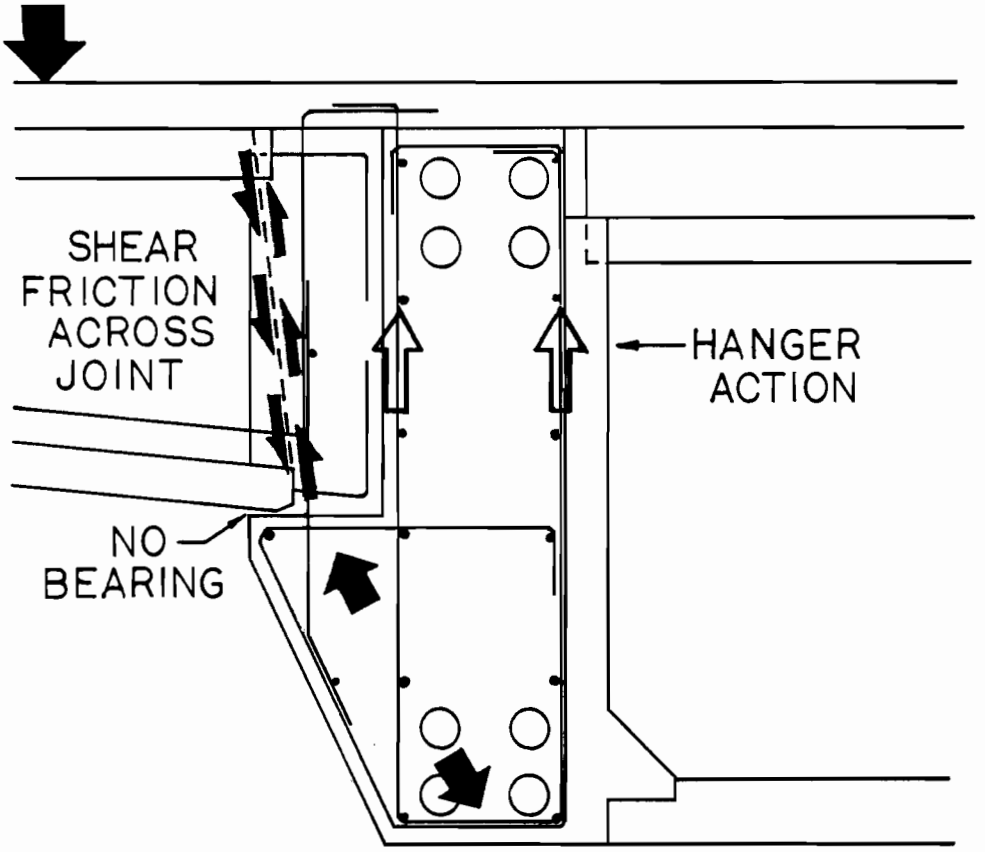

Fig. 5.7 Load path mechanism across as-designed wing-spine closure strip

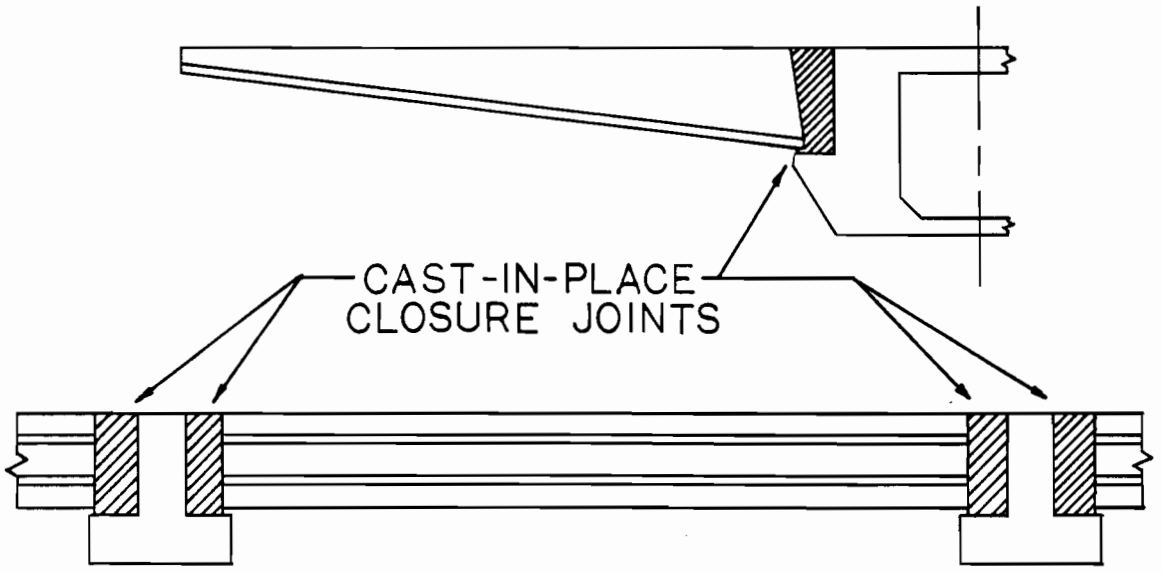

Fig. 5.8 Prestress I-girder with analogous support conditions

defined. Shear friction across a cold joint is required to transfer the entire load. The transverse post-tensioning provides the necessary normal force. This method of support would be somewhat analogous to constructing a prestressed I-girder bridge with the support conditions shown in Fig. 5.8. Extending the support ledges out and setting the wings in closer to the spine beam face, as proposed in Fig. 5.9, would result in a more positive load path mechanism. By utilizing both shear and bearing to transfer the load into the spine beam lower flange, the joint would be more efficient. The spine beam could be designed using the truss analogy to "lift" the lower flange load up to the top chord loading points using hanger rods in the form of spine beam stirrups. In combination with a neoprene bearing pad under the wing ribs and appropriate ledge corner reinforcement, the ledge spalling seen in Chapter 4 should be eliminated.

Another major modification to the wing unit subsystem would be the use of Dywidag-type threaded bars with couplers instead of seven-wire strand in the transverse direction. Figure 5.10 shows the great potential of the wing strongbacks to serve as construction barriers. With quickly coupled Dywidag bars as tension ties and temporary wedge blocks in the closure joint, the wings could be positioned and adjusted, the bars coupled, and the strongbacks removed immediately. The truss system shown in Fig. 5.11 would support the wings. The bars could be designed as conventional tensile struts at this stage and then post-tensioned at a later time when the joint closure has been completed. Alternatively, a portion of the bars could be stressed immediately to

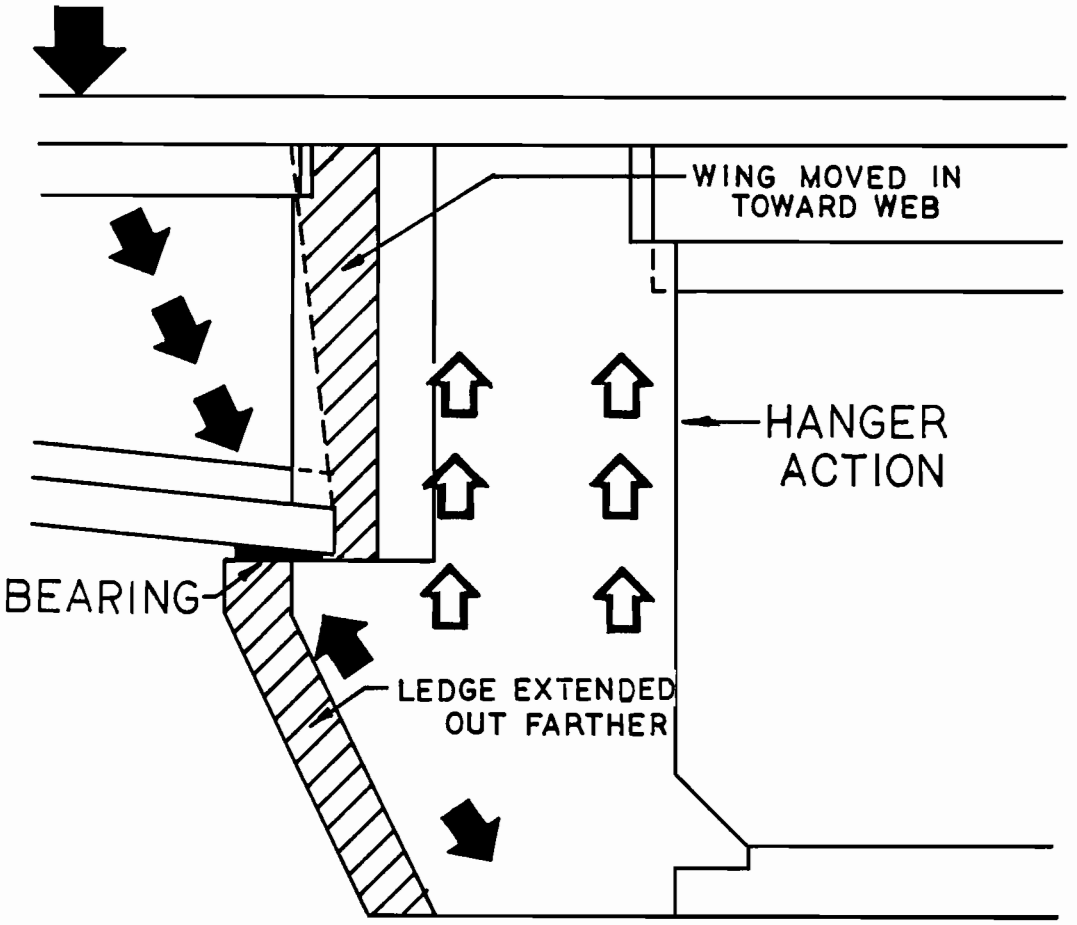

Fig. 5.9 Proposed redesign of wing-spine closure area for more efficient load transfer

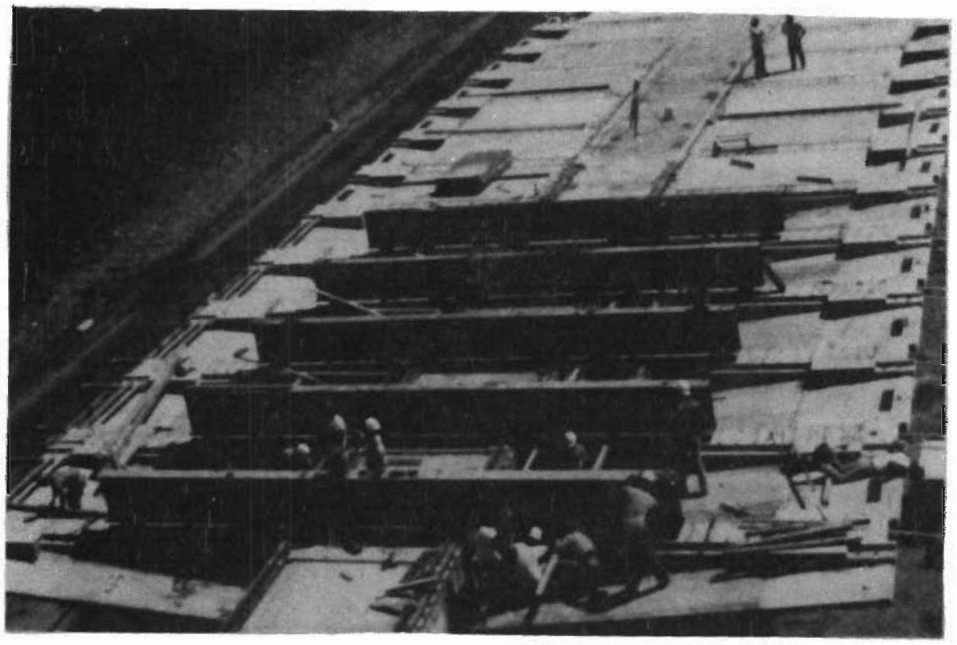

Fig. 5.10 Overhead view of wing placement operation showing construction barriers resulting from temporary strongbacks

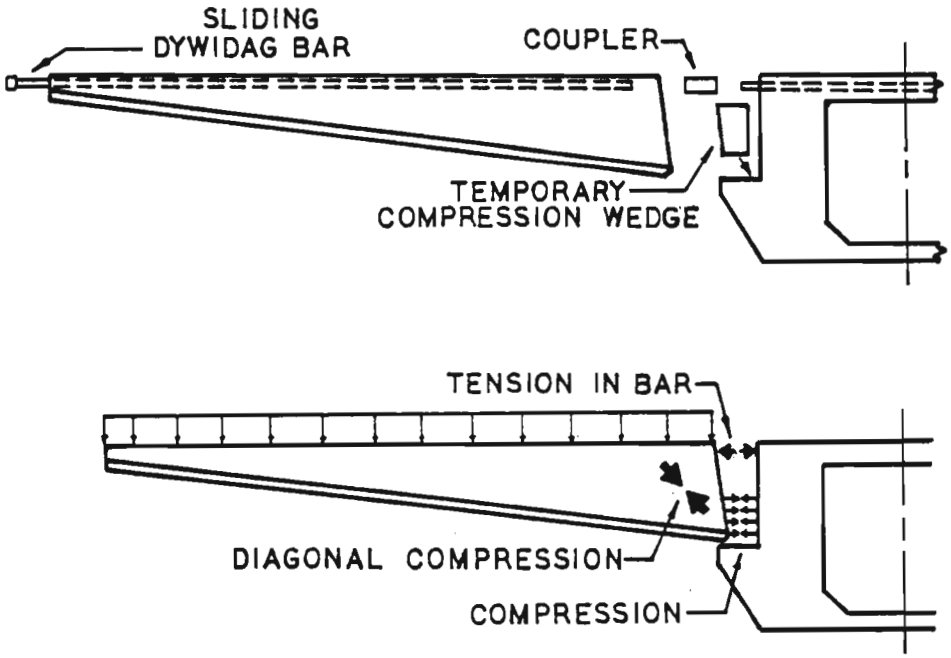

Fig. 5.11 Components of Dywidag system and truss mechanism for transferring loads with bars coupled but not yet stressed

support only the weight of the wing unit with more positive wedges or bearing plates required. The Dywidag bars, as shown in Fig. 5.12, require simpler anchorage hardware and post-tensioning jacks than conventional strands and can be grouted in a similar manner. They lend themselves to quick coupling quite easily.

There are certain drawbacks to the use of the Dywidag-type bars. They are more costly than seven-wire strand for a given level of permanent prestress. This could be overcome by using the Dywidag coupled bars for the first stage of transverse prestressing and conventional strand for the second stage. The higher unit cost of the Dywidag type prestressing should be more than offset by the increased efficiency of construction operations if the strongbacks can be removed immediately. The use of coupled bars also requires that attention be given to detailing of coupler locations. The couplers should be staggered so that only about 1/3 of the bars are coupled in a given location in the spine. This should be very easy to do since the spine beam top flange is over 9 ft wide. Three coupling zones can easily be detailed. Another positive advantage is the fact that the ram for stressing the large Dywidag bars is very light and can easily be positioned for transverse prestressing without the use of a travelling hoist. This reduces the complexity of the transverse prestressing operations.

5.3 Construction

Construction recommendations are relatively minor in scope. They include:

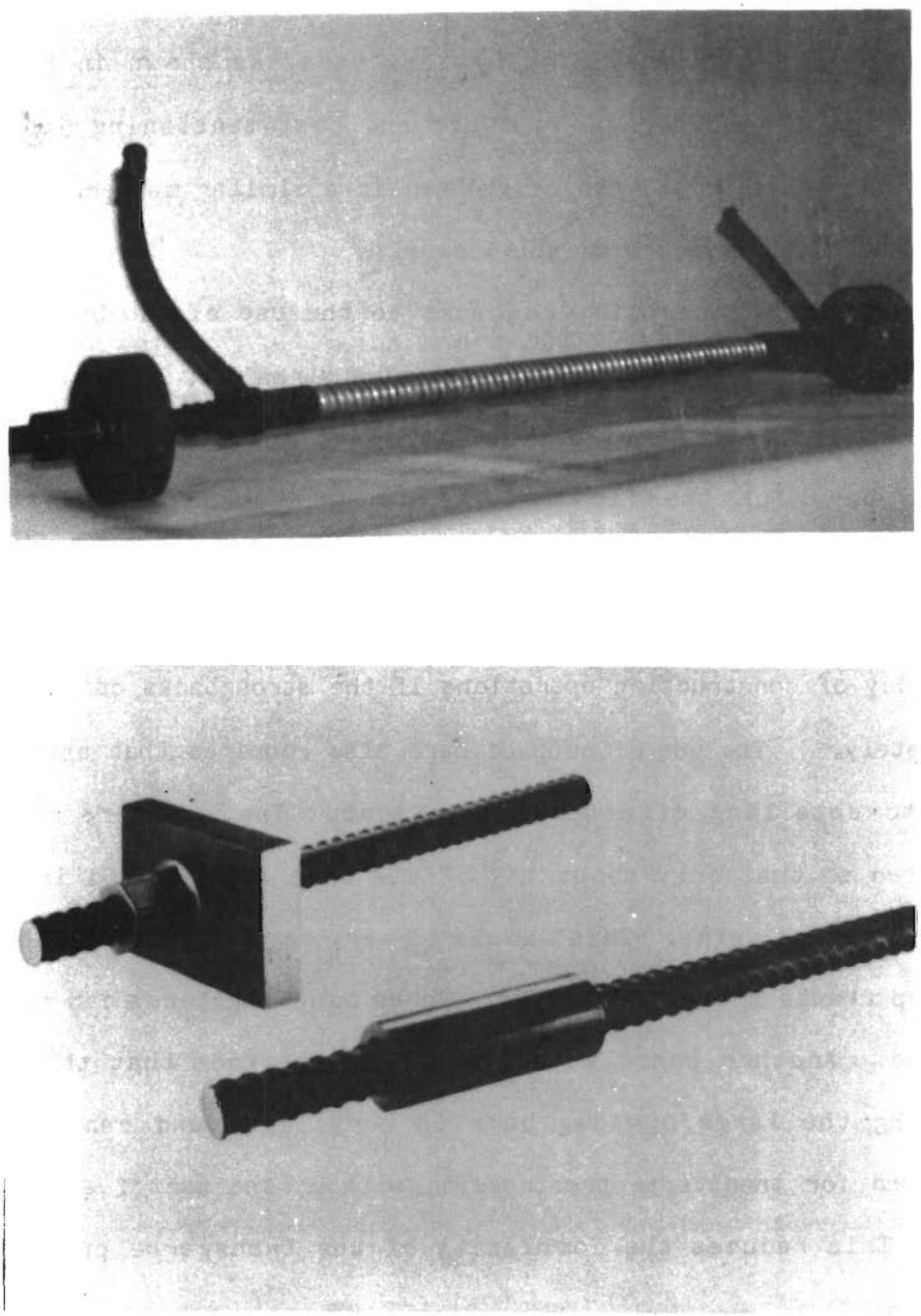

Fig. 5.12 Dywidag bars with coupling and anchorage hardware

1. When precasting the wing segments and possibly other units, the contractor should check clearance requirements closely to determine an appropriate maximum size of aggregate. After using larger aggregate sizes on the Bear Creek project, the precaster recommended a maximum aggregate size in the neighborhood of 3/4 in. in the wing units due to limited clearance.
2. Overall wing dimension tolerances and prestress hardware placement tolerances during precasting must be carefully controlled for proper positioning and alignment of the transverse tendon ducts during construction.
3. During transport to the site, the wings should only be supported along the center rib. This will eliminate some of the cracking at the wing corners.
4. On the Bear Creek project, the B1 soffit slab units were set in place on the shoring and the closure steel between adjacent units was bent in place. The bars should be prebent prior to casting or at least bent upon removal from the forms to provide greater working space for such operations. The former method would require notching the forms to facilitate removal of the finished units.
5. Finally, using the present method of casting in place the spine beam, it would be extremely desirable to pre-tie the reinforcement cage for the spine beam webs. Tying the cage in place is much too time consuming to make the cast-in-place

method of construction practical with the construction timetables envisioned.

5.3.1 General. A few general comments should be made concerning design and detailing. Several of the problems during construction alluded to in Chapter 2 were the result of inadequate detailing. The importance of coordinating drawings from all components of a structural system cannot be overemphasized. Both nonprestressed reinforcement and prestressed tendon details should be provided on common drawings. In this particular project the post-tensioning layout was not compatible with the reinforcement arrangement specified; substantial alteration of reinforcement in the field was required. Such oversights require the contractor to make engineering decisions, or at best, force a qualified engineer to make hasty, quick-fix changes. Aside from details that are altogether impossible to construct, the designer should be aware of details that are grossly impractical as well. For instance, in the authors' opinion, the spine beam webs on the Bear Creek structure were much too narrow to accommodate the large quantities of steel and conduit during fabrication and casting. Greater consideration to constructability should be used during design stages.

Other details which deserve mention relate to concrete cover requirements and reinforcement schedules. When dealing with minimum concrete cover requirements of 1 inch or 1-1/2 inches, it is advisable to specify a slightly larger cover to allow for placement errors. The additional cost is minimal, and it generally results in a more uniform, better quality structure. Finally, concerning reinforcement schedules,

bar dimensions should be specified clearly as out-to-out or center-to-center and, when possible, bend details should be given on the same drawing as the reinforcement to which they pertain.

CHAPTER 6

SUMMARY AND CONCLUSIONS

6.1 Summary of the Investigation

This investigation involved the construction monitoring and performance evaluation of the innovative "loose-fit" composite wing girder bridge at Bear Creek.

In order to better understand the load transfer behavior and assess bridge performance, appropriate instrumentation devices were implanted at various stages of construction to obtain information regarding displacements, strains, and slip. Monitoring of these devices was carried out in two distinct phases: (1) During critical stages of the construction sequence, and (2) under critical service level loadings upon completion of the bridge. Observations concerning general behavior and cracking were also made during both phases.

The design of the bridge and construction operations were detailed in Chapter 2. Special attention was given to particular items and procedures which were considered pertinent to future applications in the San Antonio project. Chapter 3 described the instrumentation program. The types and locations of instrumentation, load details, and the schedule of readings were presented for both the construction stage testing and service load testing. Sample results of the observations were given in Chapter 4 and full detail is given in Ref. 2. The plots show load response for a particular type of behavior. Also, the results of an analytical model were compared with the measured results from the

field testing program. This comparison was made to determine the model's predictive capability in analyzing similar structures to be built in the future. The model utilizes the finite element method and was modified specifically for the Bear Creek project. Finally, recommendations for improvement of the present design with regards to constructability and performance were given in Chapter 5.

6.2 Conclusions

Construction of the Bear Creek bridge proceeded as planned for the most part although at a much slower pace than originally anticipated. In regards to some of the purported advantages of the loose-fit wing girder design, the results are questionable. The idea of small and easily handled precast units is definitely beneficial in regards to transport and use of only light construction equipment. This was an obvious advantage in a job of very small scope such as Bear creek, but may actually be a liability where a very large project is involved. In very large projects the "loose-fit" system results in a very large number of small pieces and hence presents scheduling and coordination problems. The use of light equipment may be useful in urban areas such as the San Antonio site where limited access and traffic maintenance requirements place tight restrictions on construction efforts. However, experience with many large projects shows large segments can be handled in urban environments without undue traffic interruptions.

The principle of "loose-fit" with respect to construction involving precast units and cast-in-place closure areas is also an

advantage, since the tolerances required during casting, particularly when precasting is used, are easily attainable. However, the present system needs modification in terms of the tolerances required for alignment of transverse prestressing ducts to be a true "loose-fit" system. The easy assemblage of units saves time and construction effort out in the field when cast-in-place construction is used.

When examined out of context, the aforementioned features of the present wing girder concept appear ideal in meeting the stringent demands imposed by a project such as the San Antonio interstate expansion. However, the advantages discussed were never fully achieved or were overshadowed by other factors of greater significance. None of the principles of smaller units, precasting, or loose-fit was fully effective, since the concepts were not applied to the entire structure during all phases of construction. The precast spine and deck elements were light and easy to handle and transport. However, in-place construction of the spine beam was slow and difficult. A series of 10 ft precast segments of the entire spine cross section would have been much more practical in regards to limiting erection time and construction effort. This is quite apparent in light of the amount of time and effort required to assemble the formwork and reinforcement cages and to cast the spine beam webs in the field. The apparent advantage of handling the lighter, smaller precast units for the spine beam is greatly reduced when equipment must have the capacity to place wing pairs which involve weights that are nearly equal to that of a 10 ft long precast section of spine beam. The time-saving and improved

control aspects of precasting parts of the spine beam are negated by the difficulty and amount of time required for in situ casting of the webs.

The apparent advantages of "loose-fit" construction were not fully realized since certain operations still required tight tolerances to be maintained. The need for very precise transverse duct alignment between the wings and spine beam undermined the contractor's option to relax tolerance standards during casting and placement of the C1 compression struts and the wing units.

The individual features of the composite wing girder design are noteworthy in theory, but overall, the concept as demonstrated at Bear Creek does not appear to be the best alternative available. Specifically, the time required for construction, despite the familiarity gained through repetition, is much too great. A large part of this is attributable to the difficulty of the in-situ spine beam construction, which requires an extensive amount of sequential operations. This leads to a second major concern, that the number of operations involved in the field is excessive to the point of being impractical for smooth construction with a minimal occurrence of disruptions. The suggested change to precasting of the spine beam in approximately 10-ft long segments on long line beds would reduce the complexity and time required for field erection without changing the basic composite wing-spine concept.

In regards to the aesthetics and the overall structural performance of the structure, the composite wing-girder design, apart from a few details, appears to be a very satisfactory option. On the

basis of artists' renditions for the San Antonio application and from the extremely elegant appearance of the completed Bear Creek structure, the smooth, gently curving design is very attractive and appealing in the author's opinion. Although certain problems concerning cracking in the anchorage zones and along the wing panel corners (Sec. 2.3.3.7) need to be addressed in future applications, the overall load response of the structure was very good. Displacements were much smaller than originally anticipated indicating a relatively stiff structure in regards to both bending and torsion. No structural problems were noted in the service level load tests.

The relatively small levels of displacements, while desirable from a performance point of view, were not so enviable as far as the measurement program was concerned. The instrumentation used indicated qualitative agreement with expected behavior and gave useful information concerning the magnitude of response to various loads. However, in many instances the instrumentation used was not sensitive enough to give exact distributions of load behavior. Perhaps the most reliable sets of data were afforded by vertical deflection and longitudinal surface strain measurements during construction stage testing and from slope measurements during service load testing. The success of the former methods was due largely to the greater level of displacements occurring while that of the slope indicator was due primarily to the greater sensitivity of the instrumentation. The construction stage deflection measurements, however, were hampered somewhat by the inability to make all measurements on surfaces or reference points which would be

available at all stages of construction. Temperature measurements during both phases provided excellent information concerning temperature gradients over the spine beam cross section.

The results of the PUZF83 finite element analysis showed general agreement with measured behavior, but modifications are required to make the predicted results more reliable. Overall, calculated deflections and slopes in the longitudinal direction were larger than those actually measured. In the transverse direction the opposite was true. Thus, the analytical model predicts a more flexible structure in the longitudinal direction but a stiffer structure with regards to transverse bending and torsion. Only the completed bridge was modeled, so calculated results are for the service load cases alone. The construction stage analysis involved too many intermediate steps to attempt to model each stage separately.

The composite wing girder system has some very positive aspects such as the ease with which smaller units can be transported and handled and the minimization of many tolerances. However, in its present form, the design does not appear to be an optimal solution for a large project such as that proposed in San Antonio. Part of the purpose of this research program was to suggest possible changes in the concept details for consideration by the designer and owner. Several recommendations were made in Chapter 5 for improving the current design. While most involved relatively minor changes in details to improve constructability and performance without altering the basic concept, there were a few more substantial changes suggested. These were aimed at the two

critical phases of the bridge construction: (1) construction of the spine beam, and (2) placement of the wings. As discussed earlier in this section, the spine beam construction process involved an extensive amount of time and a large number of operations. In the authors' opinion, a different method of spine beam construction such as precasting the entire spine cross section in longitudinal segments and then joining the segments using epoxy adhesives, shear keys, and post-tensioning would be a much quicker, less complicated alternative. The composite wing and deck construction would then proceed in much the same manner as was successfully done at Bear Creek.

The wing-spine connection and wing support mechanism would probably benefit greatly from a redesign which makes use of bearing rather than just shear friction to transfer loads from the wing to the spine. This would more clearly define the intended load paths and would probably reduce some of the wing and spine beam ledge cracking described in Sec. 2.3.3.7.

A final proposed change to the current construction procedure for erecting the wing system would utilize threaded stressing bars rather than conventional seven-wire strands. The bars would serve as tension ties immediately upon placement of the wings. This would facilitate completion of the wing placement operation and would allow for immediate removal of the supporting strongbacks as discussed in Chapter 5.

The suggested changes need to be carefully evaluated for cost, time, and construction feasibility. Preliminary qualitative analysis

indicates all are attainable and have very positive benefits. However, no detailed pricing quotations or specific details were investigated.

The opportunity to observe and critique the construction operations of this innovative project was a most interesting and satisfying experience. The authors have attempted to phrase all comments and recommendations in the same positive and open spirit that all parties involved in this project demonstrated in sharing information. It is felt that if all recommendations were adopted, the overall concept would still be a "loose-fit composite wing girder bridge." Hopefully, the suggested revisions would result in somewhat easier and quicker construction and in improved appearance and durability at a reduced cost.

REFERENCES

1. Clark, G. T., Kreger, M. E., and Breen, J. E., "Model Test of a Composite Wing-Girder Bridge, Research Report No. 915-1F, Center for Transportation Research, The University of Texas at Austin, November 1984.

2. White, Christopher D., "Observations and Evaluation of the Composite Wing Girder Bridge at Bear Creek," unpublished M.S. thesis, The University of Texas at Austin, May 1984.

3. Plans of Proposed State Highway Improvement--F.M. Highway 1626 at Bear Creek, Texas State Department of Highways and Public Transportation, 1982.

4. Matlock, H., Panak, J. J., Vora, M. R., and Chan, J. H. C., "Field Investigation of a Skewed, Post-Stressed Continuous Slab Structure," Interim Study Report, Center for Highway Research, University of Texas, Austin, 1974.

5. Naaman, Antoine E., Prestressed Concrete Analysis and Design--Fundamentals, McGraw-Hill Inc., New York, 1982.

6. Post-Tensioning Institute, Post-Tensioning Manual, 3rd ed., USA, 1982.

7. ACI Committee 209, "Prediction of Creep, Shrinkage, and Temperature Effects in Concrete Structures," Special Publication SP-27, Designing for Effects of Creep, Shrinkage, and Temperature, American Concrete Institute, Detroit, Michigan, 1971, pp. 51-93.

8. Johnson, C. Philip, Thepchatri, Thaksin, and Will, Kenneth M., "Static and Buckling Analysis of Highway Bridges by Finite Element Procedures," Research Report 155-1F, Center for Highway Research, University of Texas at Austin, August 1973.

9. Will, Kenneth M., Johnson, C. Philip, and Matlock, Hudson, "Analytical and Experimental Investigation of the Thermal Response of Highway Bridges," Research Report 23-2, Center for Highway Research, The University of Texas, Austin, February 1977.

10. Podolny, Walter, Jr., and Muller, Jean M., Construction and Design of Prestressed Concrete Segmental Bridges, John Wiley & Sons, Inc., New York, 1982.